Development and Experimental Investigation of Direct Urea Fuel Cells

by

Ayse Sinem Meke

A thesis submitted to the
School of Graduate and Postdoctoral Studies in partial
fulfillment of the requirements for the degree of

Master of Applied Science in Mechanical Engineering

Faculty of Engineering and Applied Science

University of Ontario Institute of Technology (Ontario Tech University)

Oshawa, Ontario, Canada

June 2024

THESIS EXAMINATION INFORMATION

Submitted by: **Ayse Sinem Meke**

Master of Applied Science in Mechanical Engineering

Thesis title: Development and Experimental Investigation of Direct Urea Fuel Cells

An oral defense of this thesis took place on August 1, 2024, in front of the following examining committee:

Examining Committee:

Chair of Examining Committee	Dr. Amirkianoosh Kiani
Research Supervisor	Dr. Ibrahim Dincer
Examining Committee Member	Dr. Martin Agelin-Chaab
Thesis Examiner	Dr. Meaghan Charest-Finn

The above committee determined that the thesis is acceptable in form and content and that a satisfactory knowledge of the field covered by the thesis was demonstrated by the candidate during an oral examination. A signed copy of the Certificate of Approval is available from the School of Graduate and Postdoctoral Studies.

ABSTRACT

This thesis study considers the development and experimental investigation of Direct Urea-Hydrogen Peroxide Fuel Cells (DUHPFC). The research focuses on preparing electrodes using nickel zinc iron oxide on stainless steel foil and evaluates single cells and stacks under varying conditions. Optimal single-cell performance is achieved at 65°C with 9 M KOH and 0.5 M urea, yielding a peak power density of 46.38 mW/cm². The stack shows improved performance at 65°C, with a power output of 0.307 kW. The single cell attains an open circuit voltage (OCV) of 0.72 V, while the stack reaches 8.8 V. The energy and exergy efficiencies are 58% and 24% at 5 M KOH for single cells, and 48% and 41% at 65°C for stack, respectively. The electrochemical impedance spectroscopy (EIS) shows impedance reduction from 30 ohm.cm^2 at 25°C to 15 ohm.cm^2 at 65°C, indicating enhanced ionic conductivity and reduced resistance. These findings provide insights for advancing DUHPFC technology.

Keywords: Direct Urea-Hydrogen Peroxide Fuel Cell; Electrodeposition; Energy Efficiency; Electrochemical Impedance Spectroscopy (EIS); Fuel Cell Performance Evaluation

AUTHOR'S DECLARATION

I hereby declare that this thesis consists of original work of which I have authored. This is a true copy of the thesis, including any required final revisions, as accepted by my examiners.

I authorize the University of Ontario Institute of Technology (Ontario Tech University) to lend this thesis to other institutions or individuals for the purpose of scholarly research. I further authorize University of Ontario Institute of Technology (Ontario Tech University) to reproduce this thesis by photocopying or by other means, in total or in part, at the request of other institutions or individuals for the purpose of scholarly research. I understand that my thesis will be made electronically available to the public.

Ayse Sinem Meke

STATEMENT OF CONTRIBUTIONS

I hereby certify that I am the sole author of this thesis and that no part of this thesis has been published or submitted for publication. I have used standard referencing practices to acknowledge ideas, research techniques, or other materials that belong to others. Furthermore, I hereby certify that I am the sole source of the creative works and/or inventive knowledge described in this thesis.

ACKNOWLEDGEMENTS

First and foremost, I want to extend my heartfelt and sincere gratitude to my supervisor, Prof. Dr. Ibrahim Dincer. His unwavering support, insightful guidance, and constant encouragement have been the backbone of my research journey. Dr. Dincer, your dedication and expertise have not only been an inspiration but also a driving force that has significantly contributed to the success of this work. I am profoundly grateful for the countless hours you've invested in mentoring me, and for always pushing me to reach my full potential. Thank you from the bottom of my heart.

I would also like to express my deepest appreciation to my parents and my sister. Mom, Dad, and my dear sister, your endless love, patience, and support have been my pillar of strength. Your belief in me has been my greatest motivation, and I am incredibly thankful for the sacrifices you've made and the encouragement you've given me throughout this journey. This accomplishment would not have been possible without you by my side.

Moreover, I wish to thank all my wonderful colleagues at the Clean Energy Research Lab. Working with such a talented and dedicated group of individuals has been a truly enriching experience. Your collaboration, insightful discussions, and camaraderie have made this journey enjoyable and rewarding. I am grateful for the stimulating environment and the support you have all provided. Special thanks to Mert Temiz, Dr. Dogan Erdemir and Dr. Aysegul Yagmur Goren Kara for their invaluable assistance and support in my research. Your help and guidance have been immensely beneficial.

TABLE OF CONTENTS

LIST OF TABLES

LIST OF FIGURES

LIST OF ABBREVIATIONS AND SYMBOLS

Nomenclature

A	area (m^2)
ex	specific exergy (kJ/kg)
E	electrode potential (V)
En	energy (kJ)
$\dot{En}$	energy rate (kW)
Ex	exergy (kJ)
$\dot{Ex}$	exergy rate (kW)
F	Faraday constant (96500 C/mol)
G	Gibbs free energy (J)
h	specific enthalpy (kJ/kg)
J	current density (A/m^2 or mA/cm^2)
J_L	limiting current density (A/m^2)
J_0	exchange current density (A/m^2)
k	thermal conductivity (W/mK)
L	inductance (H)
LHV	lower heating value (kJ)
m	mass (kg)
$\dot{m}$	mass flow rate (kg/s)
$\dot{N}$	molar flow rate (mol/s)
P	pressure (Pa or kPa)
R	resistance (ohm)
R	universal gas constant (8.314 kJ/kmol K)
s	specific entropy (kJ/kgK)
$\dot{S}$	entropy rate (kW/K)
Sh	Sherwood number (-)
t	time (seconds)
T	temperature (^oC)
V	voltage (mV or V)
Z	impedance (Ω)

Greek letters

α	transfer coefficient
δ	Nernst diffusion layer thickness
Δ	change
η	efficiency
ρ	density (kg/m^3)
π	Pi number
ϕ	angle (^{o})

Subscripts

act	activation
conc	concentration
en	energy
ex	exergy
FC	fuel cell
gen	generation
imag	imaginary part
L	inductance
ohm	ohmic
R	resistance
S	specie
sc	short circuit

Acronyms

AFCs	alkaline fuel cells
AUFCs	alkaline urea fuel cells
COP	coefficient of performance
CV	cyclic voltammetry
DUFCs	direct urea fuel cells
DUHPFC	direct urea-hydrogen peroxide fuel cells
EIS	electrochemical impedance spectroscopy
LSV	linear sweep voltammetry
MCFC	molten carbonate fuel cells

MEA	membrane electrode assembly
OCP	open circuit potential
OCV	open-circuit voltage
PAFCs	phosphoric acid fuel cells
PEMFCs	proton exchange membrane fuel cells
PEMUFCs	polymer electrolyte membrane urea fuel cells
POLRES	polarization resistance
SOFCs	solid oxide fuel cells
SOUFCs	solid oxide urea fuel cells
UOR	urea oxidation reaction
UV	ultraviolet

CHAPTER 1: INTRODUCTION

In Paris, at the coefficient of performance (COP) 21 United Nations climate change conference, it was recognized that urgent and enhanced actions are necessary to meet the goals of the Paris Agreement, which was adopted on December 12, 2015 [1]. To achieve complete elimination of carbon emissions by 2050, it is necessary for governments, businesses, and individuals to make collaborative and focused endeavors. Although the necessity for change has been acknowledged, the utilization of fossil fuels has persistently increased. In 2022, there was a 0.9% rise in worldwide carbon emissions resulting from combustion and industrial operations, with a total of 36.8 Gt [2]. This demonstrates a continued dependance on fossil fuels that needs to be broken. There is an urgent requirement for the creation of practical and cost-effective, eco-friendly fuels to substitute fossil fuels and alleviate the effects of climate change.

1.1 Current State of Energy and Shift Towards Renewable and Clean Energy

Nations throughout the world are making substantial changes to the global energy system in order to decrease their reliance on fossil fuels and address the negative impacts of climate change. For many years, coal, oil, and natural gas have been the main sources of energy, supplying consistent electricity to fulfill both industrial and household requirements. Nevertheless, the ecological consequences of utilizing fossil fuels, such as the release of greenhouse gases, contamination of the air, and the depletion of resources, have forced a global reassessment of energy approaches. In 2020, fossil fuels made up 84.3% of the world's primary energy consumption, while renewables only accounted for 5.7% [3]. To address these shortfalls, there has been a noticeable transition towards renewable and environmentally friendly energy sources. Renewable energy includes solar, wind, hydropower, geothermal, and biomass energy, all of which are obtained from natural processes that are continuously renewed. Renewable energy sources possess numerous benefits compared to fossil fuels, including diminished carbon emissions, long-term viability, and less ecological footprint. Governments, corporations, and communities are progressively allocating resources to renewable energy technology to attain energy self-sufficiency, diminish carbon emissions, and foster sustainable growth. As an example, the total amount of money invested worldwide in renewable energy was $303.5 billion in 2020, which shows the increasing dedication to using cleaner sources of energy [4]. The

utilization of solar energy has experienced significant expansion because of technological improvements and decreasing costs, achieved using photovoltaic cells and solar thermal systems. The global solar capacity in 2020 reached 707.5 GW, representing a 22% growth compared to the previous year [5]. Figure 1.1 compares actual energy sector investments in fossil fuels and clean energy for the year 2021 with projected investments for 2030, based on current trends and budget forecasts, acknowledging that these projections are made from the standpoint of 2024. In 2021, investments in fossil fuels amounted to 0.9 trillion USD, while clean energy investments were 1.3 trillion USD. By 2030, fossil fuel investments are projected to decrease to 0.5 trillion USD, whereas clean energy investments are expected to rise significantly to 4.2 trillion USD, indicating a strong shift towards renewable energy sources.

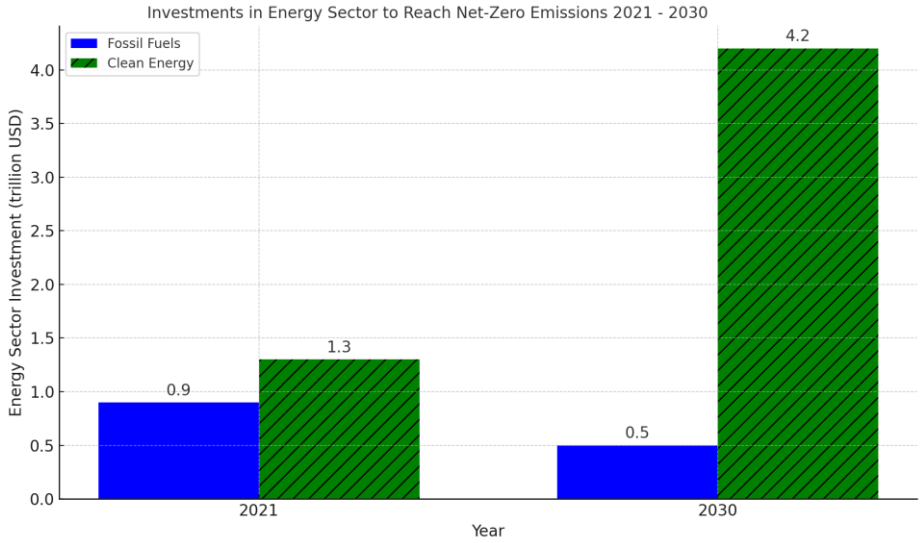

Figure 1.1 Comparison energy sector investments in fossil fuels and clean energy for the years 2021 and 2030

Wind energy, harnessed by wind turbines, has experienced significant growth, especially in areas with advantageous wind conditions. The global installed wind power capacity reached 733 GW at the end of 2020, marking a 14% increase compared to 2019 [6]. Hydroelectric power, which harnesses the energy of flowing water to generate electricity, continues to play a significant role in renewable energy. In addition, geothermal and biomass energy offer more alternatives for clean energy. The shift towards renewable energy is bolstered by global accords and domestic strategies designed to mitigate carbon emissions and advance sustainable power sources. The Paris Agreement, ratified in 2015,

is a significant treaty that brings together nations in the battle against climate change by establishing objectives for mitigating the increase in global temperatures. Countries are progressively enacting subsidies, tax incentives, and regulatory frameworks to promote the adoption of renewable energy as part of their obligations. As an illustration, the European Union has set a target of reaching a minimum of 32% renewable energy in its overall energy usage by the year 2030 [7]. There has been progress but there are still numerous obstacles to overcome to achieve widespread implementation of renewable energy. These factors include the sporadic characteristics of certain renewable sources, the requirement for significant expenditures in infrastructure, and the advancement of energy storage technologies to guarantee a consistent and dependable energy provision. Moreover, the incorporation of renewable energy into current grids necessitates the implementation of updates and creative solutions to effectively handle fluctuations and uphold the stability of the grid. By 2020, the worldwide energy storage capacity had reached 15.4 GW, indicating a significant emphasis on tackling these issues [8]. Additionally, achieving these goals will likely require infrastructure compatibility designs, ensuring that existing grid systems can accommodate the unique demands of renewable energy integration without compromising overall performance.

Ultimately, the transition to renewable and clean energy is a crucial element in worldwide endeavors to address climate change and establish sustainable energy systems. Continuous progress in technology, favorable legislation, and global collaboration are essential for overcoming obstacles and fully harnessing the promise of renewable energy. Renewable energy will have a crucial role in safeguarding the environment, fostering economic development, and maintaining energy stability as the world progresses towards a cleaner and more sustainable energy future.

Hydrogen fuel cells show up in this context as a complementing technology that works well with renewable energy systems. These fuel cells can offer a reliable and effective means of storing and using energy by transforming renewable energy sources into hydrogen, which can help with intermittency issues and improve grid resilience. Thus, investigating the possibilities of hydrogen fuel cells makes sense as we work toward a comprehensive and sustainable energy plan.

1.2 Significance of Urea as a Fuel

Urea, a molecule widely utilized in the production of fertilizers and chemicals, has recently gained attention as a potential energy carrier owing to its capacity to undergo oxidation in fuel cells. The yearly global production of urea exceeds 180 million metric tons, primarily due to its widespread use in agriculture and industrial operations [9]. The chemical structure of urea enables convenient storage and transportation, and its decomposition produces hydrogen, rendering it an appealing choice for sustainable energy solutions [9]. Studies have shown that urea can be effectively utilized in fuel cells, particularly in Direct Urea Fuel Cells (DUFCs), where it functions as an anolyte. The urea oxidation in these cells results in the production of nitrogen, carbon dioxide, and electrons, which can be utilized for power generation. Urea offers several benefits when used in fuel cells, such as its non-toxic properties, stability at normal temperatures, and the ability to utilize current infrastructure for distribution and storage [10]. Furthermore, fuel cells that utilize urea as a foundation produce fewer emissions in comparison to conventional fossil fuels. This reduction in emissions is primarily due to the absence of carbon dioxide (CO_2) production during the electrochemical reactions in urea-based fuel cells, unlike the combustion processes in fossil fuels which release significant amounts of CO_2 and other harmful pollutants. This aligns with international endeavors to decrease greenhouse gas levels and shift towards sustainable energy alternatives [11]. Multiple research projects have proved the efficacy of urea as a fuel. Urea-hydrogen peroxide fuel cells have demonstrated power densities of up to 15 mW/cm² hesitating the potential of urea in energy applications [12]. Table 1.1 shows a concise overview of the fundamental attributes of urea that render it well-suited for utilization in fuel cells:

Table 1.1 Fundamental of urea attributes of urea that render it well-suited for utilization in fuel cells

Characteristic	Value
Hydrogen content	10.1% by weight
Stability	Stable at room temperature
Toxicity	Non-toxic
Annual global production	> 180 million metric tons
Power density in DUFCs	Up to 15 mW/cm²

These properties highlight the significant role urea can play in the future energy landscape, providing a sustainable and efficient alternative to conventional fuels [13].

1.3 Challenges in Fuel Cells Utilizing Urea

Urea, having the chemical formula $CO(NH_2)_2$, poses numerous difficulties when employed as a fuel for diverse uses. The chemical stability of urea is a notable concern since it tends to undergo hydrolysis in water-based solutions. This hydrolysis process results in the formation of ammonia and carbon dioxide, which in turn decreases the concentration of urea available for reactions [14]. In addition, the electrochemical oxidation of urea is an intricate and multifaceted process that necessitates the use of effective catalysts, typically noble metals such as platinum. However, these catalysts are expensive and susceptible to being rendered ineffective by reaction intermediates, as noted by [15] in 2020. Although there have been improvements in non-precious metal catalysts, these substitutes often exhibit reduced levels of both activity and stability. Urea use can give rise to environmental concerns, including the emission of nitrogen oxides and the possibility of soil and water pollution due to inappropriate disposal [16]. The practical implementation of this project encounters obstacles such as the lack of well-established infrastructure for storing and distributing urea, as well as the requirement for substantial technological and regulatory adjustments [17]. It is essential to tackle these problems to effectively implement urea-based technology in sustainable energy systems.

1.4 Urea Production Methods

Urea production is a critical industrial process. In this part both the synthetic production of urea from ammonia and carbon dioxide, as well as innovative methods for recovering urea from wastewater is discussed [18].

1.4.1 Industrial Urea Production Methods

The industrial production of urea is carried out using various methods, primarily involving the reaction of ammonia and carbon dioxide. Table 1.2 summarizing the different methods, their reactions, and descriptions based on the literature. These methods vary in efficiency and byproducts, depending on the specific conditions and catalysts used. The choice of method not only affects the yield and purity of urea but also influences the environmental footprint and energy consumption associated with the production process. Therefore, selecting the most appropriate method is crucial for optimizing both the economic and environmental aspects of industrial urea production.

Table 1.2 Several industrial urea production methods

Method	Process Description	Key Features	Advantages	Disadvantages
Bosch-Meiser Process [19]	Involves high-pressure synthesis using ammonia and carbon dioxide	High-pressure synthesis	High conversion efficiency, well-established	High energy consumption, expensive infrastructure
Stamicarbon Process [20]	Uses a pool reactor to enhance the conversion of ammonium carbamate to urea, reducing energy consumption.	Uses a pool	Energy-efficient, high conversion rates	Complex reactor design
Snamprogetti Process [20]	Incorporates a stripper system	Incorporates a stripper system to recycle unreacted gases	High efficiency, lower energy consumption	Requires high-quality materials for stripper system
Total Recycle Process [19]	Focuses on maximizing the recycling of unreacted	Maximizes recycling of unreacted gases to improve efficiency	Minimal waste, high efficiency	High operational complexity
Montedison Process [21]	Similar to Stamicarbon but with different reactor designs and operating conditions to improve energy efficiency.	Similar to Stamicarbon	Improved energy efficiency, effective recycling	Requires specialized equipment
Concentrated Solution Process [22]	Involves multiple stages of evaporation to concentrate the urea solution before granulation.	Involves multiple stages of evaporation	Produces high-purity urea, suitable for various applications	High energy consumption, multiple stages required
Fluid Bed Granulation [23]	Produces granulated urea using a fluid bed granulator	Produces granulated urea using a fluid bed granulator	Uniform granule size, reduced dust	Initial setup cost is high, requires precise control

Urea is synthetically produced primarily through the Bosch-Meiser process, which converts ammonia and carbon dioxide at high pressure into urea. The Stamicarbon and Snamprogetti processes improve efficiency with advanced reactors and recycling systems. The total recycle and Montedison processes focus on maximizing gas recycling and energy efficiency. The concentrated solution process involves multiple evaporations for high-purity urea, while fluid bed granulation produces uniform granules. Each method has its advantages and trade-offs, suitable for different production needs based on energy use and cost.

1.4.2 Urea Production Methods from Wastewater

The utilization of wastewater for the synthesis of urea is a cutting-edge strategy that focuses on repurposing nitrogen-rich waste streams, so offering an alternative supply of urea and addressing the issue of nitrogen pollution. Multiple techniques are utilized to eliminate and retrieve urea from wastewater, each with distinct mechanisms and uses [24].

1.4.2.1 Adsorption

An established technique is adsorption, wherein wastewater is passed through a bed of adsorbent material. The urea molecules cling to the surface of the adsorbent, facilitating the collection of the treated water [25]. The adsorbent can be restored or substituted as necessary. Activated carbon, zeolites, and certain resins are commonly used as adsorbents due to their effective capacity to collect urea from wastewater.

1.4.2.2 Membrane Separation

Membrane separation is a method that use semi-permeable membranes to separate urea from water by either excluding it based on size or allowing it to pass through selectively. During this procedure, wastewater is subjected to pressure and passed across a selectively permeable membrane, which permits the passage of tiny molecules such as urea while preventing larger molecules and particles from passing through. The permeate, which is the filtered water, is gathered, while the retentate, which is the concentrated trash, is either subjected to additional treatment or disposed of. Reverse osmosis, nanofiltration, and ultrafiltration membranes are frequently employed in this procedure [26].

1.4.2.3 Biological Removal

Biological elimination utilizes microorganisms to break down urea into less complex substances, such as ammonia [27]. This process is shown in Figure 1.2. According to this figure urea-metabolizing bacteria or microbial consortia are added to a bioreactor where wastewater is injected. Commonly, this procedure employs mechanisms such as activated sludge, biofilms, or anaerobic digesters. The effluent that is produced as a result is then processed to eliminate ammonia and other impurities, rendering this technique appropriate for wastewater treatment on a wide scale.

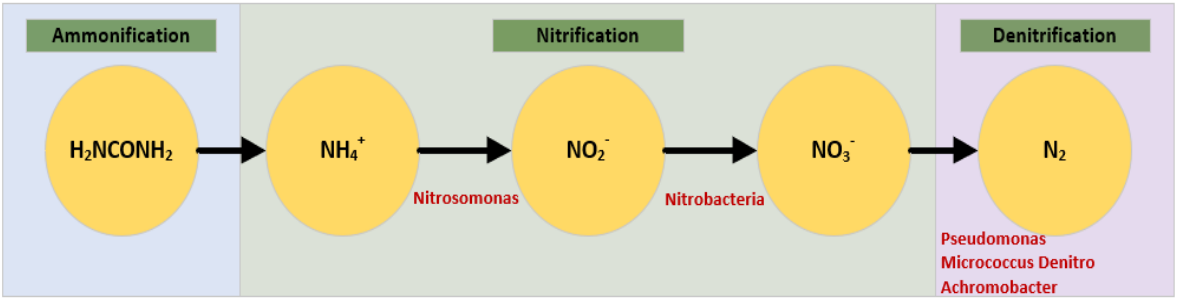

Figure 1.2 Biological removal method for urea production from wastewater

1.4.2.4 Thermal Hydrolysis

Thermal hydrolysis is a process that entails subjecting wastewater to elevated temperatures in a hydrolysis reactor, causing the decomposition of urea into ammonia and carbon dioxide. The gases produced are collected for subsequent utilization or processing. This procedure is carried out at temperatures over 100°C and is especially efficient for the treatment of effluent from ammonia facilities [28].

1.4.2.5 Enzymatic Hydrolysis

Enzymatic hydrolysis utilizes specialized enzymes, including urease, to facilitate the decomposition of urea into ammonia and carbon dioxide. Enzymes are introduced into the wastewater to expedite the hydrolysis process [29]. Subsequently, the treated water undergoes additional processing to eliminate ammonia, rendering this approach highly efficient and economically viable for applications such as hemodialysis and general wastewater treatment.

1.4.2.6 Wet Air Oxidation

Wet air oxidation is a technique in which wastewater is subjected to high pressure and temperature while being treated with oxygen or air. This process involves the oxidation of urea, resulting in the production of carbon dioxide, nitrogen gas, and water. These by-products are environmentally harmless. The typical operating conditions for this process involve temperatures ranging from 150 to 320°C and pressures ranging from 20 to 150 bar, which makes it well-suited for industrial-scale applications [30].

1.4.2.7 UV-Based Advanced Oxidation

UV-based accelerated oxidation uses ultraviolet radiation in conjunction with oxidizing chemicals such as hydrogen peroxide or ozone to break down urea [31]. This procedure entails subjecting wastewater to ultraviolet (UV) radiation, which facilitates the

decomposition of urea molecules into nitrogen gas, carbon dioxide, and water. The purified water may undergo additional purification processes to ensure the total elimination of pollutants.

1.4.2.8 Electrochemical Oxidation

Electrochemical oxidation is a process that employs an electric current to induce the oxidation of urea at the electrodes within an electrochemical cell. This process is shown in Figure 1.3. The wastewater flows through the cell, where an electric current induces the oxidation of urea at the anode, transforming it into nitrogen gas, carbon dioxide, and water. Subsequently, the effluent undergoes treatment to eliminate any residual by-products. This approach is quite effective, but it necessitates meticulous supervision of the electrolyte and electrode materials.

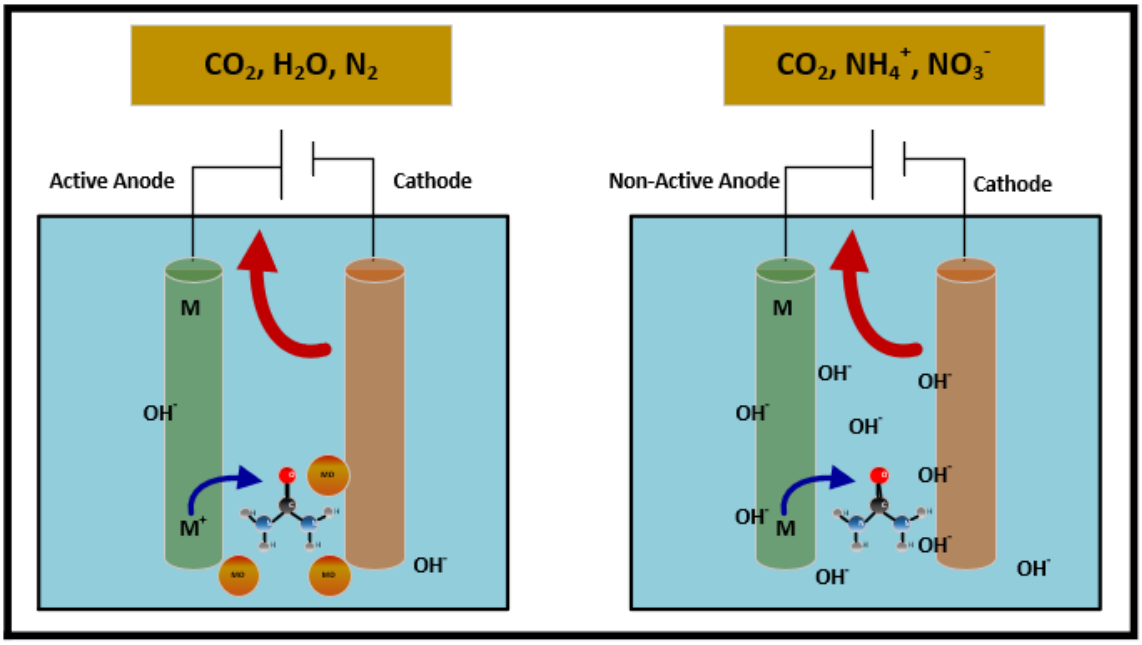

Figure 1.3 Electrochemical oxidation method for urea production from wastewater

These technologies provide diverse benefits and encounter distinct obstacles, rendering them appropriate for applications depending on their effectiveness, cost, and feasibility [32]. Integrating these technologies into wastewater treatment not only aids in controlling pollution but also facilitates the recovery of resources, thereby contributing to sustainable development.

Table 1.3 summarizes various urea production methods from wastewater, highlighting the material and energy requirements, as well as the by-products generated in

each process, providing a comparative overview of the technological approaches for effective resource recovery and pollution control.

Table 1.3 Summary of urea production methods from wastewater, detailing material and energy requirements, and by-products for each process.

Method	Material Requirement	Energy Requirement	By-product
Adsorption	Adsorbent materials (e.g., activated carbon, zeolites)	Low (mainly required for adsorption-desorption cycles)	Spent adsorbents (can be regenerated or disposed)
Membrane Separation	Semi-permeable membranes (e.g., RO, nanofiltration)	Moderate to high (for pressurizing water through membranes)	Concentrated waste stream (retentate)
Biological Removal	Microorganisms or microbial consortia	Low (requires conditions for microbial activity)	Ammonia, biomass (sludge)
Thermal Hydrolysis	Hydrolysis reactor	High (requires elevated temperatures >100°C)	Ammonia, carbon dioxide
Enzymatic Hydrolysis	Enzymes (e.g., urease)	Low to moderate (depends on the enzyme activity conditions)	Ammonia, carbon dioxide
Wet Air Oxidation	Oxygen or air, reactor	Very high (150-320°C, 20-150 bar pressure)	Carbon dioxide, nitrogen gas, water
UV-Based Advanced Oxidation	UV light source, oxidants (e.g., hydrogen peroxide)	High (for UV light generation)	Carbon dioxide, nitrogen gas, water
Electrochemical Oxidation	Electrochemical cell, electrodes, electrolyte	High (electric current for oxidation reactions)	Carbon dioxide, nitrogen gas, water

1.5 Fuel Cell Types

Fuel cells convert chemical energy directly into electrical energy through electrochemical reactions [33]. Figure 1.4 shows major fuel cell types. Each type of fuel cell operates on different principles, utilizes varying materials, and is suited for specific applications depending on the fuel source and operating conditions. The efficiency, durability, and cost of these fuel cells can vary significantly, making it essential to choose the right type based on the intended use and performance requirements. Understanding the characteristics and advantages of each fuel cell type is crucial for their effective implementation in various energy systems. In addition, advancements in fuel cell technology continue to expand the range of applications, from portable devices to large-scale power generation. Ongoing research and development are key to overcoming current limitations and enhancing the overall viability of fuel cells as a sustainable energy solution.

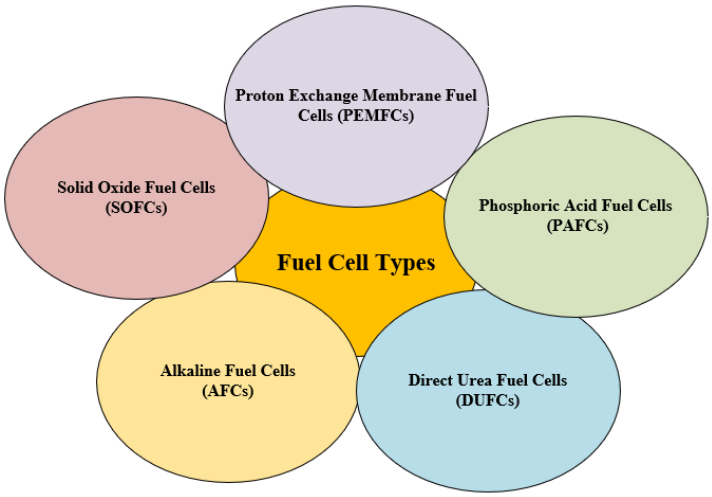

Figure 1.4 Representation of major types of fuel cells

Here are the primary types of fuel cells along with their reactions and brief descriptions.

1.5.1 Proton Exchange Membrane Fuel Cells (PEMFCs)

Uses a polymer membrane that conducts protons as the electrolyte. Renowned for its ability to operate at low temperatures and rapidly initiate. Electrochemical reactions are [34]:

Anode: $H_2 \rightarrow 2H^+ + 2e^-$ (1.1)

Cathode: $\frac{1}{2}O_2 + 2H^+ + 2e^- \rightarrow H_2O$ (1.2)

1.5.2 Solid Oxide Fuel Cells (SOFCs)

Uses a solid oxide or ceramic as the electrolyte. Operates at high temperatures (800-1000°C), allowing internal reforming of fuels [35]. SOFCs reactions are:

Anode: $H_2 + O^{2-} \rightarrow H_2O + 2e-$ (1.3)

Cathode: $\frac{1}{2}O_2 + 2e^- \rightarrow O^{2-}$ (1.4)

1.5.3 Alkaline Fuel Cells (AFCs)

Uses an alkaline electrolyte such as potassium hydroxide. Known for high efficiency and use in space applications [36]. AFCs reactions are:

Anode: $2H_2 + 4OH- \rightarrow 4H_2O + 4e^-$ (1.5)

Cathode: $O_2 + 2H_2O + 4e^- \rightarrow 4OH^-$ (1.6)

1.5.4 Phosphoric Acid Fuel Cells (PAFCs)

Uses phosphoric acid as the electrolyte. Operates at mid-range temperatures (150-200°C), suitable for stationary power generation [37]. PAFCs reactions are:

Anode: $H_2 \rightarrow 2H^+ + 2e^-$ (1.7)

Cathode: $\frac{1}{2}O_2 + 2H^+ + 2e^- \rightarrow H_2O$ (1.8)

1.5.5 Direct Urea Fuel Cells (DUFCs)

Utilizes urea as the fuel, often sourced from wastewater. Operates at moderate temperatures and offers a sustainable solution by recycling waste products [38].

Anode: $CO(NH_2)_2 + H_2O \rightarrow CO_2 + 2NH_3 + 2e^-$ (1.7)

Cathode: $O_2 + 2e^- + 2H_2O \rightarrow 4OH^-$ (1.8)

1.6 Comparison of Fuel Cell Types

Fuel cells are available in several varieties, each possessing distinct features, benefits, and uses. Table 1.4 shows a comprehensive comparison of various fuel cell types, encompassing their normal operational temperatures, efficiency, and primary applications [39].

Table 1.4 Comparison of various fuel cell types

Fuel Cell Type	Electrolyte	Operating Temperature	Efficiency (%)	Applications	Advantages	Disadvantages
Proton Exchange Membrane (PEMFC)	Proton-conducting polymer	60-100°C	40-60	Transportation, Portable Power	Quick startup, low temperature	Sensitive to fuel impurities
Solid Oxide (SOFC)	Solid oxide or ceramic	800-1000°C	45-60	Large-scale power generation, Industrial	High efficiency,	High operating temperature
Alkaline (AFC)	Potassium hydroxide	60-90°C	60-70	Space applications, Military	High efficiency, low cost,	CO_2 sensitivity
Phosphoric Acid (PAFC)	Phosphoric acid	150-200°C	40-50	Stationary power generation, CHP systems	Good tolerance to fuel impurities	Lower power density
Molten Carbonate (MCFC)	Molten carbonate salts	600-700°C	45-55	Large-scale power generation, Industrial	fuel flexibility	High operating temperature
Direct Urea (DUFC)	Alkaline medium	25-80°C	30-50	Wastewater treatment, Sustainable power sources	Utilizes waste urea	Lower efficiency

According to this table fuel cells like PEMFC, SOFC, AFC, PAFC, MCFC, and DUFC differ in electrolytes and temperatures, affecting efficiency and uses. PEMFCs (60-

100°C) are quick-start for transport; SOFCs (800-1000°C) are high-efficiency for power plants; AFCs (60-90°C) are efficient for space/military; PAFCs (150-200°C) are stable for stationary power; MCFCs (600-700°C) are efficient but corrosive for industrial use; DUFCs (25-80°C) use waste urea for sustainable power but are less efficient and still developing [39].

1.7 Fuel Cell Materials and Manufacturing

Fuel cells consist of multiple essential elements, each playing a crucial role in their operation and effectiveness. The main constituents consist of the electrolyte, electrodes (anode and cathode), and catalysts. Table 1.5 provides a concise summary of several fuel cell materials and their production methods.

Table 1.5 Summary of several fuel cell materials and their production methods

Component	PEMFC	SOFC	AFC	PAFC	MCFC	DUFC
Electrolyte	Proton-conducting polymer	Ceramic (YSZ)	Potassium hydroxide	Phosphoric acid	Molten carbonate salts	Alkaline medium
Anode Material	Platinum	Nickel-based	Platinum	Platinum	Nickel-based	Nickel-based
Cathode Material	Platinum	Perovskite or lanthanum strontium manganite (LSM)	Platinum	Platinum	Nickel-based	Nickel-based
Catalyst	Platinum	Nickel, cobalt	Platinum	Platinum	Nickel, cobalt	Nickel, cobalt

Fuel cells utilize different materials for specific applications. Proton-conducting polymer with platinum catalysts are used in PEMFCs for rapid-start transportation. Ceramic materials with nickel-based catalysts are employed in SOFCs for high-efficiency power generation. AFCs, which use potassium hydroxide and platinum, are suitable for space applications. PAFCs, which utilize phosphoric acid, provide stable stationary power. MCFCs, which employ molten carbonate and nickel-cobalt catalysts, are used in industrial settings. Finally, DUFCs, which utilize waste urea and alkaline materials, offer sustainable power generation. Manufacturing procedures like MEA, tape casting, and coating are employed to enhance the performance of each specific type [40], [41].

1.8 Motivation

Energy production and consumption have been steadily expanding worldwide over the past decades and are expected to continue to rise in the future. The ecosystem has been severely

impacted by the detrimental effects of fossil fuels, resulting in major global environmental damage, while simultaneously satisfying the increased energy requirements. Hydrogen has become recognized as a sustainable energy source and a highly promising means of storing and transporting energy. Nevertheless, the extensive utilization of hydrogen requires the creation of efficient storage methods as a result of its low density. Urea, in this particular situation, offers a promising prospect as a substance abundant in hydrogen that may be obtained from wastewater. This brings advantages in terms of both energy generation and waste disposal. The electrochemical oxidation characteristics of urea, when paired with hydrogen peroxide, offer a promising opportunity for its use in fuel cell applications. Direct Urea-Hydrogen Peroxide Fuel Cells (DUHPFCs) offer a new and eco-friendly method for utilizing urea as a fuel. DUHPFCs can utilize urea to turn waste into usable energy, which supports worldwide initiatives for sustainable development and the circular economy. DUHPFCs not only meet general energy needs, but they also contribute to specific energy production targets, like the reduction of global carbon emissions as defined in the Paris Agreement. This technology is also efficient and environmentally friendly because it complies with safety norms and regulations that are essential for renewable energy systems. This technology not only satisfies energy requirements but also aids in environmental conservation by minimizing waste and greenhouse gas emissions.

The aim of this study is to enhance and analyze the performance and efficiency of DUHPFCs. The study will investigate the electrochemical characteristics of urea when combined with hydrogen peroxide, with the goal of addressing current obstacles and improving the feasibility of DUHPFCs as an environmentally friendly energy alternative. This research aims to enhance the comprehension and implementation of DUHPFCs, with the goal of promoting the widespread use of sustainable energy technologies. Ultimately, this will help to create a future that is more sustainable and secure in terms of energy.

1.9 Objectives

While there have been studies conducted on many types of fuel cells, there has been a lack of study specifically dedicated to Direct Urea-Hydrogen Peroxide Fuel Cells (DUHPFCs). Most of the previous research has focused on traditional fuels and cell types that typically necessitate elevated operating temperatures and costly materials, hence restricting their practical utility. The electrochemical oxidation characteristics of urea, when combined

with hydrogen peroxide, present a distinct possibility for the development of fuel cells that can function optimally at moderate temperatures and employ cost-efficient materials. This work aims to create and enhance DUHPFCs as a viable and effective energy solution. The specific objectives of this study are listed below:

- To develop Direct Urea-Hydrogen Peroxide Fuel Cells (DUHPFCs) by focusing on the use of urea as the anode input and hydrogen peroxide as the cathode input. This includes the introduction of a novel nickel-based catalyst on the anode layer aimed at enhancing performance and reducing costs.
- To construct both single-cell and multi-cell stacks of DUHPFCs, incorporating the optimized membrane and electrode materials developed in the previous step. This ensures that the new designs are effectively integrated into practical fuel cell systems.
- To optimize the performance of the constructed DUHPFC systems by conducting comprehensive evaluations under varying conditions, such as different temperatures, urea concentrations, and KOH concentrations. This objective includes assessing the energy and exergy efficiencies of the systems through detailed electrochemical analyses.
- To enhance the durability and stability of DUHPFCs by identifying and mitigating factors that negatively impact long-term performance. This includes conducting parametric studies to understand the effects of different operating parameters on system performance, with the goal of improving reliability over extended periods of operation.
- To evaluate the environmental benefits and sustainability of DUHPFCs, with a focus on their potential for waste management, reduction of greenhouse gas emissions, and the feasibility of using urea derived from wastewater as a sustainable fuel source.

1.10 Novelties

There were various novelties introduced in this thesis project as part of three main integrals. Firstly, new approaches for developing and optimizing Direct Urea-Hydrogen Peroxide Fuel Cells (DUHPFCs) are established. The main innovation is the utilization of urea as a fuel source combined with hydrogen peroxide as an oxidant. The second element where

novelties are present includes the development and application of a novel nickel-based catalyst. The final component where contributions were introduced pertains to the comprehensive performance and sustainability analysis of the DUHPFCs. The novelties in the thesis are listed as follows:

- Introduction of urea as a sustainable fuel and innovative use of hydrogen peroxide as an oxidant, optimizing electrochemical reactions within DUHPFCs to achieve higher efficiency at moderate temperatures.
- Development of a novel nickel-based catalyst applied to the anode, significantly enhancing urea oxidation and improving the overall performance and efficiency of DUHPFC systems.
- Design, construction, and systematic performance assessment of single-cell and multi-cell DUHPFC stacks, providing insights into optimal operating conditions and contributing to the practical application of these fuel cells.
- Comprehensive energy, exergy, and electrochemical analyses, along with parametric studies, guide the enhancement of efficiency and reliability in DUHPFC systems, supporting their broader implementation in sustainable energy solutions.

These contributions provide valuable advancements in the field of fuel cell technology, offering new perspectives on how DUHPFCs can be developed and optimized for better performance and sustainability. The outcomes of this research highlight the potential of DUHPFCs for practical applications and lay the groundwork for future studies to further refine and enhance these systems. Additionally, the methodologies and findings from this thesis may serve as a useful reference for ongoing research in sustainable energy solutions. Moreover, the insights gained from this work could inspire the exploration of novel materials and configurations, potentially leading to breakthroughs that further increase the efficiency and adaptability of DUHPFC technology. As the demand for clean energy continues to grow, the relevance of these findings in contributing to a more sustainable energy future cannot be overstated.

CHAPTER 2: BACKGROUND AND LITERATURE REVIEW

In this chapter background and literature review of the research study are discussed.

2.1 Background Information

Comprehending the background and technological underpinnings of DUHPFCs is essential for recognizing their potential and tackling their obstacles. This section offers a comprehensive examination of the fundamental ideas, technologies, and approaches associated with DUHPFCs. We shall examine the diverse classifications of urea fuel cells, elucidate their operational principles, and analyze the significant operating parameters that impact their efficiency. This extensive background provides the foundation for the following examination and advancement of DUHPFC technologies, with the goal of enhancing their utilization in sustainable energy generation.

2.1.1 Direct Urea Fuel Cell (DUFC)

Direct Urea Fuel Cells (DUFCs) are a novel method of producing environmentally friendly electricity by using urea as a fuel. Urea, a molecule abundant in nitrogen, which is frequently present in wastewater and agricultural runoff, presents a viable and economical substitute for conventional hydrogen-powered fuel cells. The primary function of a DUFC entails the electrochemical process of oxidizing urea at the anode, resulting in the release of electrons and protons. Simultaneously, oxygen reduction takes place at the cathode, producing electricity, water, and nitrogen as by-products [42]. The chemical reactions of a DUFC can be summarized in the following manner:

Overall Reaction: $CO(NH_2)_2+O_2 \rightarrow CO_2+N_2+2H_2O$ (2.1)

Direct Urea Fuel Cells (DUFCs) produce environmentally friendly electricity by the oxidation of urea, a readily available and inexpensive material commonly present in wastewater. This process generates power, water, and nitrogen, providing benefits such as waste management and decreased emissions of greenhouse gases. Dual-use fuel cells (DUFCs) function effectively at moderate temperatures, rendering them well-suited for use in portable power and decentralized energy systems. Nevertheless, DUFCs encounter obstacles such as enhancing catalysts, handling ammonia by-products, and guaranteeing long-term durability. The research is centered on enhancing these areas using nickel-based catalysts and the integration of DUFCs with wastewater treatment processes, in order to improve sustainability. Additionally, there are a number of benefits that DUFCs have over

traditional fuel cells, such as the use of a widely accessible and affordable fuel, the ability to integrate with wastewater treatment systems, and a decrease in harmful emissions. Because of these advantages, DUFC technology is a promising means of producing sustainable energy.

2.1.2 Urea Fuel Cell Types

Urea fuel cells are a potential technique for generating sustainable energy by using urea as a fuel. Various variants of urea fuel cells have been created to enhance efficiency and meet specific requirements of different applications [43]. Table 2.1 represents a tabular overview outlining the primary categories of urea fuel cells, their notable characteristics, and practical uses, followed by a concise elucidation.

Table 2.1 Representation of urea fuel cell types

Fuel Cell Type	Electrolyte	Operating Temperature	Key Features	Applications
Direct Urea Fuel Cells (DUFCs)	Various	Moderate	Uses urea directly, eco-friendly, cost-effective	Portable power, decentralized energy systems
Alkaline Urea Fuel Cells (AUFCs)	Potassium hydroxide (KOH)	Moderate	High efficiency, non-noble metal catalysts	Industrial applications, waste treatment
Urea-Hydrogen Peroxide Fuel Cells (UHPFCs)	Various	Moderate	Uses hydrogen peroxide, high efficiency	Applications requiring high power densities
Solid Oxide Urea Fuel Cells (SOUFCs)	Solid oxide/ceramic	High (600-1000°C)	High efficiency, fuel flexibility	Large-scale, stationary power generation
Polymer Electrolyte Membrane Urea Fuel Cells (PEMUFCs)	Proton-conducting polymer	Low (60-100°C)	Compact design, quick startup	Portable and small-scale applications

The table highlights the different types of urea fuel cells, each with unique advantages and applications. DUFCs and AUFCs are efficient at moderate temperatures with cost-effective catalysts, ideal for decentralized and industrial uses. UHPFCs, using hydrogen peroxide, offer high efficiency and power density for high-demand applications. SOUFCs provide high efficiency for large-scale power generation but require high temperatures [44]. PEMUFCs are compact and quick-starting, suitable for portable applications. Continued research is essential to optimize these technologies and expand their practical applications.

2.1.3 Working Principles of Direct Urea-Hydrogen Peroxide Fuel Cell (DUHPFC)

Direct Urea-Hydrogen Peroxide Fuel Cells (DUHPFCs) function by using urea as the fuel at the anode and hydrogen peroxide as the oxidant at the cathode. This combination synergistically boosts the electrochemical reactions, hence optimizing the overall efficiency and energy output of the fuel cell. Figure 2.1 illustrates the working principles of DUHPFCs with different configurations of cation and anion exchange membranes.

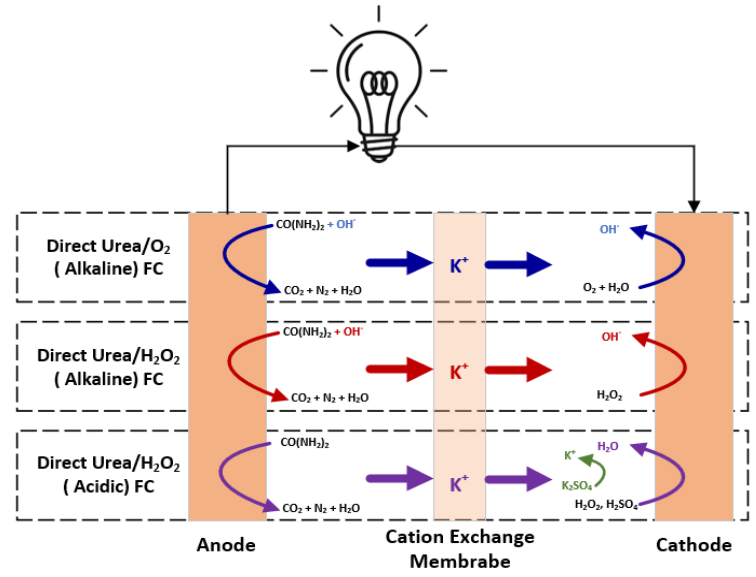

(a)

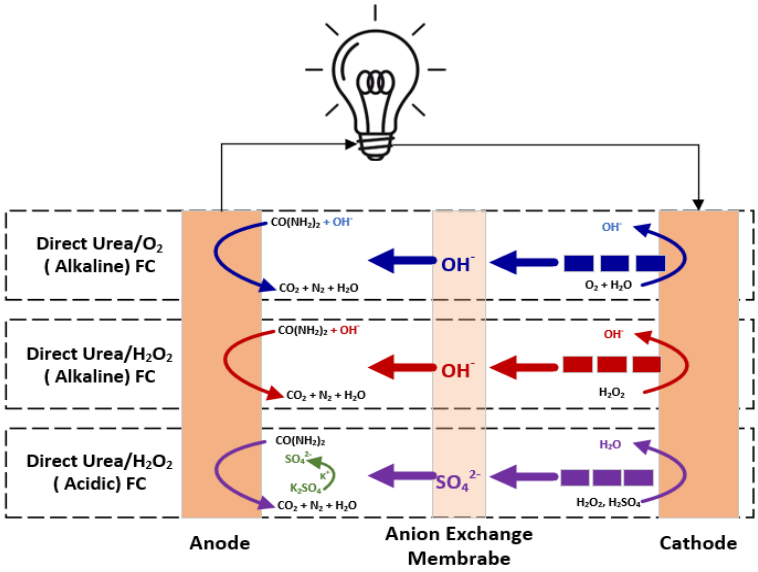

(b)

Figure 2.1 Illustration of the working principles of DUHPFCs (a) with cation exchange membrane (b) with anion exchange membrane configurations

The left side displays designs with cation exchange membranes, through which potassium ions (K^+) traverse to maintain charge equilibrium. The first row displays a Direct Urea/O_2 (alkaline) fuel cell, the second row exhibits a Direct Urea/H_2O_2 (alkaline) fuel cell, and the third row portrays a Direct Urea/ H_2O_2 (acidic) fuel cell. The by-products and efficiency of each arrangement differ depending on the specific electrolyte and membrane employed. The picture on the right illustrates configurations including anion exchange membranes, through which hydroxide ions (OH^-) or sulfate ions (SO_4^{2-}) can pass. The reactions and ion movements exhibit similarities, however, the precise ions engaged vary depending on the kind of membrane used. Through the optimization of membrane type and efficient management of reactants, DUHPFCs have the potential to attain high efficiency and energy output, positioning them as a promising technology for sustainable energy production. This figure demonstrates the versatility and adaptability of DUHPFCs in diverse chemical conditions, showcasing their potential for a wide range of applications depending on unique system needs [45].

2.1.4 Important Operating Parameters for Electricity Production in DUHPFC

To achieve optimal performance in Direct Urea-Hydrogen Peroxide Fuel Cells (DUHPFCs), it is necessary to effectively control and monitor certain critical operational parameters. The fuel cell's power production and efficiency are substantially influenced by the concentration of urea and hydrogen peroxide, requiring appropriate amounts to achieve a balance between performance and safety. The operating temperature is a critical factor that affects both the reaction rates and the thermal stability of cell materials. The selection of electrolyte, whether it is alkaline or acidic, has an impact on the transportation of ions and the overall efficiency. Similarly, the choice of ion exchange membrane, whether it is cation or anion, impacts the specific mechanism of ion transport and the by-products produced. Nickel-based catalysts are crucial for effective urea oxidation, and current research aims to enhance their durability and performance. Furthermore, it is crucial to meticulously regulate the flow rates of urea and hydrogen peroxide to avoid insufficient fuel supply and maintain a steady power output. Through the optimization of these parameters, DUHPFCs have the potential to attain elevated efficiency and dependable electricity generation, positioning them as a promising technology for sustainable energy solutions [46].

Building on the importance of these operating parameters, a deeper exploration of each factor's influence on DUHPFC performance provides valuable insights into optimizing this technology for practical applications. Both batteries and fuel cells have benefits over one another. Batteries are more energy dense and efficient, which makes them perfect for portable devices and short-term uses. On the other hand, batteries lose capacity over time and need more time to recharge. While they usually have lesser efficiency and require a constant fuel supply, fuel cells, on the other hand, offer stable power output and quick refilling capabilities, making them suited for long-duration applications like transportation and backup power. The requirements of the application, such as the length of operation, the influence on the environment, and the requirement for rapid refilling or charging, will determine which option is best.

2.2 Literature Review

Each year, global energy demands continue to rise, even though most energy generation still relies on fossil fuels [47]. Hence, it is imperative to explore additional options for clean, eco-friendly, and affordable energy sources. The utilization of wastewater as a viable energy source has garnered significant interest due to two primary issues: the need for energy and the treatment of wastewater, both of which may be effectively addressed. An arduous endeavor involves utilizing urine as a source of fuel in direct urea fuel cells (DUFCs) [48,49,50,51]. Urea, which is commonly present in wastewater, is an organic substance composed of carbon, hydrogen, and oxygen. The hydrogen content in urea is around 6.67 weight percent. Thus, urea, which is present at a concentration of around 2-2.5% by weight in wastewater (urine), is considered a suitable feedstock for direct urea fuel cells (DUFC) in an alkaline environment [52]. Urea is an energy source with favorable attributes. It has a high energy density of 16.9 MJ L^{-1}, which is ten times greater than hydrogen. Additionally, urea is safe and suitable for transportation, as it is non-flammable and non-toxic [53]. Conversely, a fuel cell is a highly efficient device that converts fuel energy into electricity through electrochemical processes [54]. Several varieties of fuel cells have been documented. In addition to the widely used proton exchange membrane fuel cell (PEMFC), there are several more types of fuel cells available. These include the solid oxide fuel cell (SOFC), the molten carbonate fuel cell (MCFC), the alkaline fuel cell, and urea fuel cell. The DUFC technique is a promising and efficient

approach for generating energy using urea, urine, and wastewater as fuel sources [55]. This device utilizes electrochemical oxidation of urea or urine to generate carbon dioxide, nitrogen gas, water, and energy. Oxygen is essential for carrying out oxidation reactions. It is well-established that H_2O_2 can serve as a substitute for O_2 due to its ability to offer a significantly greater electrode potential, approximately twice as high, in an alkaline environment [56]. In addition, the direct urea/H_2O_2 fuel cell has a more condensed structure due to the fact that urea and H_2O_2 are in their liquid forms [57]. The reaction that occurred is largely analogous, except for using H_2O_2 at the cathode, which consequently affects the overall reactions.

Cathode: $3H_2O_2+6H^++6e^- \rightarrow 6H_2O$, E0=1.763V (vs SHE) (2.2)

Overall: $CO(NH_2)_2+3H_2O_2+6H^++8OH^- \rightarrow CO_2^{-3}+ N_2+12H_2O$, E0=−0.40V (vs SHE) (2.3)

Figure 2.2 depicts the standard schematic diagram of DUFCs. The cathode catalyst facilitates the electrochemical reduction reaction of O_2 or H_2O_2 in the cathode chamber, resulting in the production of OH^- ions. These ions then pass via the anion exchange membrane to reach the anode chamber. Within this enclosure, the OH^- ions undergo a chemical reaction with urea, resulting in the release of electrons. These electrons are subsequently transmitted to the cathode through the external circuit, generating electricity.

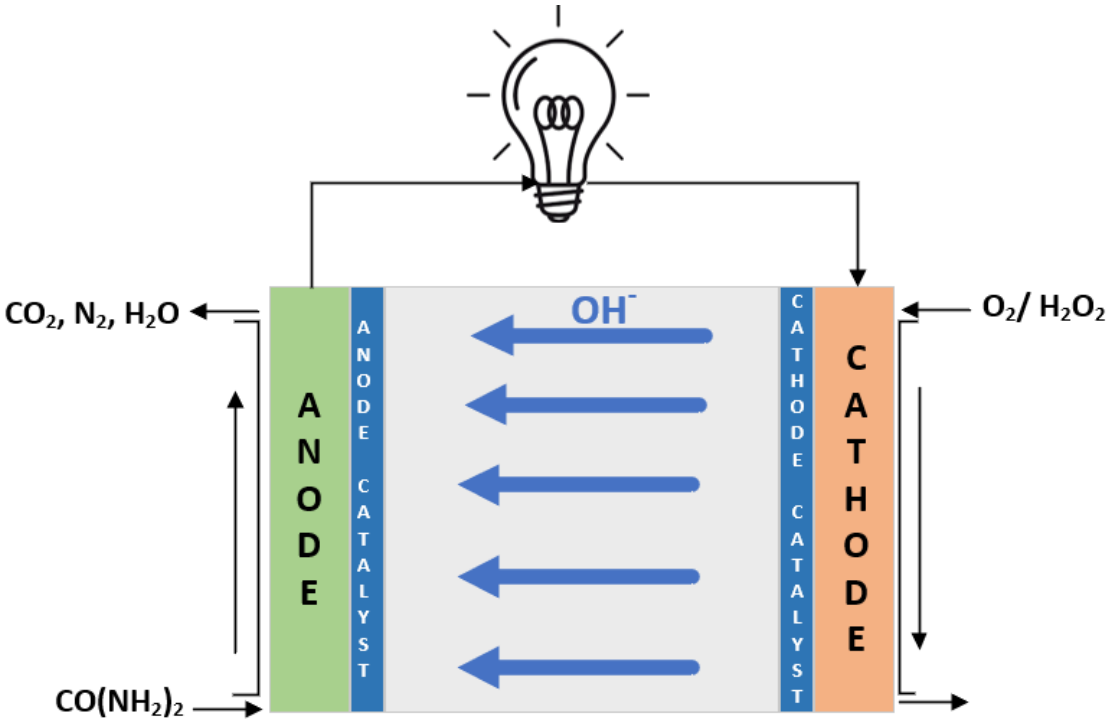

Figure 2.2 Schematic diagram of DUFC

The investigation into the utilization of urea for electricity production began in 1973, employing platinum as the electrodes for both the anode and cathode. An anion exchange membrane was used to separate the anode and cathode chambers. The examination determined that urea has the potential to undergo oxidation, resulting in the formation of carbon dioxide, nitrogen gas, and water. However, additional research and refinement are required to fully understand and optimize this process. In 2010, Lan et al. [58] conducted a study on the use of urea, urine, and AdBlue (a 32.5% urea aqueous solution) as fuels for DUFCs. An analysis was conducted to compare the anode materials Pt and Ni/C, while using Ag/C and MnO_2/C as the cathode materials. At an operating temperature of 50°C, the maximum power density achieved was 1.7 mW cm^{-2} using Ni/C as the anode and MnO_2/C as the cathode. The fuel used was a 1 M solution of urea. Thus far, researchers have explored the creation of anode catalysts for DUFCs with the aim of optimizing the power density of these fuel cells. Various catalysts, both noble and non-noble metals, have been investigated to improve the efficiency of this fuel cell.

This chapter provides a summary of the current advancements in technology, focusing specifically on the utilization of supporting anode catalysts and their impact on the performance of DUFCs. The text included a detailed discussion of the benefits and drawbacks of catalysts, as well as a comprehensive method for improving their fabrication.

Furthermore, an examination of the impacts of external factors, as well as the obstacles and potential opportunities, is conducted to optimize performance.

2.2.1 Mechanism of Urea Electro-Oxidation

Urea can be oxidized in alkaline, neutral, or acidic environments, leading to the formation of nitrogen gas (N_2) and carbon dioxide (CO_2). However, differences in the responsiveness of final products and intermediate products may be found in various pH supporting electrolytes. Figure 2.3 shows the Schematic diagram of the urea molecule. This figure provides a clear representation of the molecular structure, highlighting the arrangement of atoms within the urea molecule. Understanding this structure is crucial for analyzing its behavior in electrochemical reactions within the fuel cell.

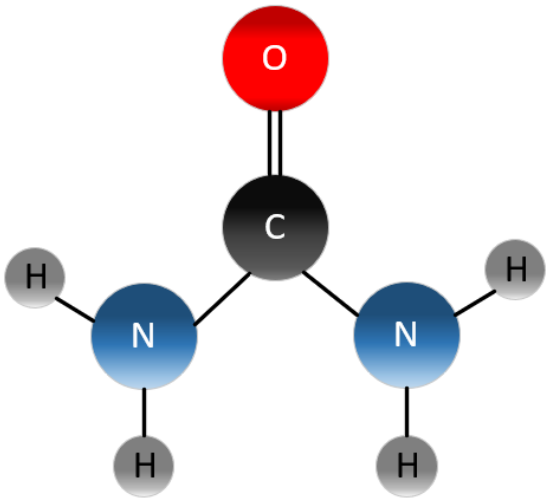

Figure 2.3 Schematic diagram of the urea molecule

2.2.1.1 Neutral Medium Mechanism

In a neutral medium, for example, NaCl solution as the electrolyte, Cl^- is oxidized into Cl_2 which is disproportionated in aqueous solution to form HOCl. HOCl will be reduced back to Cl^-, while urea is electro-oxidized according to the following reactions [59]:

$$6Cl^- \rightarrow 3Cl_2 + 6e^- \quad (2.4)$$

$$3Cl_2 + 3H_2O \rightarrow 3HOCl + 3H^+ + 3Cl^- \quad (2.5)$$

$$3HOCl + 3CO(NH_2)_2 \rightarrow N_2 + CO_2 + 3H^+ + 3Cl^- + 2H_2O \quad (2.6)$$

$$\text{Overall reaction: } CO(NH_2)_2 + H_2O \rightarrow N_2 + CO_2 + 6H^+ + 6e^- \quad (2.7)$$

In this circumstance, the generation of H^+ occurs. Therefore, an anode catalyst that is resistant to acid is required, such as RuO_2 and IrO_2. The study documented the effective oxidation of urea into CO_2 and N_2 using a titanium electrode covered with RuO_2-TiO_2 [59].

2.2.1.2 Alkaline Medium Mechanism

When urea is exposed to an alkaline environment, it can be inexpensively electro-oxidized by utilizing nickel as the catalyst. Moreover, studies suggest that using Ni metal, nickel hydroxides, or Ni composites as the catalyst produces better outcomes in urea electro-oxidation compared to other noble metal catalysts such as Pt, Pt-Ir, and so on. It is feasible to get reduced oxidation potentials and increased current densities. Guo et al. [60] investigate the electro-oxidation of urea in an alkaline solution using electrochemical impedance spectroscopy (EIS). The researchers conducted a study to explore the impact of polarization potential and KOH concentration on impedance. Nyquist plots display two

depressed semicircles: one remains constant in the first quadrant at higher frequencies, while the other oscillates between the first and second quadrants at lower frequencies in response to variations in polarization potential. The work uncovers both indirect and direct routes in the urea electro-oxidation cycle. The occurrence of the reverse loop in Nyquist plots is ascribed to the detrimental effect of CO_2 poisoning on the catalyst, which has been confirmed through the use of chronoamperometry. The rate-limiting stages of urea electro-oxidation are contingent upon the concentration of KOH.

Electro-oxidation of urea by Ni catalyst in alkaline medium is proposed to occur in two possible mechanisms, including indirect mechanism and direct mechanism. The indirect mechanism, which is the most used explanation for urea electro-oxidation, involves NiOOH as the active catalyst. In this mechanism, NiOOH, formed from the electro-oxidation of $Ni(OH)_2$, oxidizes urea molecules and is subsequently reduced back to $Ni(OH)_2$. NiOOH formed from the electro-oxidation of Ni $(OH)_2$ oxidizes the urea molecules and is reduced back to $Ni(OH)_2$ according to the following equation:

$$CO(NH_2)_{2(aq)}+6OH^- \rightarrow N_2(g)+5H_2O(l)+CO_2(g)+6e^- \quad (2.8)$$

In the direct mechanism, urea is oxidized by Ni in the form of NiOOH which is not reduced back to the Ni $(OH)_2$ form. The oxidation process will use OH^- and the NiOOH will be reduced at the reverse scan.

Botte et al. conducted a study on the process of urea degradation through electro-oxidation using DFT computation [61]. The electrophilic atoms of urea established many plausible processes by interacting with the nucleophilic atoms of NiOOH and undergoing reversal. The formation of NiOOH as the active catalyst occurs through the interaction of Ni atoms with N and O in urea, while the bridging O interacts with the C atom in urea.

Cyclic voltammetry can be used to explain the electro-oxidation process of urea. Vedharathinam and Botte conducted a study on the electro-oxidation of urea using a cyclic voltammogram at a nickel electrode in a potassium hydroxide solution with a concentration of 5 M. The experiment was conducted both with and without the presence of urea [62]. In the absence of urea, the cyclic voltammogram exhibits a redox peak in both the anodic and cathodic areas at 387 and 260 mV, respectively. This indicates the occurrence of a redox process involving Ni^{2+}/Ni^{3+}. Upon the addition of urea to the electrolyte solution, there is a noticeable rise in the current density at the oxidation potential of around 0.35 V (versus

Hg/HgO). This indicates that the process of urea electro-oxidation has taken place on the surface of the nickel electrode. In their study, Yan et al. [63] observed the same phenomenon of urea electro-oxidation in Ni-Co hydroxide electrodes. This was demonstrated through the cyclic voltammograms of the Ni-Co hydroxide electrodes under the same conditions as the previous experiment. An oxidation peak is detected at a potential of 0.42 V, which suggests the conversion of Ni $(OH)_2$ into NiOOH. An intense oxidation current commences at a potential of 0.40 V in the presence of urea. The observed potential is analogous to the potential formation of NiOOH, suggesting that NiOOH serves as the catalytically active form for the oxidation of urea.

Table 2.2 displays the performance of different anode catalysts in the process of urea electro-oxidation [65].

Table 2.2 Investigation of the performance of several anode catalysts in the electro-oxidation of urea

Anode catalysts	**Preparation methods**	**Electrolytes**	**Onset potential**	**Anodic peak**	**Current density, $mAcm^{-2}$**
Ni NPs/Ti rod	Electrodeposition	0.3 M urea in 5 M KOH	0.35 V vs Hg/HgO	0.46 V vs Hg/HgO	>90
Ni/carbon sponge	Electrodeposition	0.1 M urea in 1 M NaOH	0.40 V vs Hg/HgO	0.52 V vs Hg/HgO	>50
Ni-decorated graphene	Calcination	2.0 M urea in 1 M KOH	0.35 V vs Hg/HgO	0.59 V vs Hg/HgO	~80
Ni NPs/commercial carbon paper	Pulsed laser deposition	0.3 M urea in 1 M KOH	0.25 V vs SCE	0.55 V vs MMO	4.8
Ni-WC/MWCNT	Impregnation	0.3 M urea + 1 M KOH	0.45 V vs Hg/HgO	0.55 V vs Hg/HgO	200
Ni-Mn/MWCNT	Electrodeposition	0.3 M urea + 1 M KOH	0.45 V vs Hg/HgO	0.55 V vs Hg/HgO	85
CB@ds-Ni	Electrodeposition	0.3 M urea + 1 M KOH	0.45 V vs Hg/HgO	0.58 V vs Hg/HgO	13
NiCo LDH/NiCo(OH)2	Solution methods at room temp.	0.3 M urea + 1 M KOH	0.25 V vs SCE	0.56 V vs Hg/HgO	300
NiO/graphite	Chemical precipitation	0.3 M urea + 0.5 M KOH	0.57 V vs SCE	0.57 V vs SCE	30.94
NiO/GC	Electrodeposition	0.3 M urea + 0.5 M KOH	0.30 V vs Ag/AgCl	0.57 V vs Ag/AgCl	150
Ultrafine NiO nanoparticles/GC	Electrochemical deposition	0.3 M urea + 1 M KOH	0.25 V vs Ag/AgCl	0.57 V vs Ag/AgCl	300
Ni-Co hydroxide/Ti foil	Electrodeposition	0.3 M urea + 1 M KOH	0.35 V vs Hg/HgO	0.55 V vs Hg/HgO	~160
Ni-Co NWAs	Galvanostatic electrodeposition	1 M urea in 3 M KOH	0.20 V vs Hg/HgO	0.45 V vs Hg/HgO	280
Ni-Zn-Co/Ti foil	Electrodeposition, alkaline leaching	0.3 M urea in 1 M KOH	0.45 V vs Ag/AgCl	0.55 V vs Ag/AgCl	560

2.2.1.3 Effect of KOH Concentration in The Anolyte Solution

According to a report, using KOH as the electrolyte in the electrochemical oxidation of urea has been found to offer superior performance compared to LiOH and NaOH. This is evident in terms of a lower onset potential and a larger current density. The activity of urea oxidation follows the order of LiOH < NaOH < KOH [65]. The presence of $PtOH^{-}M^{+}$ (H_2O) x at the interface reduces the hydration energy of alkali metals and hinders the active sites. This inhibition occurs in the following order: $Li^{+} > Na^{+} > K^{+}$. Higher concentrations of KOH have been found to enhance the current density of urea oxidation. Increasing the concentration of KOH leads to a decrease in the onset potential of urea oxidation and a simultaneous increase in current density. This is due to the substantial impact of OH^{-} on the growth of NiOOH.

2.2.1.4 Effect of Urea Concentration

In addition to altering the concentration of KOH, researchers have also examined the impact of modifying the content of urea. Experimental evidence demonstrates that an elevation in urea concentration directly corresponds to an increase in the oxidation peak of urea. The reason for this could be the presence of sufficient urea for the oxidation process. According to the research, when the concentration exceeds 0.2 M, the current density decreases because the catalyst surface becomes covered with urea molecules. This coverage reduces the rate of urea oxidation by depriving the reaction of OH^{-} ions, which is a limitation imposed by the kinetics of the reaction [47].

2.2.2 Progress of Anode Catalyst For DUFC

The incorporation of anode catalyst in a direct urea fuel cell (DUFC) significantly influences the outcome by enhancing power density and improving the electrical efficiency of the DUFC. There are several methods to enhance the performance of DUFC. These include augmenting the number of active sites on the catalyst's surface, raising the open circuit voltage (OCV) by employing oxidants, and, most significantly, advancing the anode catalyst of DUFC. Traditionally, noble metal catalysts including Ti/Pt, Ti/(Pt-Ir), and Ti/RuO_2 [45] have been employed as anode catalysts in DUFC. However, these catalysts have shown themselves to be ineffective and expensive. Alternatively, it has been claimed that utilizing a cost-effective catalyst made from a non-noble metal as the anode catalyst in a urea fuel cell yields a remarkably efficient outcome in DUFC. Nickel, in the form of

NiOOH, has been identified as a highly effective catalyst for the electro-oxidation of urea, and has the potential to enhance the electrical efficiency of DUFC. There are multiple methods to enhance the reactivity of nickel, including the creation of different structures of nickel, employing catalysts with a large surface area, and combining nickel with diverse metals.

2.2.3 DUFC Performances

The Direct Urea Fuel Cell is a highly promising renewable energy option that efficiently generates electricity by utilizing waste materials. DUFC is advantageous since it utilizes urea-containing wastewater, unlike PEMFC which relies on hydrogen. Although hydrogen is considered a clean energy source, it encounters obstacles in terms of manufacturing, storage, and transportation, which impede its widespread use. On the other hand, DUFC, which relies on urea as its energy source, provides convenient storage and transportation, is not harmful, and can make use of the plentiful urea present in human and animal urine as well as industrial effluent. The crucial factor in achieving high electricity production in DUFC is the urea electro-oxidation process, which requires improvements in anode catalysts to boost their catalytic activity. The DUFC configuration closely resembles that of traditional fuel cells, typically consisting of a dual-chamber cell with an anode and a cathode chamber that are divided by an ion exchange membrane. The catalysts in each chamber serve as both the working and counter electrodes. DUFC applications commonly employ a flow cell configuration. Li et al. [66] aimed to develop a novel catalyst for urea oxidation and test a stacked membraneless direct urea fuel cell (DUFC) using raw urine as fuel. They synthesized molybdenum nickel phosphides on nickel foam (MoNiP/NF) through a combined hydrothermal and phosphating method. Among the various catalysts tested, the honeycomb-like MoNiP/NF catalyst with a Mo/Ni molar ratio of 0.50 (MoNiP/NF-0.50) exhibited the highest electrocatalytic activity for urea oxidation. The researchers constructed a stacked membraneless DUFC using the MoNiP/NF-0.50 electrode as the anode and a gas diffusion cathode. With an electrode spacing of 5 mm and 6 electrode pairs, the cell achieved a maximum voltage of 0.55 V and a power density of 0.115 mW cm^{-2} at an external resistance of 1000 Ω. This performance represented a power output 5.32 times higher than that of an individual membraneless DUFC. Additionally, the urea removal efficiency reached 65.8% at an external resistance of 100 Ω within 192 hours.

The impressive performance of the DUFC is attributed to the high catalytic activity of the MoNiP/NF-0.50 catalyst, reduced electrode spacing, and the use of multiple electrode pairs. These findings suggest a promising potential for scalable DUFC applications with efficient urine treatment.

In another study, Wang et al. [67] focused on addressing the sluggish kinetics of the urea oxidation reaction (UOR), which significantly limits the efficiency of direct urea fuel cells (DUFCs) using urea/urine-containing electrolytes. In their study, they prepared copper and nickel-based composite oxides by meticulously controlling the galvanic reaction of copper ions with metallic nickel, followed by a high-temperature oxidation process. Through systematic electrochemical characterization, they optimized the nano-architectures for UOR performance, achieving a low potential of 1.39 V vs. RHE to drive a current density of 100 mA cm^{-2} in alkaline solution. The button-like DUFCs constructed with these catalysts demonstrated a maximum power density of 1.19 mW cm^{-2}. Moreover, the DUFCs assembled with bio-urine from humans, dogs, cats, and rats, used as electrolytes without further purification, showed comparable voltage performance. These results indicate a promising direction for converting bio-waste into valuable energy sources.

The DUFC exhibits significant potential as a substitute for fossil fuels in the production of energy, however additional refinement is required. The catalysts in both the cathode and anode play a crucial role in this system, with the anode requiring a significant surface area to ensure effective interaction with urea. It is crucial to improve the surface area and corrosion resistance of the anode catalyst. Additionally, utilizing H_2O_2 in an acidic environment at the cathode is necessary to get better performance. Anion exchange membranes are essential, but they must possess both stability and high anionic conductivity. Assessing the efficacy of a catalyst through the utilization of electrochemical impedance spectroscopy is crucial to comprehend its resistance prior to implementation. Conducting stability tests and utilizing authentic wastewater samples, such as urine and industrial waste, are essential for practical implementation. Once optimized, DUFCs have the potential to substitute fossil fuels and offer efficient solutions for wastewater treatment and electricity generation.

2.3 Gaps in the Literature

Further research is necessary due to many gaps in the present literature about the promising potential of Direct urea fuel cells as an alternative energy source. Although progress has been achieved in the field of catalyst creation, there is a lack of thorough investigations into their enduring stability and effectiveness in actual operational circumstances. In addition, most research utilizes synthetic urea solutions instead of actual wastewater, which contains contaminants that may impact the efficiency of cells. Further research is needed to examine the stability and effectiveness of anion exchange membranes, as well as determine the best conditions for integrating H_2O_2 cathode electrolytes. The potential of electrochemical impedance spectroscopy (EIS) investigation to comprehend resistance and conductivity in catalyst systems has not been fully utilized. In this study, the development of a Direct Urea-Hydrogen Peroxide Fuel Cell (DUHPFC) are comprehensively investigated. The research focuses on the electrode preparation, specifically the electrodeposition of nickel zinc iron oxide onto stainless steel foil and evaluates the performance of single cells and fuel cell stacks under varying conditions. This study addresses several gaps in the current literature by optimizing electrode materials and configurations for DUHPFCs, which have been underexplored despite the high potential of urea as a fuel source due to its nitrogen content and availability. Additionally, the research examines the optimal operating conditions, including temperature and KOH concentration, to enhance efficiency and stability, areas often overlooked in previous studies. By providing insights into the electrochemical processes involved in urea oxidation and hydrogen peroxide reduction, the study aims to improve the practical application of DUHPFCs and lays the groundwork for future research in sustainable energy technologies. The outcomes of this research not only contribute to the advancement of DUHPFC technology but also offer a foundation for the development of more efficient and durable energy systems that can utilize low-cost and readily available fuels. Furthermore, the methodologies employed in this study can be adapted and applied to other emerging fuel cell technologies, potentially leading to broader impacts across the field of renewable energy.

CHAPTER 3: EXPERIMENTAL APPARATUS AND PROCEDURE

This chapter entails the description of the experimental procedures conducted and the apparatus utilized. A detailed description of each piece of equipment used is included. The experimental methodology followed is also discussed, outlining the steps taken from the preparation of the anode electrode to the parametric tests and performance evaluations of the single cell and fuel cell stack.

3.1 Electrode Preparation and Coating Techniques

The process of preparing and coating electrodes is crucial in the development of high-performing fuel cells, as it guarantees that the electrodes possess the required qualities for maximum efficiency. These approaches encompass a range of processes used to prepare and apply coatings to electrodes, with the aim of improving their electrochemical properties. Electrode preparation and coating for DUHPFC systems commonly employ techniques such as chemical vapor deposition (CVD), physical vapor deposition (PVD), and electrochemical deposition. The selection of these procedures is based on the required characteristics of the electrodes, such as conductivity, stability, and catalytic activity [68]. The anode electrode in this investigation was constructed using stainless steel foil as the substrate. An electro-deposition process was used to coat the stainless-steel foil with nickel zinc iron oxide. The selection of this approach was based on its capacity to provide a consistent and cohesive coating, which is crucial for the optimal functioning of the DUHPFC.

3.1.1 Electrode Selection for Anode Layer

The selection of the appropriate material for the anode layer is crucial in the development of efficient DUHPFC systems. The chosen material must possess outstanding electrical conductivity, corrosion resistance, superior mechanical strength, and surface characteristics that provide effective catalyst support. The study utilized stainless steel foil as the substrate for the anode layer, which was then coated with nickel zinc iron oxide by an electro-deposition method. The choice of stainless-steel foil was made after considering several compelling factors. Stainless steel has a significant amount of electrical conductivity, which is essential for minimizing ohmic losses in the fuel cell. This attribute ensures the seamless flow of electrons between the electrode and the external circuit, hence enhancing the overall efficiency of the DUHPFC. Moreover, a significant hindrance to the

operation of fuel cells is the existence of a corrosive environment within the cell. Stainless steel is widely recognized for its remarkable capacity to withstand corrosion, thereby guaranteeing the longevity and endurance of the anode layer, even under difficult operating conditions. Moreover, the robustness of the stainless-steel foil enhances the structural integrity of the anode layer. This strength is essential for maintaining the electrode's integrity during handling and operation, hence preventing any deformation or mechanical failure. Stainless steel has favorable surface properties that are suitable for the use of catalysts. The electro-deposition of nickel zinc iron oxide onto stainless steel foil results in the formation of a coating that is both homogeneous and firmly bonded. The application of this coating is essential for guaranteeing the optimal catalytic efficiency required in DUHPFC operations. The product details of stainless-steel foil used are provided in Table 3.1 [69].

Table 3.1 Product details of stainless-steel foil used

Property	Value
Material	Stainless Steel
Width	76.2 mm
Length	2.74 m
Overall Thickness	0.1016 mm
Material Thickness	0.0508 mm
Temperature Range	-34.4°C to 121.1°C
Tensile Strength	262 N/cm width
Adhesion to Steel	65.7 N/cm width

The selection of stainless-steel foil as the anode layer in this study was based on its remarkable electrical conductivity, resistance to corrosion, robust mechanical properties, and suitable surface features for catalyst deposition. The indicated characteristics ensure the anode layer performs at its best and is reliable, hence improving the overall effectiveness of the DUHPFC system.

3.1.2 Selection of Anode Catalyst in DUHPFC

The selection of anode catalysts in DUHPFC is vital for improving the efficiency and performance of the fuel cell. In general, anode catalysts are selected based on their catalytic activity, stability, electrical conductivity, and cost-efficiency. The catalysts must effectively facilitate the oxidation of urea at the anode, guaranteeing a high-power output and overall efficiency of the fuel cell.

The anode catalysts commonly employed in DUHPFCs consist of noble metals like platinum and palladium, chosen for their exceptional catalytic characteristics. Nevertheless, these materials are costly and can substantially augment the expense of the fuel cell. Hence, there is an increasing inclination towards the development of catalysts made from non-noble metals that provide similar performance but at a reduced expense.

For the DUHPFC, we chose nickel zinc iron oxide as the anode catalyst in this investigation. The selection of this material was based on its significant catalytic activity, which is crucial for facilitating the oxidation of urea at the anode. In addition, nickel zinc iron oxide has exceptional electrical conductivity, guaranteeing effective electron transfer during electrochemical operations. The anode's endurance is improved by its steadiness throughout operation, making it a dependable option for extended periods of use. In addition, nickel zinc iron oxide is a more cost-effective catalyst compared to noble metals, making it a financially feasible choice that does not compromise on performance.

3.1.3 Electrodeposition Method on Anode Electrodes

The electrodeposition method is a commonly employed technique for applying a thin film of material onto substrates, allowing for exact manipulation of the content and thickness of the deposited layer. The substrate for the anode electrode in this work was stainless steel foil, which was coated with nickel zinc iron oxide using the electrodeposition process. At first, a 400 ml electrolyte solution was created, consisting of nickel zinc iron oxide, hydrochloric acid (HCl), Copper (II) chloride, and distilled water. The addition of Copper (II) chloride was intended to enhance the adherence of the coating to the surface. The procedure requires a specific amount of HCl, as insufficient HCl leads to inadequate adherence of the nickel zinc iron oxide to the stainless-steel foil. The stainless-steel foil was precisely trimmed to the necessary measurements and meticulously purified using acetone, thereafter, washed with distilled water to eliminate any impurities on the surface. The stainless-steel foil that had been cleansed was utilized as the working electrode, while a platinum electrode was employed as the counter electrode. The electrodes were positioned in the prepared electrolyte solution, and a direct current power source was utilized to provide a consistent voltage of 2 V between the working and counter electrodes. The process of electrodeposition was conducted for a period of 30-40 minutes to achieve a consistent and firmly attached layer of nickel zinc iron oxide on the stainless-steel foil.

Throughout the deposition process, the electrolyte solution was constantly agitated to guarantee even dispersion of ions and consistent application onto the substrate. Following the electrodeposition process, the stainless-steel foil that had been coated was taken out of the electrolyte solution and washed extensively with distilled water to eliminate any remaining electrolyte. Subsequently, it was dried.

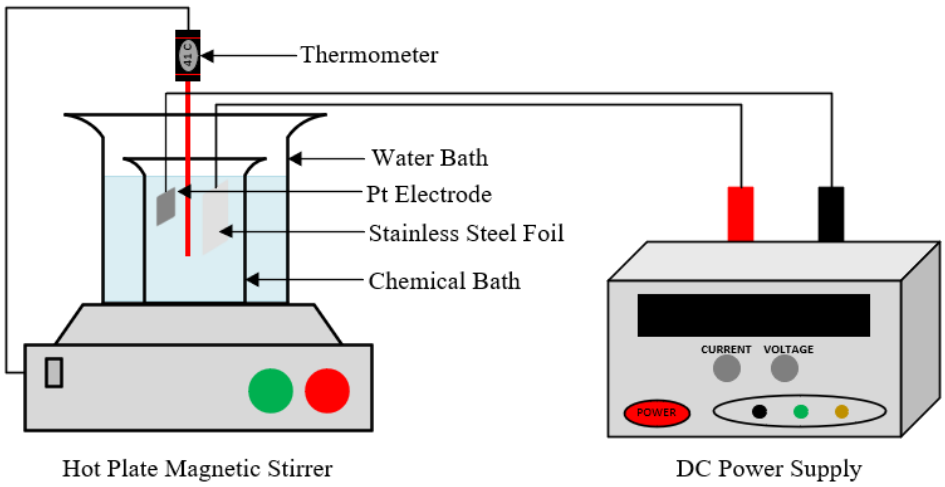

Figure 3.1 Illustration of electrodeposition method

This electrodeposition method provided a controlled and efficient means of coating stainless steel foil with nickel zinc iron oxide, resulting in a high-quality anode electrode for the DUHPFC. The process ensured uniform coating thickness and good adhesion, which are critical for the optimal performance of the fuel cell.

3.2 System Components and Materials

This section provides a thorough summary of the experimental settings and procedures used for different stages of the study, such as electrodeposition, H-cell investigations, single cell tests, and fuel cell stack evaluations. The document provides a comprehensive description of the equipment, chemicals, and procedures employed in each experimental configuration for electrochemical testing. This ensures a comprehensive comprehension of the essential components and materials involved in the research. All components used in the designed fuel cell are given in Table 3.3.

3.2.1 Fuel Cell Components

This section outlines the various components used in the fuel cell systems, including the materials and devices essential for constructing and operating the fuel cells. Detailed descriptions of each component, their roles, and the rationale behind their selection will be provided to give a clear understanding of the fuel cell architecture and its functionality. The representation of all layers for built single cell is given in Figure 3.2.

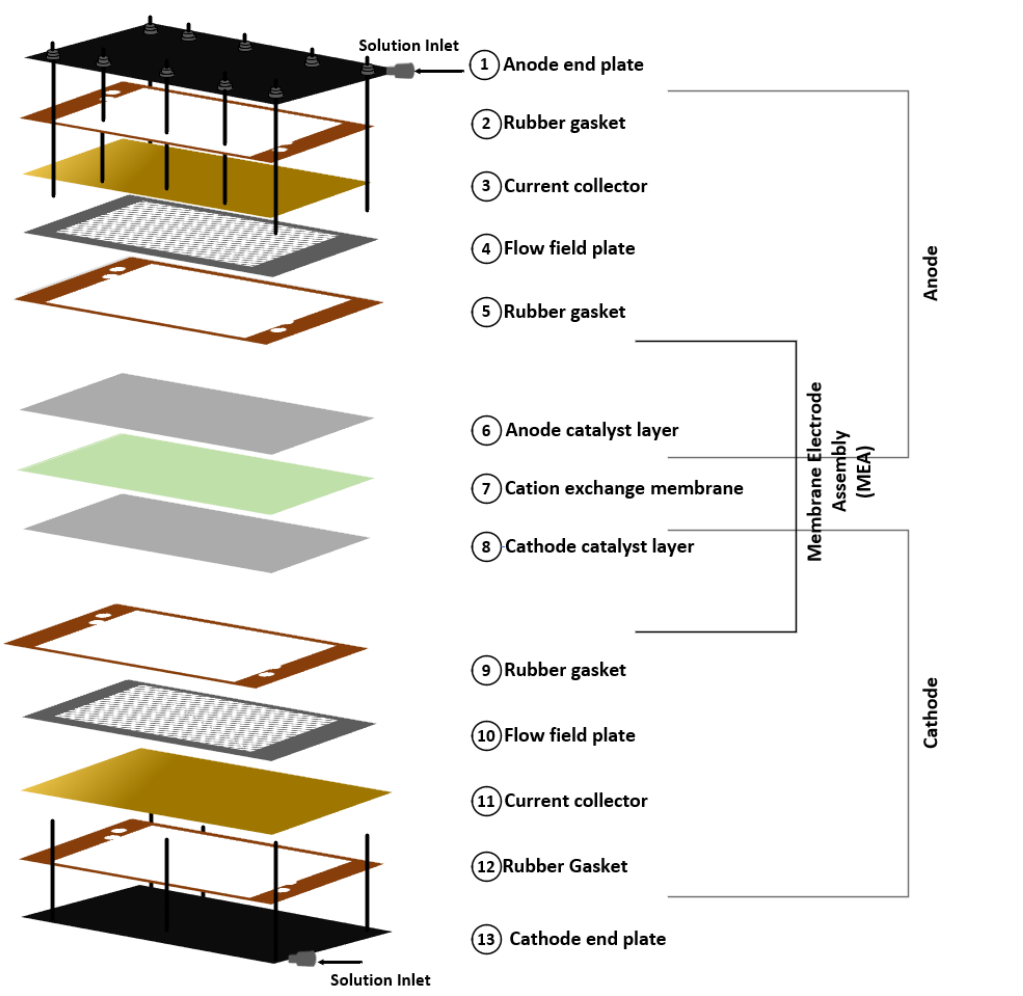

Figure 3.2 Illustration of the layers contained in DUHPFC single-cell arrangements

3.2.1.1 Cation Exchange Membrane

The cation exchange membrane plays a crucial role in the fuel cell system, particularly in the DUHPFC. The study utilized a membrane made of polystyrene cross-linked with divinylbenzene, known as CXM-200S.

The membrane is essential for the functioning of the DUHPFC as it selectively permits the passage of cations while preventing anions and other contaminants from passing through. The selective permeability is crucial for preserving the ionic equilibrium and enabling the electrochemical processes in the fuel cell. The membrane facilitates the movement of positively charged ions from the anode compartment to the cathode compartment, thereby creating a barrier between the fuel (urea) in the anode compartment and the oxidant (hydrogen peroxide) in the cathode compartment, thereby preventing undesired secondary chemical reactions. The membrane in the fuel cell ensures smooth functioning by maintaining electrical neutrality and balancing the charge transfer between the electrodes. The CXM-200S membrane has exceptional chemical stability even in the highly alkaline environment of the DUHPFC, guaranteeing both durability and long-term performance. Technical specifications of cation exchange membrane used is given in Table 3.2.

Table 3.2 Technical specifications of cation exchange membrane used

Technical Specification	**CXM-200S (CMI-7000S)**
Functionality	Strong Acid Cation Exchange Membrane
Polymer Structure	Gel polystyrene cross-linked with divinylbenzene
Functional Group	Sulphonic Acid
Ionic Form as Shipped	Sodium
Color	Beige/Brown
Standard Size (US)	48 in x 120 in
Standard Size (Metric)	1.22 m x 3.05 m
Standard Thickness (mils)	18 ± 1
Standard Thickness (mm)	0.45 ± 0.025
Electrical Resistance ($Ohm \cdot cm^2$)	< 30 (0.5 mol/L NaCl)
Maximum Current Density (A/m^2)	< 500
Permselectivity (%)	94 (0.1 mol KCl/kg / 0.5 mol KCl/kg)
Total Exchange Capacity (meq/g)	1.6 ± 0.1
Water Permeability ($ml/hr/ft^2$) @ 5 psi	< 3
Mullen Burst Test Strength (psi)	> 80
Thermal Stability (°C)	90
Chemical Stability Range (pH)	1-10
Preconditioning Procedure	Immerse the membrane in either the application solution or a 5% NaCl solution for 12 hours to allow for membrane hydration and expansion.
Storage	Store at room temperature and low humidity in sealed airtight container. Storage period not to exceed one year.

The CXM-200S (CMI-7000S) cation exchange membrane is a very acidic membrane that contains a gel structure made of polystyrene cross-linked with divinylbenzene polymer. The compound possesses a functional group known as sulphonic acid and is transported in the form of sodium ions, exhibiting a hue ranging from beige to brown. The membrane has a standard size of 48 inches by 120 inches (1.22 meters × 3.05 meters) and a standard thickness of 18 ± 1 mils (0.45 ± 0.025 mm). The membrane has an electrical resistance of less than 30 Ohm·cm² in a 0.5 mol/L NaCl solution, and it has a maximum current density capacity of less than 500 A/m². The perm selectivity of the substance is 94% when tested in a solution containing 0.1 mol of KCl per kilogram and 0.5 mol of KCl per kilogram. Additionally, it has a total exchange capacity of 1.6 ± 0.1 milliequivalents per gram. The water permeability is below 3 ml/hr/ft² at 5 pressures, but the Mullen burst test strength exceeds 80 psi [70].

The CXM-200S membrane exhibits thermal stability up to a temperature of 90°C and demonstrates chemical stability within a pH range of 1 to 10. Prior to utilization, the membrane necessitates a process of preconditioning, which involves immersing it in either the solution intended for application or a 5% NaCl solution for a duration of 12 hours. This step is crucial as it allows for the membrane to undergo hydration and expansion. For optimal storage conditions, it is recommended to keep the item in a sealed airtight container at room temperature with low humidity. The storage duration should not exceed one year.

3.2.1.2 Anode Layer

The anode layer in the DUHPFC is a crucial component responsible for the oxidation reactions necessary to generate electricity. For this study, stainless steel foil coated with nickel zinc iron oxide was used as the anode layer. This specific combination of materials was chosen for its excellent electrical conductivity, corrosion resistance, and catalytic properties. The main purpose of the anode layer in the DUHPFC is to enable the oxidation of the fuel, specifically urea. During the functioning of the fuel cell, urea undergoes an electrochemical oxidation reaction at the anode, liberating electrons and generating carbon dioxide and other secondary substances. The liberated electrons in this reaction traverse an external circuit, producing an electrical current that can be utilized for power generation. The nickel zinc iron oxide layer on the stainless-steel foil has multiple significant functions. Firstly, it functions as a catalyst, expediting the oxidation of urea and enhancing the overall

efficiency of the fuel cell. The nickel-zinc iron oxide exhibits a high catalytic activity, which promotes the occurrence of electrochemical reactions at an accelerated rate, hence improving the performance of the anode. Furthermore, the stainless-steel foil serves as a durable and conductive base, guaranteeing effective electron transport and preserving the structural stability of the anode layer.

Additionally, the corrosion resistance of stainless steel is crucial in the highly alkaline environment of the DUHPFC, ensuring the longevity and durability of the anode layer. The combination of nickel zinc iron oxide and stainless steel creates a synergistic effect, optimizing the performance of the anode and, consequently, the entire fuel cell system.

To sum up, the anode layer composed of nickel zinc iron oxide coated on stainless steel foil plays a vital role in the DUHPFC by facilitating the oxidation of urea, enhancing catalytic activity, and ensuring efficient electron transfer and corrosion resistance. These properties are essential for the efficient and reliable operation of the fuel cell.

3.2.1.2 Cathode Layer

The cathode layer of the DUHPFC plays a crucial role in facilitating the reduction processes required for energy generation. The selection of this material was based on its exceptional electrical conductivity and robust mechanical strength. The main purpose of the cathode layer in the DUHPFC is to enable the reduction of the oxidant, specifically hydrogen peroxide. During the functioning of the fuel cell, hydrogen peroxide performs an electrochemical reduction reaction at the cathode, where it consumes electrons and produces water and oxygen. The electrons utilized in this reaction are sourced from the external circuit, thereby establishing an electrical circuit and facilitating uninterrupted electricity production. The carbon paper fulfills multiple crucial functions within the cathode layer. Firstly, it functions as a highly conductive medium, facilitating efficient electron passage from the external circuit to the reaction sites. Carbon paper's strong electrical conductivity minimizes resistive losses, hence improving the fuel cell's overall efficiency. Furthermore, the carbon paper's permeable structure enables efficient gas diffusion, enabling hydrogen peroxide to access the active spots on the cathode surface where the reduction reaction takes place.

Moreover, the carbon paper's robust mechanical strength enhances the structural integrity of the cathode layer, enabling it to endure the operating strains of the fuel cell. The chemical inertness of carbon paper guarantees its stability and prevents degradation during electrochemical reactions, hence enhancing the longevity and durability of the cathode layer. Essentially, the carbon paper cathode layer is crucial in the DUHPFC as it enables the reduction of hydrogen peroxide, improves electron transfer, and ensures efficient gas transport and structural stability. These qualities are crucial for the effective and dependable functioning of the fuel cell.

3.2.1.2 Flow Channel

The flow channel in the DUHPFC plays a crucial role in evenly spreading the fuel and oxidant across the electrode surfaces. The bipolar parallel flow channel design was utilized in this study. The selection of this flow channel design was based on its capacity to optimize mass transport, reduce pressure drop, and improve the overall performance of the fuel cell. The main purpose of the flow channel in the DUHPFC is to guarantee the uniform dispersion of urea as the fuel to the anode and hydrogen peroxide as the oxidant to the cathode. The flow channel's parallel design efficiently guides the reactants, guaranteeing a consistent distribution over the electrode surfaces. This design optimizes the contact area and promotes electrochemical reactions throughout the electrodes. The uniform distribution is essential for ensuring consistent cell performance and minimizing the formation of isolated hot spots or concentration gradients. The design of parallel flow channels also has a substantial impact on reducing the pressure drop within the fuel cell. Through the optimization of the course and cross-sectional area of the flow channels, the system can accomplish efficient fluid transport while minimizing energy loss. It is crucial to maintain the overall efficiency of the fuel cell and ensure that the reactants are delivered to the reaction sites with adequate pressure.

Furthermore, the design of the parallel flow channel makes it easier to eliminate the byproducts that are produced because of the electrochemical processes. For example, the design enables the efficient elimination of carbon dioxide generated at the anode and water generated at the cathode, preventing the buildup of these waste products and ensuring the cell operates under ideal conditions.

3.2.1.3 Gaskets

The gasket in the DUHPFC plays a vital role in creating a secure seal between the various layers of the fuel cell. This seal is essential for preventing any leaks and preserving the structural integrity of the cell. The selection of this material was based on its exceptional sealing qualities, chemical resistance, and flexibility. The main purpose of the gasket in the DUHPFC is to ensure a tight and reliable seal between the different parts of the fuel cell, such as the anode, cathode, and flow channels. The rubber gasket serves to contain the fuel (urea) and the oxidant (hydrogen peroxide) within their designated compartments, effectively avoiding any mixing or unintended release. Ensuring the efficiency and safety of the fuel cell is crucial.

Rubber gaskets provide numerous benefits in the DUHPFC system. First and foremost, their remarkable flexibility enables them to adapt to the unevenness of the fuel cell components, guaranteeing a secure and airtight seal. It is crucial to maintain pressure and prevent leaks when operating under different conditions. Additionally, rubber gaskets provide excellent chemical resistance, a critical characteristic in the extremely alkaline setting of the DUHPFC. This guarantees that the gaskets maintain their integrity and do not experience any deterioration or loss of their ability to create a seal as time passes. The chemical durability of rubber gaskets is crucial, especially due to the existence of corrosive chemicals like urea and hydrogen peroxide. Their chemical resistance guarantees the fuel cell's enduring robustness and dependable functionality. In addition, rubber gaskets have excellent thermal stability, ensuring that their sealing capabilities remain effective across a broad spectrum of working temperatures. This characteristic is crucial for maintaining constant operation of the DUHPFC.

Essentially, the rubber gasket in the DUHPFC has a crucial function of creating a secure seal between the different parts of the fuel cell. This seal is essential for preventing any leakage and ensuring that the cell operates with maximum effectiveness and efficiency. The material's flexibility, resistance to chemicals, and capacity to withstand high temperatures make it an excellent option for use in the DUHPFC, ensuring the fuel cell operates reliably and for a long period.

3.2.1.4 End Plates

The end plates of the DUHPFC are crucial elements that offer structural reinforcement and guarantee consistent compression of the fuel cell stack. The plates used in fuel cells are typically constructed from robust and inflexible materials to endure the operational pressures of the fuel cell. The study utilized stainless steel end plates. The selection of this material was based on its exceptional mechanical strength, resistance to corrosion, and capacity to dissipate thermal energy, ensuring consistent performance under operational conditions.

The major purpose of the end plates in the DUHPFC is to offer mechanical support and uphold the structural integrity of the fuel cell stack. The end plates secure the many components of the fuel cell, such as the electrodes, gaskets, and flow channels, in a stable position. Homogeneous compression is essential for preserving efficient contact among the layers, guaranteeing excellent performance, and preventing any leaks or separation.

Steel end plates provide numerous benefits in the DUHPFC system. Their exceptional mechanical strength enables them to endure the compressive stresses necessary for maintaining a secure seal between the fuel cell components.

It is crucial to prevent leaks and maintain constant operation even when pressure conditions change. Furthermore, stainless steel has exceptional resistance to corrosion, a crucial characteristic in the highly alkaline surroundings of the DUHPFC. This guarantees the preservation of the end plates, preventing their deterioration over time, which enhances the fuel cell's long-lasting resilience. The thermal stability of stainless-steel end plates is crucial as it enables them to retain their structural integrity and deliver constant compression across a broad spectrum of working temperatures.

The reliable performance of the DUHPFC is contingent upon temperature stability, as fluctuations in temperature can have an adverse effect on the fuel cell's sealing and overall efficiency.

All fuel cell layers are summarized in Table 3.3. This table presents a graphical overview of the primary layers involved in the construction of the Direct Urea-Hydrogen Peroxide Fuel Cell (DUHPFC). Every part of the fuel cell, from the end plates to the cation exchange membrane, is essential to its effective functioning.

Table 3.3 Representation of all fuel cell layers

Name	Layer
Cation Exchange Membrane	
Anode	
Cathode	
Flow Field Channel	
Rubber Gasket	
End Plates	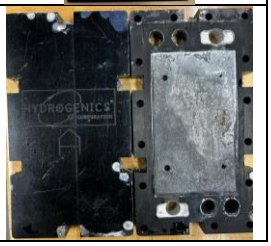

The physical layout of the DUHPFC is represented in the table, which provides a clear reference to each component that has previously been covered in detail. It acts as a

succinct synopsis, enhancing the thorough explanations offered and showing how these parts are integrated into a coherent and working fuel cell system. The comprehension of how each layer affects the DUHPFC's overall durability and performance is strengthened by this synopsis.

3.2.1.5 Fuel Cell Single Cell and Stack Assembly

The construction of both the individual cell and the stack of fuel cells in the DUHPFC is a crucial procedure that guarantees the correct alignment and operation of all the fuel cell components. The procedure entails the meticulous arrangement of many layers, such as the anode, cathode, flow channels, gaskets, and end plates, to create a unified and efficient fuel cell system. The single cell assembly process commences by meticulously aligning the anode and cathode layers. The anode, which is covered with nickel zinc iron oxide, and the cathode, which is constructed from carbon paper, are strategically positioned to optimize contact with the flow channels. The parallel layout of the flow channels enables the uniform distribution of urea as the fuel and hydrogen peroxide as the oxidant over the electrode surfaces. Rubber gaskets are inserted between these layers to ensure a tight seal and prevent any escape from the reactants. The assembly is finalized by positioning stainless steel end plates, which offer the essential mechanical reinforcement and consistent compression, so preserving the structural integrity and guaranteeing optimal contact among all the layers. A representation of the built single cell is given in Figure 3.3. Also, the experimental setup for single-cell assembly is given in Figure 3.8 (a) and (b) respectively.

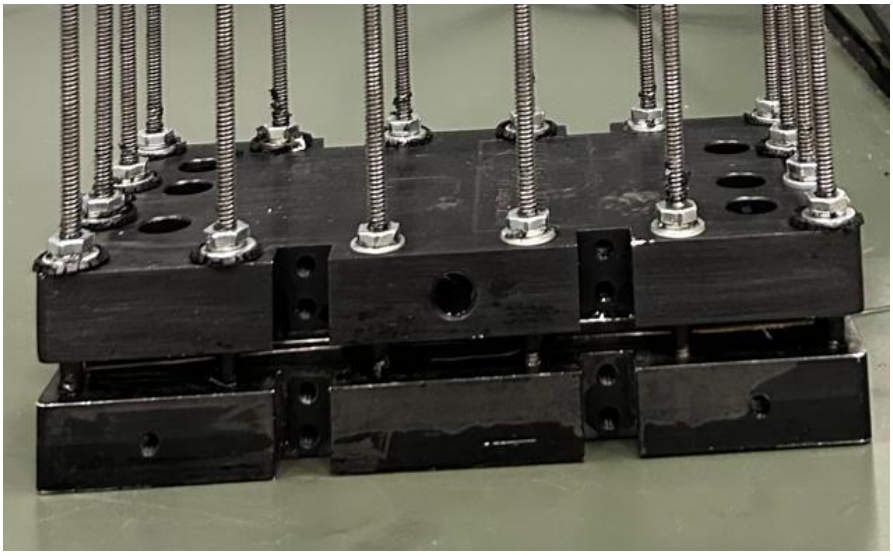

Figure 3.3 Built single-cell assembly

Regarding the fuel cell stack assembly, the procedure is comparable but necessitates repeating the individual cell assembly procedures for numerous cells. These cells are subsequently interconnected in either a series or parallel configuration to attain the intended power output. Every individual cell inside the stack is meticulously positioned to guarantee optimal contact and effective distribution of fuel and oxidant. The gaskets, flow channels, and end plates serve identical crucial functions as in the single cell assembly, ensuring sealing, distribution, and mechanical reinforcement. The stack is subsequently fastened with bolts to guarantee a sturdy and long-lasting structure. A representation of the 16-cell stack assembly is given in Figure 3.4.

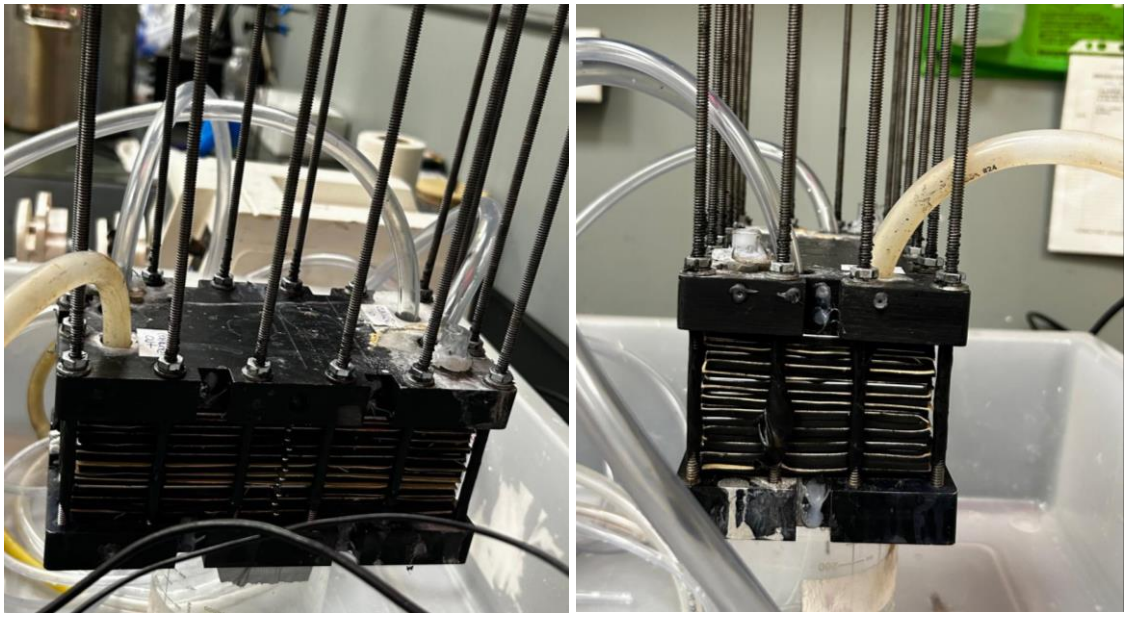

Figure 3.4 16-cell stack assembly

Ensuring the correct arrangement of both the individual cell and the stack of fuel cells is essential for achieving the highest level of performance and efficiency in the DUHPFC. Performance losses, leaks, or damage to the fuel cell components might occur if there is any misalignment or faulty sealing.

Hence, meticulous focus is given to the alignment, sealing, and compression during the assembly procedure to guarantee dependable and uniform functioning. This method guarantees the effective operation, structural soundness, and peak performance of the fuel cell, hence enhancing its efficiency and dependability.

3.2.2 H-type Electrolytic Cell Components

The H-type electrolytic cell is an essential apparatus employed in the preliminary phases of testing for the DUHPFC to assess the performance of the membrane electrode assembly (MEA) under controlled circumstances. This configuration enables the accurate quantification of several electrochemical parameters, yielding useful data that guides the enhancement of the fuel cell components. A representation of this H-type electrolytic cell is given in Figure 3.5.

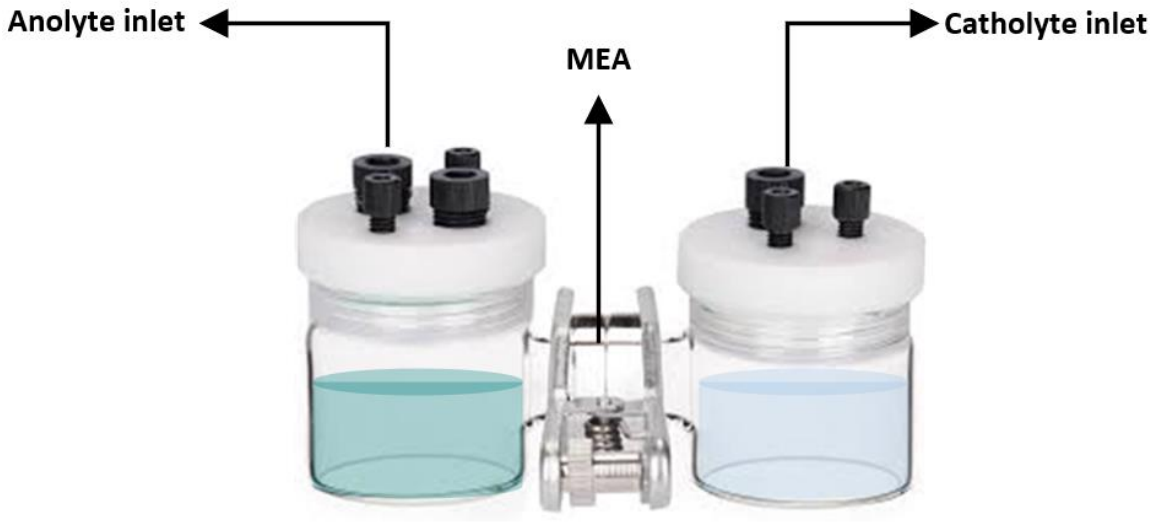

Figure 3.5 H-type electrolytic cell assembly

The main constituents of the H-type electrolytic cell consist of the anode chamber, cathode chamber, and the center compartment where the membrane electrode assembly (MEA) is positioned. The MEA is composed of an anode layer covered with nickel zinc iron oxide, a cathode layer produced from carbon paper, and a cation exchange membrane (CXM-200S). It is positioned between the anode and cathode chambers. This structure enables the independent delivery of fuel and oxidant into their individual chambers, guaranteeing controlled and accurate reactions. The anode chamber is filled with a solution of urea, while the cathode chamber contains a solution of hydrogen peroxide. Rubber gaskets are employed to guarantee a secure and airtight connection between the MEA and the chambers, effectively avoiding any leakage and preserving the cell's integrity.

The presence of stainless-steel end plates serves to offer structural reinforcement and guarantee even compression of the MEA and gaskets, so preserving a consistent level of contact and preventing any deviations or misalignments during the testing process.
The end plates are fastened together using bolts, ensuring the complete assembly is securely held in place and enabling consistent and replicable measurements. The H-type electrolytic cell is furnished with electrodes for the application of an external potential and the measurement of the resultant current.

This allows for the evaluation of diverse electrochemical characteristics, including open-circuit voltage (OCV), current density, and power density. This configuration is essential for assessing the performance attributes of the MEA, including its conductivity, catalytic activity, and overall efficiency.

3.2.3 Equipment Specifications

This section offers comprehensive explanations of the many instruments and devices used in the experimental techniques. This encompasses the detailed specifications and operational capabilities of crucial equipment, such as the Gamry Reference 3000 potentiostat/galvanostat, peristaltic pumps, and other necessary gear employed in the preparation, assembly, and testing of the DUHPFC system. Comprehending the requirements of every equipment component is vital to guarantee precise and replicable experimental outcomes. Equipment and component specifications are summarized in Table 3.4.

This detailed understanding of the equipment not only ensures accurate data collection but also aids in troubleshooting and optimizing the experimental setup. Proper calibration and maintenance of these instruments are essential for the reliability of the results. The information provided in Table 3.4 serves as a quick reference, ensuring that each component is utilized to its full potential in the experimental procedures. By carefully adhering to these specifications, researchers can minimize variability and enhance the consistency of the experimental data. This attention to detail is crucial for achieving meaningful comparisons between different sets of experiments and for validating the overall performance of the DUHPFC system under various conditions.

Table 3.4 Equipment and component specifications

Name	Image	Specifications
Wanptek DC Power Supply DPS3010 U		Output Voltage: 0-30 V Output Current: 0-10 A Temperature: 0-40 ºC Resolution: 00.01 V, 0.002 A.
Fisher Scientific Isotemp Hotplate with Magnetic Stirrer		Stirring Range: 60- 1200 rpm Temperature Range: 5 to 400 ºC Plate Capacity: 35 lbs.
Mettler Toledo, AB204-S/FACT Scale		Range: Up to 220 g Temperature Sensitivity (10 to 30 ºC): 2.5 ppm/ºC Time (setting): 4s.
Mastercraft 052-0060-2 Multimeter		Resistance Readability: 200, 2k, 20k, 200k, 2000kΩ Temperature: 0 to 50 ºC Readings accurate after 1 year of calibration at 18 to 28 ºC.
Wagner Furno Heat Gun		Two Speeds: Low, High Heating Setting (Drying Paint): Low.
Platinized Titanium Mesh electrode	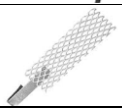	Dimensions (mesh): 50 mm (length) by 25 mm (width).
316 Stainless Steel Foil	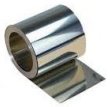	Dimensions: 124mm (length) x 71 mm (width).
Gamry Reference 3000 Potentiostat/ Galvanostat		Used for electrochemistry analysis.
Ag/AgCl Reference Electrode		Reference electrode used in electrochemical testing setup.
Urea Flowmeter		The Urea Flowmeter is used to regulate the flow rate of urea sent from the anolyte side.
Thermocouple		The thermocouple is used to regulate the temperature on the anolyte side.

3.2.4 Chemical Specifications

The Chemical Specifications section outlines the specific chemicals and materials used in the experimental setups. This includes details on the anolyte and catholyte solutions, electrode materials, and other reagents involved in the electrodeposition process and electrochemical testing. The precise composition and properties of these chemicals are critical for achieving the desired reactions and optimizing the performance of the DUHPFC system. Chemical specifications are given in Table 3.5.

Table 3.5 Chemicals and specifications

Name	Image	Specifications
Nickel Zinc Iron Oxide ($NiZnFe_4O_4$)		Nickel Zinc Iron Oxide is used for anode catalyst for DUHPFC.
Potassium Hydroxide (KOH)		Potassium Hydroxide is used in the anolyte to provide ionic conductivity, maintain an alkaline pH for optimal urea oxidation, and prevent corrosion of the fuel cell components.
Urea ($CO(NH_2)_2$)		Urea is used for anolyte solution in DUHPFC.
Hydrogen Peroxide (H_2O_2)		Hydrogen Peroxide is used for catholyte solution in DUHPFC.
Sulfuric Acid (H_2SO_4)		Sulfuric Acid is used in the catholyte to enhance the reduction of hydrogen peroxide.
Hydrochloric Acid (HCl)		Hydrochloric Acid is used in electrodeposition for nickel-based catalyst coating.
Copper (II) Chloride ($CuCl_2$)		Copper (II) Chloride is used in electrodeposition to improve the adhesion of the nickel zinc iron oxide coating to the stainless-steel foil.

3.3 Experimental Setup and Procedure

This section provides a comprehensive overview of the methodologies and equipment used throughout the research to evaluate the performance and efficiency of the DUHPFC system. This section includes detailed descriptions of the experimental setups, including the preparation and coating of electrodes, the assembly of single cells and fuel cell stacks, and the configurations of H-type electrolytic cells. Additionally, it outlines the electrochemical testing procedures carried out using the Gamry Reference 3000 potentiostat/galvanostat to ensure precise and reliable data acquisition for performance analysis.

3.3.1 Experimental Setup for Electrodeposition and Electrochemical Test of Coating

The experimental setup for electrodeposition and electrochemical testing of the coating, as depicted in the photographs, employs a meticulous and methodical approach to guarantee the efficient application and assessment of the nickel zinc iron oxide coating on stainless steel foil. The electrodeposition procedure starts by preparing a 400 mL solution consisting of nickel zinc iron oxide, hydrochloric acid (HCl), and Copper (II) chloride. This experimental setup is shown in Figure 3.6. This solution is crucial for attaining a consistent and cohesive covering. The stainless-steel foil is submerged in the solution, while a DC power supply administers a consistent voltage of 2V across the electrodes. Platinum is employed as the counter electrode to expedite the electrochemical processes. The process of electrodeposition is conducted for a duration of 30-40 minutes, providing ample time for the deposition of nickel zinc iron oxide onto the surface of the stainless steel. The addition of Copper (II) chloride improves the bonding of the coating, while the concentration of HCl assures the best possible deposition by assisting in the electrochemical process.

Following the process of electrodeposition, the stainless-steel foil that has been coated is meticulously washed with distilled water to eliminate any remaining chemicals and loose particles. The efficacy of the coating is subsequently evaluated through a sequence of electrochemical examinations.

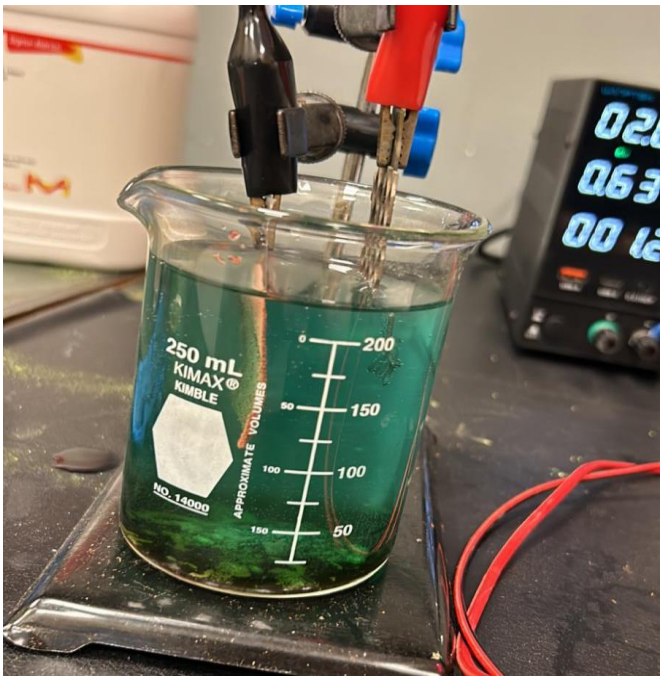

Figure 3.6 Experimental setup for electrodeposition

To conduct these experiments, the coated electrode is immersed in an electrolyte solution and linked to a potentiostat/galvanostat. The Gamry Reference 3000 equipment is utilized for performing a range of measurements, such as cyclic voltammetry (CV), linear sweep voltammetry (LSV), and electrochemical impedance spectroscopy (EIS). The experimental setup for electrochemical test for coating is given in Figure 3.7.

During the electrochemical testing step, the performance of the electrode with a coating is thoroughly assessed. The procedure involves submerging the electrode in the electrolyte solution and making the necessary connections to the reference, working, and counter electrodes. Data is gathered and examined to ascertain the electrochemical properties of the coating, including its conductivity, catalytic efficacy, and overall appropriateness for utilization in the DUHPFC. This complete methodology guarantees that the electrodeposition process and subsequent electrochemical testing yield precise and dependable data, which is crucial for maximizing the performance of the DUHPFC. Additionally, this rigorous approach ensures that any potential issues with the electrode coating are identified and addressed early in the development process.

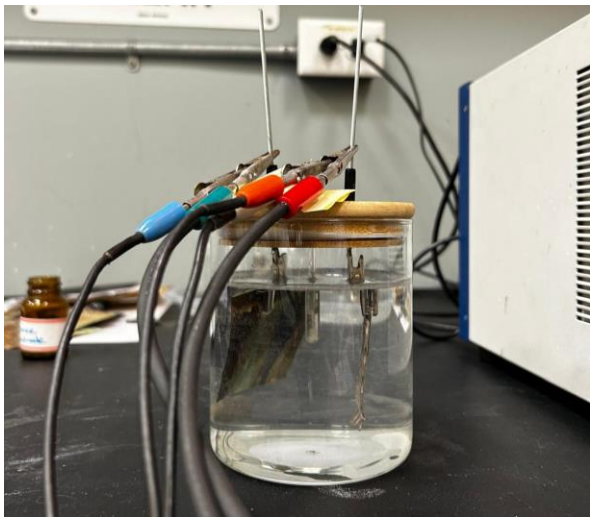

(a)

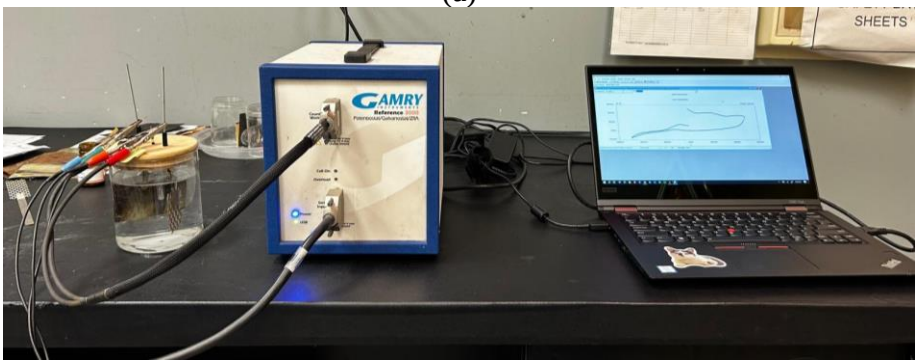

(b)

Figure 3.7 Illustration of (a) prepared solution (b) experimental setup for electrochemical test for coating

3.3.2 Experimental Setup for H-type Electrolytic Cell

The H-type electrolytic cell experimental setup, depicted in Figure 3.11, comprises an anode chamber filled with urea solution and a cathode chamber holding hydrogen peroxide solution. The MEA is positioned between the two chambers. The MEA consists of an anode layer made of stainless-steel foil coated with nickel zinc iron oxide, a cathode layer made of carbon paper, and a cation exchange membrane (CXM-200S) that separates the two layers. The utilization of rubber gaskets and stainless-steel end plates guarantees a secure seal and consistent compression, so preventing any leakage and preserving the structural integrity. The configuration includes inlets and outlets for anolyte and catholyte to enable uninterrupted flow. It also incorporates a reference electrode (RE), working electrode (WE), and counter electrode (CE) to provide accurate electrochemical measurements. The process entails the preparation of solutions, the assembly of the cell, the filling of the

chambers, the connection of the electrodes, and the utilization of a potentiostat/galvanostat to apply a potential and measure the current. During this process, data such as open circuit voltage (OCV), current density, and power density are recorded. Following the studies, the cell is dismantled, thoroughly cleansed, and preserved for subsequent utilization. This configuration enables precise and controlled assessment of the electrochemical performance of the DUHPFC.

3.3.3 Experimental Setup for Single Cell Assembly

The experimental configuration for the assembly and testing of individual cells, as illustrated in the image, comprises various essential elements and meticulous methods to guarantee precise assessment of the performance of the DUHPFC. The individual cell is constructed by combining the prearranged anode and cathode layers, which are divided by a cation exchange membrane (CXM-200S). The anode layer is composed of stainless-steel foil that is coated with nickel zinc iron oxide, whilst the cathode layer is constructed from carbon paper. The layers are stacked together with the membrane in the middle, forming the MEA. The experimental setup for single cell assembly is shown in Figure 3.8.

The consolidated individual cell is positioned into a testing apparatus, comprising a clamp to secure the cell and guarantee even distribution of pressure. The cell is linked to a Gamry Reference 3000 potentiostat/galvanostat to facilitate electrochemical testing. The configuration involves the utilization of a peristaltic pump to facilitate the circulation of the anolyte and catholyte solutions throughout the cell. The anolyte solution commonly comprises urea and potassium hydroxide (KOH), whereas the catholyte solution is composed of sulfuric acid and hydrogen peroxide. During the testing process, the anolyte and catholyte solutions are injected into their respective compartments within the cell using a pump. The Gamry apparatus is utilized for conducting a range of electrochemical examinations, including open circuit potential (OCP), linear sweep voltammetry (LSV), polarization resistance (POLRES), and electrochemical impedance spectroscopy (EIS). These tests yield information regarding the voltage, current density, power density, and impedance characteristics of the cell.

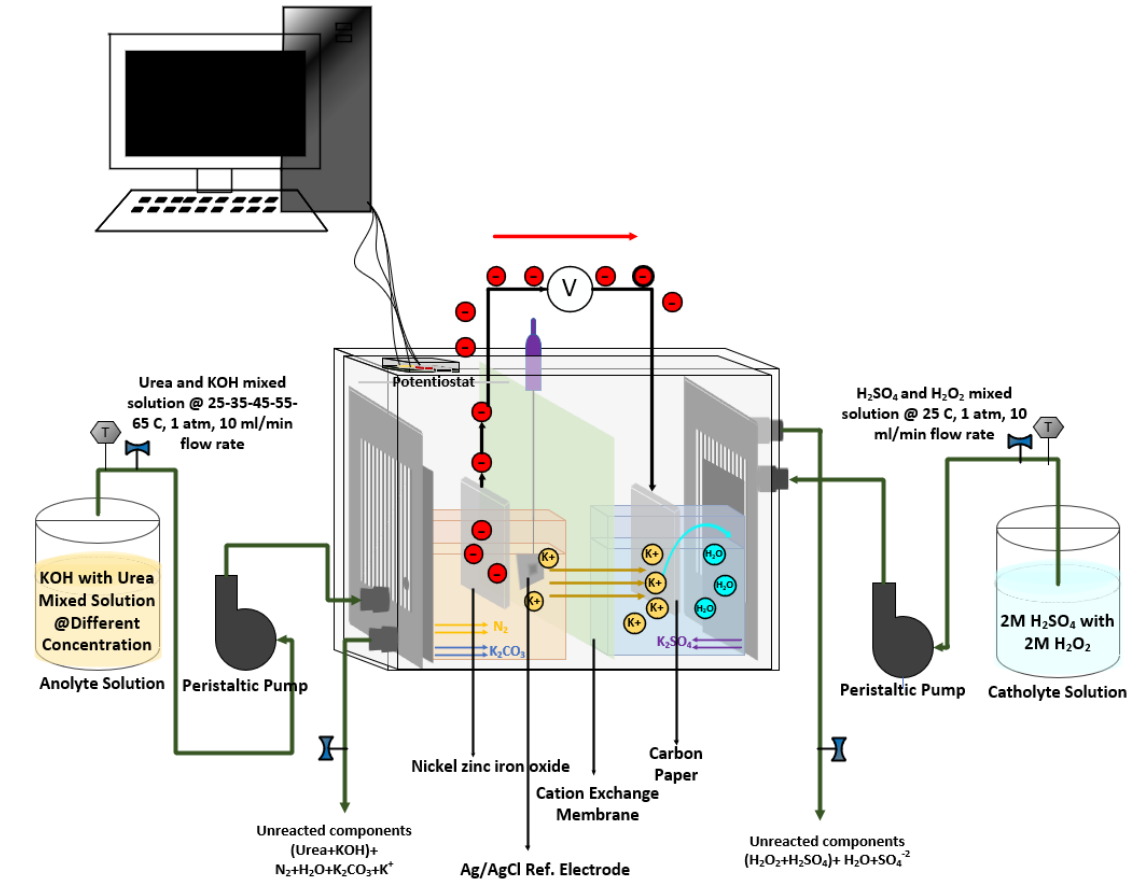

(a)

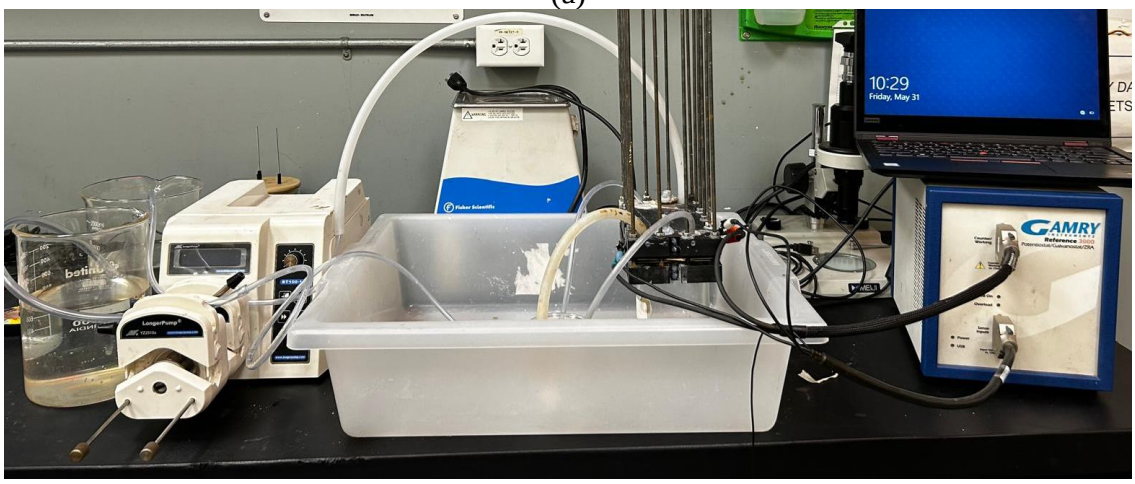

(b)

Figure 3.8 Illustration of a (a) schematic (b) real experimental setup for single cell assembly

In addition, the system includes a computer that is linked to the Gamry equipment to facilitate the capture and interpretation of data. The performance of the individual cell is assessed using the gathered data, and the findings are utilized to enhance the design and

operational parameters of the cell. The complete experimental approach guarantees that the assembly and testing of the single cell are carried out in controlled and repeatable settings, resulting in dependable and precise performance data for the DUHPFC.

3.3.4 Experimental Setup for Fuel Cell Stack Assembly

The experimental setup for the 16-cell stack assembly and testing, depicted in the image, entails a meticulous arrangement to guarantee a thorough assessment of the performance of the DUHPFC stack. The 16-cell stack is created by arranging numerous individual cells in a series configuration. Each cell is composed of pre-made anode and cathode layers, separated by cation exchange membranes (CXM-200S). The anode layer consists of stainless-steel foil that is coated with nickel zinc iron oxide, whilst the cathode layer is composed of carbon paper. The stack is positioned securely within a holder that has been specifically constructed for it, to evenly distribute pressure over all cells. This design ensures that there is consistent contact and minimizes any resistance. The configuration consists of a peristaltic pump that continuously moves the anolyte and catholyte solutions across the stack. The anolyte solution is composed of a 9 M potassium hydroxide (KOH) solution with 0.5 M urea. On the other hand, the catholyte solution consists of a 2 M sulfuric acid solution with 2 M hydrogen peroxide. The experimental setup for fuel cell stack assembly is given in Figure 3.9.

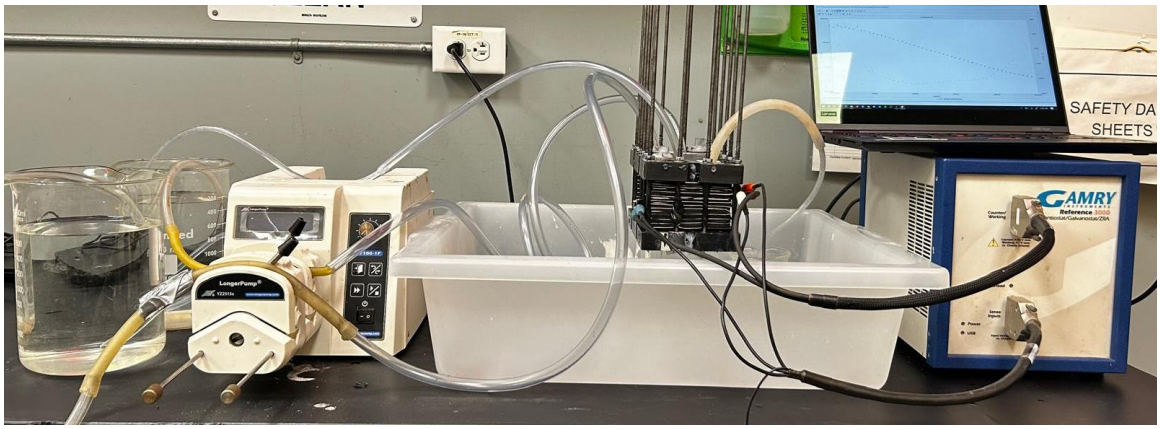

Figure 3.9 Experimental setup for fuel cell stack assembly

The stack is connected to a Gamry Reference 3000 potentiostat/galvanostat for electrochemical testing. This setup enables the performance of various electrochemical tests, such as OCP, LSV, POLRES, and EIS. These tests provide essential data on the stack's voltage, current density, power density, and impedance characteristics. The

experimental configuration comprises a computer that is connected to the Gamry apparatus for the purpose of acquiring and analyzing data. The gathered data aids in assessing the stack's performance across various operating situations, encompassing fluctuations in temperature. The complete experimental approach guarantees that the stack building and testing are carried out in controlled and replicable settings, resulting in dependable and precise performance data for the DUHPFC. This comprehensive configuration enables a full examination of the performance of the 16-cell stack, so contributing to the improvement of the DUHPFC system.

3.3.5 Electrochemical Testing

Electrochemical testing plays a crucial role in evaluating the performance of the DUHPFC components, single cells, and stacks. Utilizing the Gamry Reference 3000 potentiostat/galvanostat, various electrochemical measurements were conducted to understand the system's electrochemical behavior, efficiency, and functionality. Prior to testing, the Gamry instrument was carefully calibrated to ensure accurate and reproducible results, eliminating systematic errors and providing precise control over applied voltage and current. The calibration setup is given in Figure 3.10.

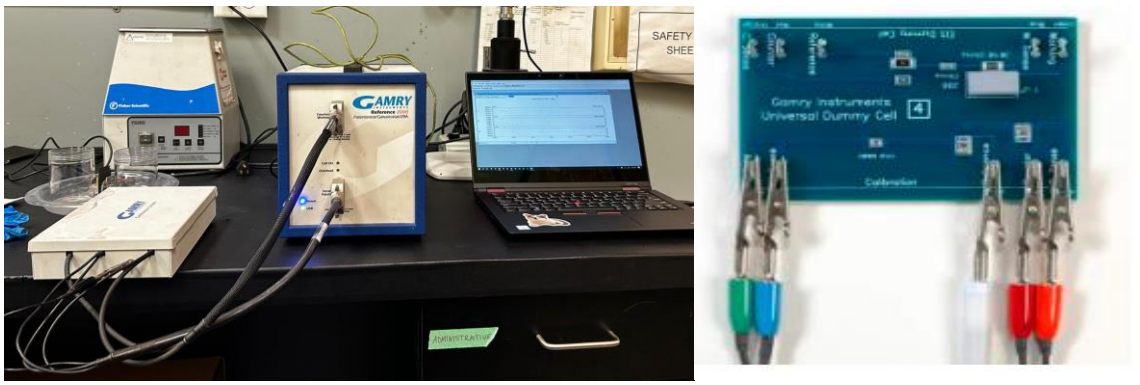

(a) (b)

Figure 3.10 Illustration of the (a) calibration setup (b) calibration cell of Gamry Reference 3000 potentiostat/galvanostat

The calibration process is critical for obtaining valid and interpretable data. Several tests were performed, including OCP to measure the cell's inherent voltage, LSV to assess catalytic activity and reaction onset potentials, POLRES to evaluate charge transfer resistance and reaction kinetics, and EIS to analyze resistive and capacitive elements of the system over a range of frequencies. These tests involved immersing the electrodes in

electrolyte solutions and connecting them to the reference, working, and counter electrodes, with data acquisition and analysis carried out using Gamry software. The insights gained from these measurements are essential for optimizing the design and operating conditions of the DUHPFC, contributing to the development of more efficient and reliable energy conversion systems.

3.4 Experimental Uncertainty and Error Analysis

Error analysis is crucial for accurately analyzing studies and the resulting data. Evaluating the uncertainties linked to the experimental components employed for measurements is crucial, as any inaccuracies in the experiment can directly influence the results if not adequately evaluated. Table 3.6 enumerates the distinct mistakes linked to the different experimental components employed in this study. These inaccuracies are derived from the manuals given by the individual manufacturers. Experimental uncertainties can be categorized into systematic mistakes and random errors. Systematic errors are inherent to the equipment and typically originate from the manufacturer. The study provides a comprehensive breakdown of the systematic errors associated with the components utilized in the tests. The specific details may be found in Table 3.6.

Table 3.6 Error analysis of experimental devices

Component	**Parameter**	**Component Accuracy/Error**
Wanptek DC Power Supply DPS3010 U	Input Voltage	± 10%
Gamry Reference 3000 Potentiostat/ Galvanostat	Applied potential	≤ 0.1% ± mV offset
Mastercraft 052-0060-2 Multimeter	Resistance (Range)	200Ω: ±1.2%+5 2kΩ, 20kΩ, 200kΩ: ±1.0%+5 2000kΩ: ±1.5%+5
Urea Flowmeter	Calibration Accuracy	±5%

Random mistakes occur during studies and can be affected by several factors, such as human error or other variables that lead to oscillations in the collected data. The identification of these faults is solely possible through the utilization of the collected data. To mitigate and assess the impact of unpredictable errors, experiments and measurements are replicated three times. The uncertainty associated with the various measured parameters can be determined using Equation 3.1:

$$U=\sqrt{(R^2 + S^2)} \tag{3.1}$$

where U is the experimental error (%), R is the random error (%), and S is the systematic error (%).

The random errors can be calculated by equation 3.2:

$$R=\frac{\text{SD}}{\text{AVG}} \text{ x } 10 \quad (3.2)$$

where R is the error (%) due to random errors, SD is the standard deviation, and Avg is the average of the measurements recorded.

This approach is used to assess the uncertainty of the measured parameters. The experimental uncertainties presented in Table 3.7 are determined by considering both systematic and random errors. To determine the random error, three distinct measurements are obtained for every parameter.

The table highlights the uncertainty associated with each system component used in the experiments. The highest uncertainty is observed with the Wanptek DC Power Supply, showing an uncertainty of 12.62%, largely due to a higher systematic error. The Gamry Reference 3000 Potentiostat/Galvanostat and the Mastercraft Multimeter have lower uncertainties of 7.11% and 4.27%, respectively, indicating more reliable measurements. The Urea Flowmeter shows an uncertainty of 6.43%, reflecting a balance of random and systematic errors. Overall, the uncertainties are within acceptable ranges, ensuring the reliability of the experimental data.

Table 3.7 Errors and uncertainties of the system components

Component	**Parameter**	**Reference Measurement**			**Systematic Error (%)**	**Uncertainty (%)**
		1	**2**	**3**		
Wanptek DC Power Supply DPS3010 U	Voltages (V)	1.98	1.98	1.97	0.0033	0.0058
Gamry Reference 3000 Potentiostat/ Galvanostat	Applied potential (V)	81.34	81.35	81.33	0.01	0.01
Mastercraft 052-0060-2 Multimeter	Resistance (Ω)	0.74	0.73	0.73	0.0067	0.0058
Urea Flowmeter	Volumetric flow (ml/min)	10	9.59	9.59	0.27	0.24

CHAPTER 4: ANALYSIS AND MODELLING

In this chapter, we conduct a comprehensive analysis and modelling of Direct Urea-Hydrogen Peroxide Fuel Cells using advanced electrochemical techniques. The performance of the fuel cells is evaluated under various conditions, with data from electrochemical tests analyzed using Gamry ECHEM Analyst 2 software. This analysis provides detailed insights into the efficiency, stability, and overall functionality of the DUHPFCs, helping to understand key factors influencing their performance and potential improvements.

4.1 Thermohydrolysis of Urea in DUHPFC

The thermohydrolysis of urea is a crucial process in the functioning of a direct urea-hydrogen peroxide fuel cell. This process entails the decomposition of urea into its constituent products through the application of heat and water. It significantly influences the fuel cell's efficiency and overall performance. In a DUHPFC, the thermohydrolysis of urea involves several essential chemical reactions that are fundamental to its operation.

The primary thermohydrolysis reaction in a DUHPFC begins with the decomposition of urea, as given by:

$$CO(NH_2)_2 \rightarrow NH_3 + HNCO \quad (4.2)$$

In this reaction, urea ($CO(NH_2)_2$) decomposes in the presence of heat to form ammonia (NH_3) and isocyanic acid (HNCO). This initial step is crucial as urea breaks down due to the application of heat. The ammonia produced is a key reactant in subsequent electrochemical reactions within the fuel cell, while the isocyanic acid (HNCO) serves as an intermediate product that undergoes further hydrolysis. Isocyanic acid reacts with water to produce additional ammonia (NH_3) and carbon dioxide (CO_2).

$$HNCO + H_2O \rightarrow NH_3 + CO_2 \quad (4.3)$$

This stage guarantees the complete conversion of the intermediate isocyanic acid into beneficial chemicals. The electrochemical processes in the fuel cell depend on the ammonia produced in this step as well as the CO_2.

Combining the above two reactions, the overall thermohydrolysis reaction of urea can be summarized as:

$$CO(NH_2)_2 + 2H_2O \rightarrow 2NH_3 + CO_2 \quad (4.4)$$

This coupled reaction shows how urea completely breaks down into carbon dioxide and ammonia. This reaction emphasizes the function of water as a reactant and the significance of keeping the fuel cell system's water levels at a suitable level.

Ammonia and carbon dioxide, the byproducts of thermohydrolysis, subsequently take part in the fuel cell's electrochemical operations. The ammonia produced in Equation 4.3 is further oxidized at the anode as shown in Equation 4.4 and plays an important role in generating electrons and driving the overall reaction.

$$2NH_3 + 6OH^- \rightarrow N_2 + 6H_2O + 6e^- \quad (4.5)$$

In the presence of KOH, the overall reactions produce additional products, integrating into the overall anode reaction as given by:

$$CO(NH_2)_2 + 8KOH \rightarrow N_2 + 6H_2O + K_2CO_3 + 6K^+ + 6e^- \quad (4.6)$$

The cathode reaction involves hydrogen peroxide in the presence of sulfuric acid. In the cathode size, hydrogen peroxide reacts with protons (H^+) from sulfuric acid and electrons (e^-) from the external circuit. This reaction produces water (H_2O) and sulfate ions (SO_4^{2-}), completing the electrochemical circuit. Its given as:

$$3H_2O_2 + 3H_2SO_4 + 6e^- \rightarrow 6H_2O + 3SO_4^{2-} \quad (4.7)$$

Combining the anodic and cathodic reactions, the overall reaction for the DUHPFC is:

$$CO(NH_2)_2 + 8KOH + 3H_2O_2 + 3H_2SO_4 \rightarrow N_2 + K_2CO_3 + 12H_2O + 3K_2SO_4 \quad (4.8)$$

These reactions demonstrate how the inclusion of a nickel-based catalyst greatly enhances the complex chemical processes involved in the thermohydrolysis of urea in a DUHPFC. While producing electrical energy, the anode reaction with KOH and the cathode reaction with H_2SO_4 and H_2O_2 result in harmless byproducts like water and nitrogen. The efficient and effective operation of the fuel cell depends on comprehending and optimizing these processes as well as using catalysts and electrolytes appropriately.

4.2 Thermodynamic and Electrochemical Modelling

The thermodynamic and electrochemical analysis of the proposed system is detailed in this section. In the proposed system, the urea is fed to the anode side to be used as fuel. The half-cell chemical reaction occurring in the presence of a nickel-based catalyst is given by Equation (4.5). The half-cell chemical reaction for the reduction reaction occurring at the cathode is expressed by Equation (4.6). The overall reaction for the DUHPFC is shown by

Equation (4.7). The Gibbs Energy Minimization (GEM) method can be used to determine the thermodynamic equilibrium of overall reaction:

$$(\Delta G_{System})_{T,P} = 0 \quad (4.8)$$

where the total of the product of moles of chemical species I multiplied by the corresponding specific Gibbs energy at constant temperature and pressure is the system's Gibbs energy:

$$G = \sum_i n_i G_i \quad (4.9)$$

The aim is to reduce the system's total Gibbs free energy, which is the sum of the Gibbs free energies of all the participating species. During the operation of a fuel cell, the chemical energy of the reactants undergoes conversion into electrical energy. The electrical cell potential and current output demonstrate the transformation of electrical energy. The maximum cell potential is attained under reversible operating circumstances. The term used to describe this cell potential is the reversible cell potential. The reversible cell potential is stated as the potential difference between two electrodes under standard conditions of 1 atmosphere of pressure and a temperature of 25 °C [71].

$$Er^0 = - \frac{(\Delta GSystem)T,P}{nF} \quad (4.10)$$

where n denotes the number of moles of electrons transferred and F denotes the Farady's constant, $\Delta G(T0,P0)$ denotes the change in Gibbs function at standard conditions. The reversible cell potential varies with changing partial pressures or concentrations of products and reactants of a given reaction. The Nernst equation can be utilized to obtain an expression for the reversible fuel cell potential as a function of these parameters:

$$E_{FC} = E_r - \frac{RT}{nF} \ln(K) \quad (4.11)$$

where K represents the equilibrium constant. The equilibrium constant is defined as the ratio of the molar fractions of reactants to products. The reversible potential is slightly affected at low temperatures when inert gases like nitrogen are present in the reactant streams. The term "EFC" denotes the electrical potential difference across a cell while there is no current flowing through it. When electrical current is extracted from the fuel cell, it experiences several voltage losses within the fuel cell that must be considered. The fuel cell voltage can be represented or described as:

$$V_{FC} = E_{FC} - V_{act} - V_{ohm} - V_{conc} \quad (4.12)$$

The activation overpotential, denoted as $Vact$, arises from the resistance of the electrochemical reaction at the electrodes. Moreover, in electrochemical processes, the atoms and molecules of the reactant are absorbed onto the surface of the electrode. The concurrent physiochemical processes also impact the activation overpotential. The Butler-Volmer equation establishes a relationship between the activation overpotential and the current density.

$$J=J_0\{\exp(\frac{\alpha nFVact}{RT})- \exp(-\frac{(1-\alpha)nFVact}{RT})\} \quad (4.13)$$

where J_0 represents the exchange current density. The exchange current density refers to the current density at which the rates of the backward and forward reactions are in equilibrium. Therefore, the charges passing through the boundary between the electrolyte and electrode are identical, resulting in an equal reduction of products and oxidation of reactants in the electrochemical reaction occurring in the half-cell. Furthermore, the exchange current density serves as an indicator of the level of ease with which an electrochemical reaction takes place. The variable α represents the transfer coefficient. The transfer coefficient is contingent upon the electrode reaction. The temperature is represented by T, the gas constant is represented by R, the number of moles of electrons transported is represented by n, and Faraday's constant is represented by F. The activation overpotential is denoted by the symbol $Vact$. Equation (4.13) can be rearranged for large electrode over potentials, to obtain a general expression for the activation overpotential:

$$V_{activation}= \frac{RT}{\alpha nFVact}\ln(\frac{J}{J0}) \quad (4.14)$$

The equation mentioned above is commonly known as the Tafel equation. The overall activation overpotential for the fuel cell can be calculated by adding together the cathodic and anodic activation overpotentials.

$$V_{act}=V_{act,C} + V_{act,A} \quad (4.15)$$

where the cathodic and anodic over potentials can be determined according to equation (4.14):

$$V_{act,\,i} = \frac{RT}{\alpha nF}\ln(\frac{J}{J0,i}) \quad (4.16)$$

The subscript i indicates whether it refers to the anode or cathode. Equations for DUHPFC indicate that a total of 6 moles of electrons (n) are involved in the electrochemical reactions. The anodic and cathodic exchange current densities fluctuate

based on the processes taking place nearby. An increase in fuel cell current density leads to a corresponding rise in the rate of electrochemical reaction, which is necessary to meet the demand for electron transfer. As the reaction rates escalate, the reactants are depleted more rapidly at the electrodes. Nevertheless, the rate at which the reactants are transferred is restricted. As a result, the presence of reactants near the potential sites for reaction is restricted. In addition, as the reactants provided by the feed are transformed into products, these products have the potential to excessively accumulate at the locations of the reaction.

Additionally, this impedes the transportation of fresh reactant molecules to the sites of the reaction. This phenomenon imposes a maximum threshold on the quantity of electric current that can be extracted from the cell. The greatest current density that may be extracted from the fuel cell is known as the limiting current density. As the current density nears the maximum current density, the maximum rate of mass transfer prevents any further rise. The phenomena of polarization loss resulting from this is referred to as concentration overpotential ($Vconc$). For a given half-cell reaction at an electrode, the limiting current density can be expressed as:

$$J_L(x) = \frac{\mathrm{nFCi,avg}}{\mathrm{L/D^{eff}_{a-b}}} \tag{4.17}$$

where n denotes the number of moles of participating electrons, F represents the Faraday's constant, Ci,avg denotes the average concentration of specie i, L denotes the thickness of the porous layer, $D^{eff}{}_{a-b}$ represents the effective diffusion coefficient of specie a in specie b. The average concentration of specie a can be determined as:

$$C_{a,avg}(x)=C_{a,avg,i}\ e^{-hmx/bvavg} \tag{4.18}$$

where $C_{a,avg,i}$ denotes the average concentration of specie a at the inlet of the flow channel, b represents the width of the flow channel, $vavg$ denotes the average velocity of flow, x represents the flow distance, hm denotes the mass transfer coefficient that can be obtained from:

$$Sh = \frac{\mathrm{hmDh}}{\mathrm{D}} \tag{4.19}$$

The symbol Sh indicates the Sherwood number, D represents the diffusion coefficient, and Dh represents the hydraulic diameter. The concentration polarization can be calculated based on the value of the limiting current density. The total concentration overpotential can be expressed as:

$$Vconc = Vconc,a + Vconc,c \quad (4.20)$$

In addition, when current is extracted from the cell, the voltage losses caused by the electrical resistances within the cell are referred to as Ohmic overpotentials. The Ohmic overpotential ($Vohm$) can be determined by doing calculations.

$$Vohm = JR \quad (4.21)$$

where R represents the total electrical resistance within the cell and J denotes the current density.

4.3. Electrochemical Impedance Spectroscopy Modeling

Electrochemical cells contain many sorts of impedances. These impedances obstruct the flow of electric current through the cell. A perfect resistor limits the passage of electric current in accordance with the mathematical relationship known as Ohm's law:

$$I = VR \quad (4.22)$$

A perfect resistor's resistance remains constant regardless of the frequency and always follows Ohm's law. Nevertheless, there are additional varieties of circuit components that rely on the frequency of signals. These components consist of inductors and capacitors. The impedance of a resistor can be determined solely by its resistance, as the flow of electrons is unaffected by the frequency:

$$Zresis = R \quad (4.23)$$

In the case of a capacitor, the relation between the capacitance, impedance and frequency can be expressed as follows:

$$Zcap = \frac{1}{\mathrm{jwC}} \quad (4.24)$$

where C denotes the capacitance and w represents the frequency. Furthermore, the impedance of an inductor element can be evaluated from the relation:

$$Zind = jwL \quad (4.25)$$

where L denotes the element inductance and w denotes the frequency. Opposite charges can accumulate at the interfaces of components in an electrochemical cell, resulting in the formation of an electrical double layer. This exhibits the characteristics of a capacitor, which is an electrical circuit component that experiences charge separation. An inductor is an electrical conductor that releases or stores energy by creating a magnetic field because of the flow of electric current. Within a fuel cell, there are electrical conductors that exhibit comparable behavior to an inductor when current flows through them. Furthermore, the

fuel cell exhibits additional resistances, such as charge transfer resistance and mass transfer resistance. The charge transfer resistance refers to the limitations placed on the movement of electrons and ions within the electrochemical cell. Mass transfer resistance refers to the impediment that affects the diffusion of interacting substances within the fuel cell.

Electrochemical impedance spectroscopy (EIS) utilizes methodologies to assess the impedances within the cell. The potentiostat generates abrupt voltage pulses in a sinusoidal rhythm. The currents that are produced are measured and recorded, including their magnitudes and phase angles. There are multiple models available that accurately depict the impedance elements within the cell. The EIS approach is gaining more interest because it is a non-destructive testing technique [72,73]. The impedances comprise of real and imaginary parts and the magnitudes can be determined as:

$$|Z|=\sqrt{Zreal^2 + Zimag^2} \tag{4.26}$$

In addition to this, the phase angle can be expressed as:

$$\phi = \tan{-}1\frac{\mathrm{Zimag}}{\mathrm{Zreal}} \tag{4.27}$$

The EIS approach yields data that are seen using Nyquist and Bode graphs. The Nyquist plot is a graphical representation of impedance data, where the real parts are plotted on the x-axis and the imaginary parts are plotted on the y-axis, with different frequencies being considered.

The energy and exergy efficiencies of the fuel cell system can be defined as the total useful energy or exergy output divided by the total energy or exergy input:

$$\eta en, _{FC} = \frac{W_{FC}}{N_{urea} LHV_{urea}} \tag{4.28}$$

$$\eta ex, _{FC} = \frac{W_{FC}}{N_{urea} ex_{urea}} \tag{4.29}$$

where WFC denotes the power output of the fuel cell, Nurea represents the molar flow rate of the urea input and LHV_{urea} denotes the lower heating value of urea and ex_{urea} represents the specific molar exergy of urea.

CHAPTER 5: RESULTS AND DISCUSSION

In this chapter, the modeling and experimental results for the developed DUHPFC are presented, analyzed, and discussed for both single cell and fuel cell stack configurations. Comprehensive electrochemical tests were conducted on both the single cell and the stack at different concentrations and cell temperatures to evaluate the performance of the fuel cell. Before constructing the fuel cell, parametric studies were carried out using an H-type electrolytic cell to determine the optimum conditions by evaluating cell performance at various cell temperatures, urea, and KOH concentrations. The analysis and discussion of the test results from these parametric studies are also included in this section. Additionally, the newly developed anode electrode for the DUHPFC, with its catalyst coating, was electrochemically tested, and the results of these tests are discussed here. All electrochemical tests were performed using the Gamry Reference 3000 instrument.

5.1 New Anode Electrode Layer Developed For DUHPFC

In this section, we present the performance results of the newly developed anode electrode layer for DUHPFC, which employs stainless steel foil coated with nickel zinc iron oxide through an electrodeposition technique, showcasing its enhanced catalytic activity, electrical conductivity, and stability under operational conditions, as evidenced by electrochemical tests.

5.1.1 Coated Electrode and Deformations

The newly developed anode electrode for the DUHPFC is presented here. Stainless steel foil coated with nickel zinc iron oxide was used as the anode electrode. The catalyst was deposited onto the stainless-steel foil using an electrodeposition technique at 2 V.

Nickel zinc iron oxide was chosen as the anode catalyst due to its numerous advantages. Firstly, it exhibits high catalytic activity, which is essential for promoting the oxidation of urea at the anode, thereby enhancing the overall efficiency and power output of the fuel cell. Additionally, nickel zinc iron oxide possesses excellent electrical conductivity, ensuring efficient electron transfer during electrochemical reactions. This property is crucial for the effective operation of the anode and contributes significantly to the fuel cell's performance. The material's stability under operating conditions is another important factor; it resists corrosion and degradation, which prolongs the anode's lifespan and maintains consistent performance over time. Moreover, compared to noble metal

catalysts like platinum, nickel zinc iron oxide is more cost-effective, making the production of fuel cells economically viable without compromising on performance.

The electrodeposition technique used for coating the anode electrode involves a series of well-defined steps. Initially, an electrolyte solution containing nickel zinc iron oxide, hydrochloric acid (HCl), and Copper (II) chloride is prepared. The nickel zinc iron oxide provides the catalytic material, while HCl acts as a supporting electrolyte, enhancing the solution's conductivity. Copper (II) chloride assists in the electrodeposition process by facilitating the transfer of metal ions.

During the electrodeposition process, the stainless-steel foil (working electrode) and a platinum (Pt) counter electrode are placed in the prepared electrolyte solution. The electrodes are connected to a power supply, and a constant voltage of 2 V is applied between the working electrode and the counter electrode. This voltage drives the reduction of metal ions in the solution, causing the nickel zinc iron oxide to deposit onto the surface of the stainless-steel foil. The platinum counter electrode facilitates this process by providing a stable and inert reference point for the current flow.

The deposition process is carried out for 30-40 minutes, which is critical to ensure a uniform and complete coating of nickel zinc iron oxide on the stainless-steel foil. The extended deposition time allows the catalyst layer to build up to an optimal thickness, enhancing its electrochemical performance. The application of 2 V causes the nickel zinc iron oxide particles in the solution to migrate towards the stainless-steel foil and adhere to its surface, resulting in a uniform and adherent layer.

Once the electrodeposition process is complete, the coated stainless-steel foil is removed from the electrolyte solution and thoroughly rinsed with deionized water to remove any residual chemicals. The coated foil is then dried and inspected to ensure that a uniform and adherent layer of nickel zinc iron oxide has been achieved. The successful application of this electrodeposition technique results in a robust anode electrode with enhanced catalytic properties, contributing to the improved performance and efficiency of the DUHPFC.

The state of the anode electrode, prepared to enhance the fuel cell's performance using the specified methods, immediately after coating and 1-2 days post-coating is shown in Figure 5.1.

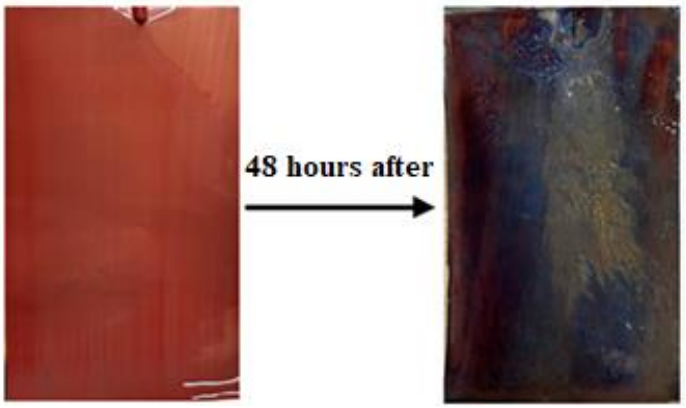

(a) (b)

Figure 5.1 The state of the prepared anode catalyst, (a) immediately after coating and (b) 48 hours after coating

Upon examining the state of the prepared anode catalyst immediately after coating and 48 hours after coating, several observations can be made regarding the changes and potential reasons behind them. Immediately after coating, the surface of the anode catalyst is smooth and uniformly coated with a reddish-brown color, indicative of a fresh nickel zinc iron oxide layer. The uniform appearance suggests that the electrodeposition process was successful in depositing a consistent layer of the catalyst on the stainless-steel foil. In contrast, 1-2 days after coating, the anode catalyst exhibits significant changes. The surface shows signs of discoloration, with a noticeable shift to darker hues, including areas of blue and black. Additionally, there are visible signs of corrosion or oxidation, with irregular patterns and spots on the surface. The overall appearance indicates degradation and potential chemical reactions that occurred over the 1–2-day period.

The discoloration from reddish-brown to darker hues can be attributed to the oxidation and chemical reactions occurring on the surface of the nickel zinc iron oxide coating. When exposed to the environment, especially in the presence of moisture and oxygen, nickel zinc iron oxide can undergo further oxidation, forming nickel and iron oxides or hydroxides that exhibit darker colors. The visible corrosion and surface degradation are likely due to the interaction between the anode catalyst and the ambient environment. Factors such as humidity, temperature fluctuations, and exposure to atmospheric gases (e.g., oxygen, carbon dioxide) can accelerate corrosion processes. The presence of HCl in the initial electrolyte solution might also leave residual traces that contribute to ongoing chemical reactions, further degrading the surface. The blue and black

spots observed could be the formation of nickel and iron hydroxides or oxides. These compounds form because of the reaction between the metallic elements in the coating and water or oxygen in the air. The process is typically accelerated in environments with higher humidity or other reactive substances.

The prepared anode catalyst showed a significant transformation from its initial state immediately after coating to 1-2 days later. These changes are primarily due to oxidation, corrosion, and the formation of various metal oxides and hydroxides. This highlights the importance of protecting the anode catalyst from environmental exposure and considering additional treatments or coatings to enhance its stability and longevity.

5.1.2 Electrochemical Test Results of Anode Electrode

The electrochemical tests for the developed anode electrode were conducted using the Gamry Reference 3000 instrument. The electrochemical tests performed using the Gamry device included CV, LSV, and EIS. For these tests, the coated anode layer was immersed in a 1 M KOH solution. A platinum electrode served as the counter electrode, while an Ag-AgCl electrode was used as the reference electrode. Once the experimental setup was established, the electrochemical tests were carried out.

These electrochemical tests are crucial for evaluating the performance of the anode coating. CV is employed to study the redox behavior of the electrode material and to determine the potential window in which the electrode operates effectively. LSV is used to assess the electrocatalytic activity of the anode by measuring the current response as the potential is swept linearly. This helps in understanding the oxidation and reduction reactions taking place at the electrode surface. EIS provides insights into the resistance and capacitive behavior of the electrode, which are important for evaluating the charge transfer processes and overall stability of the coating.

By conducting these tests, a comprehensive understanding of the electrochemical properties and performance of the coated anode layer is obtained, ensuring its suitability and efficiency for use in the DUHPFC. Figure 5.2 shows the LSV test measurements conducted on the developed anode layer. This test was repeated three times, and the results from each individual test are presented.

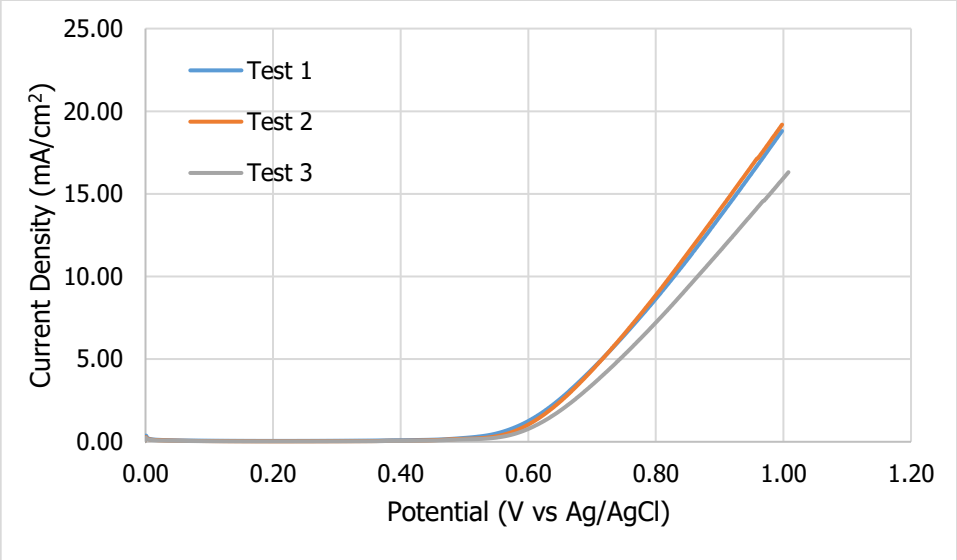

Figure 5.2 LSV measurements of anode electrode in 1 M KOH solution at 25°C

The results from the three tests are remarkably consistent under the same conditions, as indicated by the overlapping nature of the curves. This consistency suggests that the electrodeposition process produced a uniform and stable coating on the stainless-steel foil. The reproducibility of the results is critical in confirming the reliability of the anode's performance under similar conditions. The increase in current density with increasing potential demonstrates the electrocatalytic activity of the anode. At potentials above approximately 0.6 V, a sharp rise in current density is observed, indicating the onset of significant electrochemical reactions. This behavior is typical for anodic oxidation processes, where higher potentials facilitate greater electron transfer rates and thus higher current densities.

The maximum current density achieved in these tests approaches 25 mA/cm^2, which is a positive indication of the anode's capability to facilitate efficient oxidation reactions. The similar performance observed across all three tests indicates that the anode layer may maintain its integrity and catalytic activity over multiple uses, which could be beneficial for practical applications in fuel cells. The potential at which current density begins to increase significantly is around 0.6 V vs Ag/AgCl. This onset potential is a critical parameter, as it indicates the voltage required to initiate the oxidation reactions effectively. The relatively low onset potential observed here suggests that the nickel zinc iron oxide

coating provides a favorable environment for electrochemical reactions, likely due to its high catalytic efficiency and good electrical conductivity.

Figure 5.3 shows the Bode plot obtained from the EIS electrochemical test for the anode electrode.

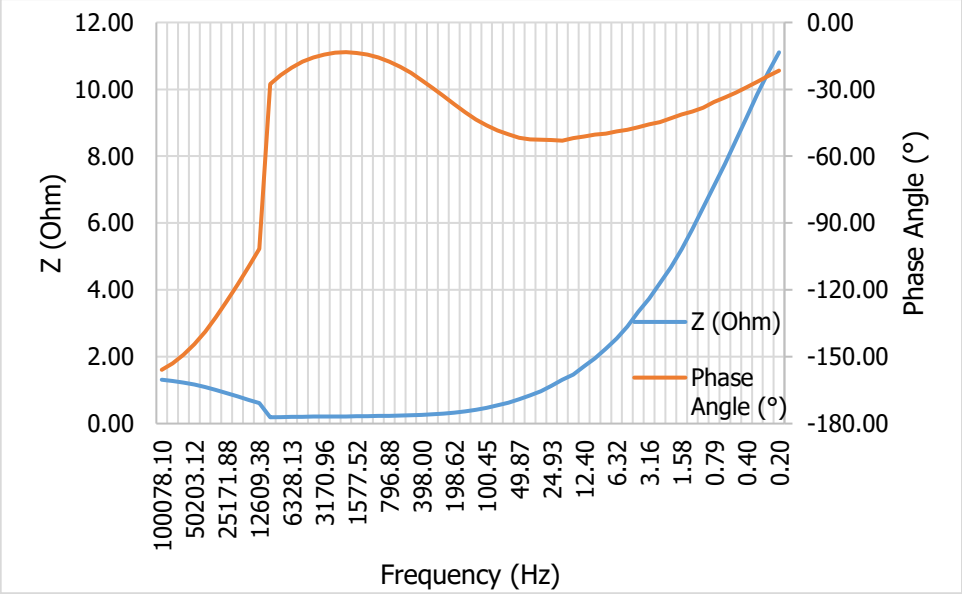

Figure 5.3 Bode plot of anode electrode obtained from the EIS

From the Bode plot, several key observations can be made. At high frequencies, the impedance is relatively low, which is characteristic of the resistive behavior of the electrolyte and the electrode material. As the frequency decreases, the impedance increases, indicating the capacitive behavior of the electrode interface. This increase in impedance at lower frequencies suggests the presence of charge transfer resistance and double-layer capacitance at the electrode surface. The phase angle curve shows a peak at mid frequencies, which corresponds to the frequency range where the capacitive and resistive behaviors intersect. This peak indicates the presence of a dominant time constant in the electrochemical system, likely related to the charge transfer processes at the electrode interface.

The shape of the Bode plot is typical for electrochemical systems, where a combination of resistive and capacitive elements influences the impedance response. The low impedance at high frequencies indicates good conductivity of the electrode material, while the increase at low frequencies suggests some resistance to charge transfer, which

could be due to surface phenomena or the inherent properties of the nickel zinc iron oxide coating.

Figure 5.4 shows the Nyquist plot obtained from the EIS electrochemical test for the anode electrode.

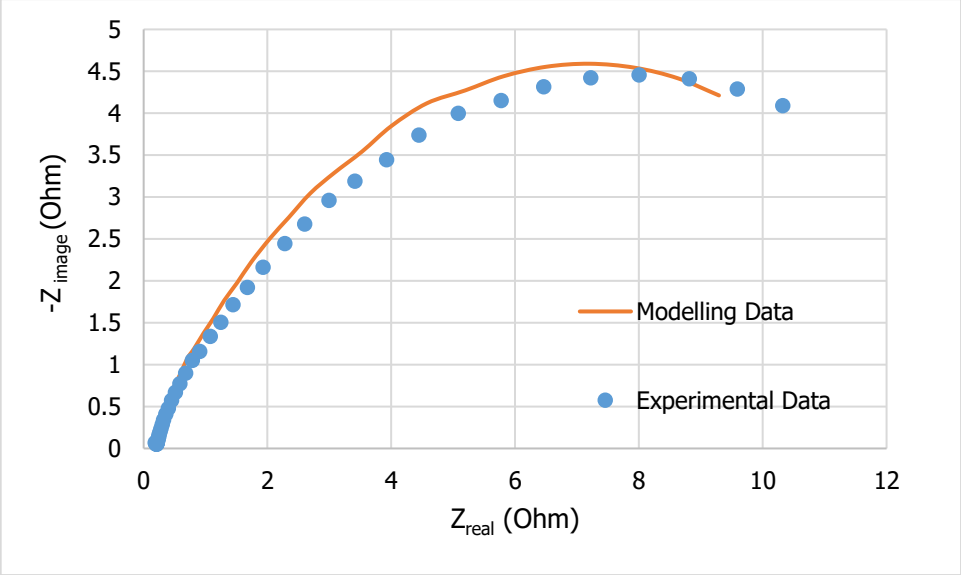

Figure 5.4 Nyquist plot of anode electrode obtained from the EIS

In the Nyquist plot, the data points form a semicircular arc, which is indicative of a single charge transfer process dominating the impedance response. The diameter of the semicircle corresponds to the charge transfer resistance of the electrode. A smaller semicircle would indicate lower charge transfer resistance, suggesting more efficient electrochemical activity. In this plot, the experimental data (blue dots) closely follow the modeling data (orange line), indicating a good fit between the experimental measurements and the theoretical model. In this Nyquist plot, the blue dots represent the raw experimental data collected during the electrochemical impedance spectroscopy (EIS) analysis, while the orange line represents the modeling data, which is a theoretical interpretation generated from the same experimental dataset using Gamry Echem software. This modeling data is not the result of curve fitting; rather, it is directly based on the experimental measurements and provides a calculated response that represents the expected behavior of the system under the given conditions. The close correspondence between the experimental and modeling data indicates that the model accurately captures the key characteristics of the electrochemical system. The semicircular arc observed in the plot, with a charge transfer

resistance of approximately 9.5 Ohms (as inferred from the diameter of the semicircle), signifies a dominant charge transfer process. This alignment between the experimental and modeled data underscores the reliability and consistency of the electrochemical analysis performed.

The intercept at the Z axis (real part of the impedance) at high frequencies represents the solution resistance, which includes the resistance of the electrolyte and any other series resistances in the system. The semicircle's size and shape provide valuable information about the kinetics of the electrochemical reactions occurring at the electrode surface.

The good agreement between the experimental data and the modeling data suggests that the electrochemical behavior of the nickel zinc iron oxide coated anode can be accurately described by the equivalent circuit model used. This model typically includes elements representing the solution resistance, charge transfer resistance, and double-layer capacitance. Together, these EIS plots demonstrate that the nickel zinc iron oxide coating exhibits good conductivity and moderate charge transfer resistance, making it a promising candidate for use in DUHPFCs. Further composition could potentially reduce the charge transfer resistance and enhance the overall electrochemical performance [75,76,77].

5.2 The Parametric Tests Conducted Using an H-Type Electrolytic Cell For DUHPFC

Before conducting single-cell and stack tests and analyses, parametric studies were performed using an H-type Electrolytic Cell to evaluate the performance of the DUHPFC. These parametric studies involved varying urea concentrations, KOH concentrations, and cell temperatures. The primary objective was to observe the conditions under which the membrane electrode assembly (MEA) operates optimally by altering these parameters. By adjusting the parameters, the voltage values produced by the cell over time were measured. This approach allowed for a comprehensive assessment of the performance under different conditions to identify the optimal operating parameters for the MEA.

5.2.1 Investigation of Effect of Cell Temperature on DUHPFC

Under this heading, the effect of temperature on cell performance was investigated through parametric studies conducted using an H-type electrolytic cell. The urea concentrations were set at 0.33 M, 0.5 M, and 1 M, while the KOH concentrations were established at 1 M, 5 M, and 9 M. These specific concentrations were chosen to cover a wide range of

operating conditions, from low to high concentration, to thoroughly understand their influence on the performance of the cell. By keeping the urea and KOH concentrations constant, the voltage values produced by the cell over time were measured at temperatures of 25°C, 35°C, 45°C, 55°C, and 65°C. The selection of these urea concentrations was based on common ranges used in similar fuel cell studies to optimize the balance between fuel availability and catalytic efficiency. Lower concentrations such as 0.33 M provide a baseline for performance, while higher concentrations up to 1 M ensure sufficient fuel presence to drive the reactions. Similarly, the KOH concentrations were chosen to explore the effect of electrolyte strength on cell performance. A 1 M KOH solution represents a standard electrolyte concentration, 5 M KOH provides a medium strength condition, and 9 M KOH represents a highly concentrated scenario. This range helps in identifying the optimal electrolyte concentration that balances conductivity and minimizes resistive losses. By systematically varying the temperature while keeping the urea and KOH concentrations constant, the study aims to identify the temperature at which the cell operates most efficiently.

In this part, the anolyte parameters were continuously varied, while the catholyte solution consisted of 2 M H_2SO_4 with 2 M H_2O_2. Figure 5.5 illustrates the measured voltage values of the cell containing 1 M KOH with 0.5 M urea as the anolyte at different temperatures.

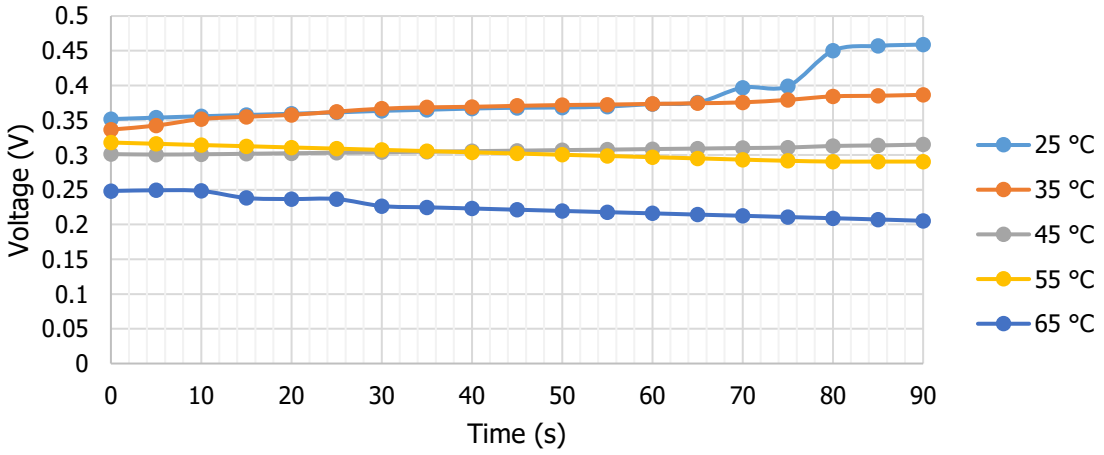

Figure 5.5 The voltage values of the cell containing 1 M KOH with 0.5 M urea as the anolyte at different temperatures over time

The results indicate that the cell voltage is inversely proportional to temperature at certain ranges, with the lowest voltage observed at 25°C, approximately 0.23 V, and the highest voltage observed at 55°C, around 0.37 V. This suggests that while an increase in temperature generally enhances electrochemical activity up to a certain point, beyond 55°C, the voltage begins to decline slightly, indicating that excessively high temperatures may negatively impact cell performance.

Figure 5.6 illustrates the measured voltage values of the cell containing 5 M KOH with 0.5 M urea as the anolyte at different temperatures.

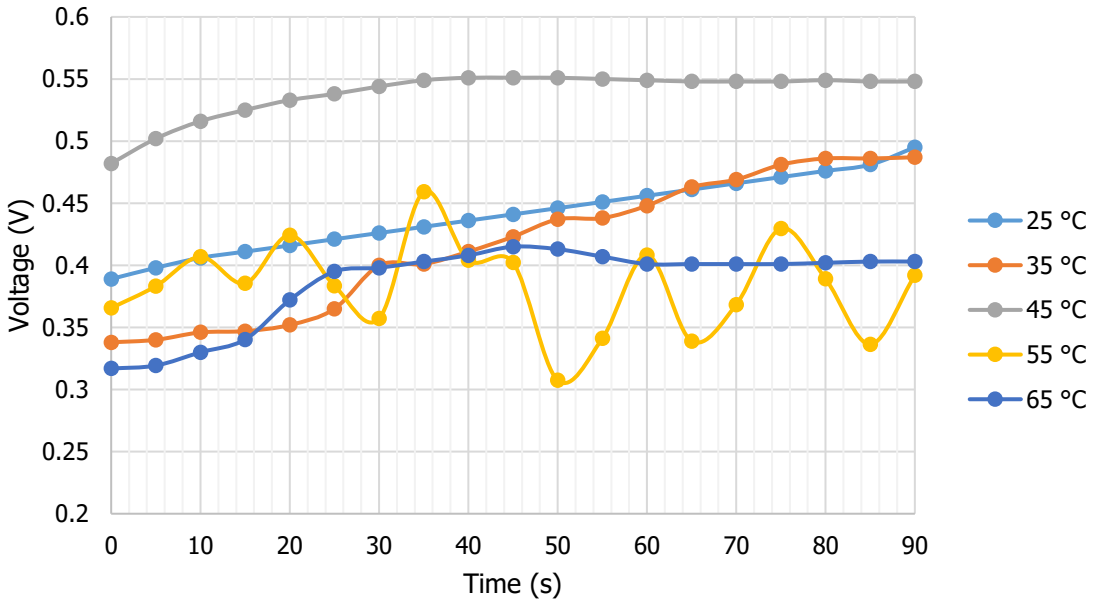

Figure 5.6 The voltage values of the cell containing 5 M KOH with 0.5 M urea as the anolyte at different temperatures over time

The results indicate that while higher temperatures generally improve the voltage output, there is an optimal temperature range (around 45°C) where the performance is maximized, reaching approximately 0.55 V. This behavior can be attributed to the increased reaction kinetics at moderate temperatures, which enhance the electrochemical activity and efficiency of the cell. However, at temperatures of 55°C and above, the voltage shows significant fluctuations and begins to decline. This decline is likely due to the onset of instability within the cell, possibly caused by increased electrolyte degradation or side reactions that occur at these higher temperatures, leading to reduced efficiency.

This pattern was not as prominent in previous tests with lower KOH concentrations, suggesting that the higher concentration used in this test amplifies the thermal sensitivity of the cell. This difference highlights the importance of optimizing both temperature and electrolyte concentration to maintain stable and efficient cell operation.

Figure 5.7 illustrates the measured voltage values of the cell containing 9 M KOH with 0.5 M urea as the anolyte at different temperatures.

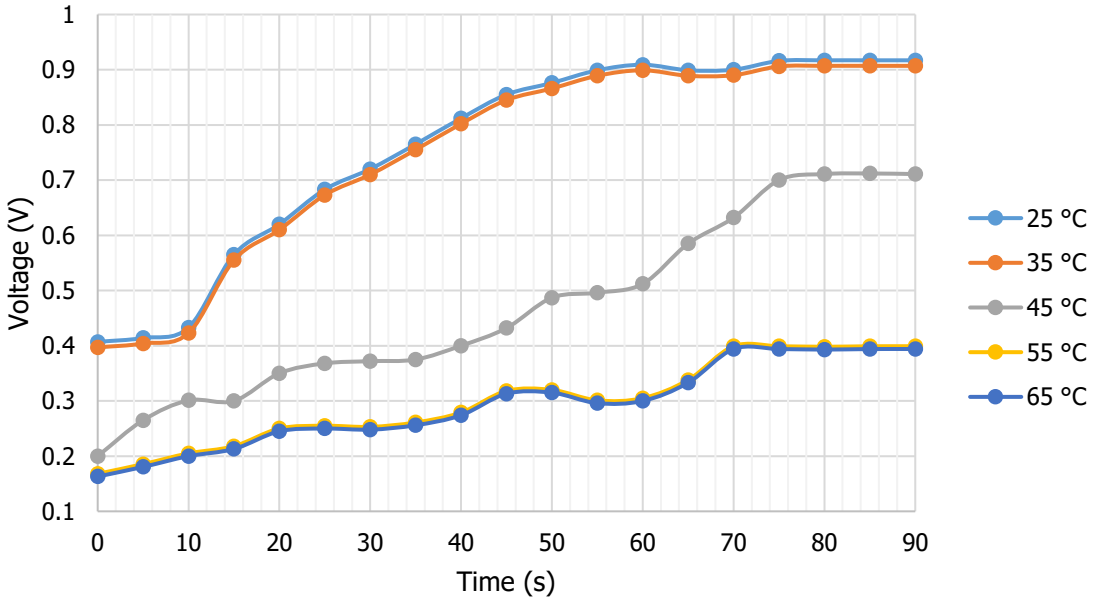

Figure 5.7 The voltage values of the cell containing 9 M KOH with 0.5 M urea as the anolyte at different temperatures over time

In the graph, the cell voltage at 25°C consistently performs better than at 35°C, with the voltage reaching higher levels and maintaining stability throughout the duration of the test. At 25°C, the voltage rises steadily and stabilizes around 0.9 V, which is higher than the voltage at 35°C, where it stabilizes just below 0.9 V. This suggests that the cell operates more efficiently at 25°C compared to 35°C. At 45°C, the voltage stabilizes at a lower value of around 0.7 V, indicating that while the cell still functions, it is less efficient than at lower temperatures. At 55°C and 65°C, the voltage values are even lower, stabilizing around 0.5 V and 0.4 V, respectively, indicating a significant decrease in cell performance at these higher temperatures. Overall, the graph demonstrates that 25°C is the most optimal temperature for this cell, providing the highest and most stable voltage, while higher temperatures lead to decreased efficiency and performance.

Figure 5.8 illustrates the measured voltage values of the cell containing 1 M KOH with 1 M urea as the anolyte at different temperatures.

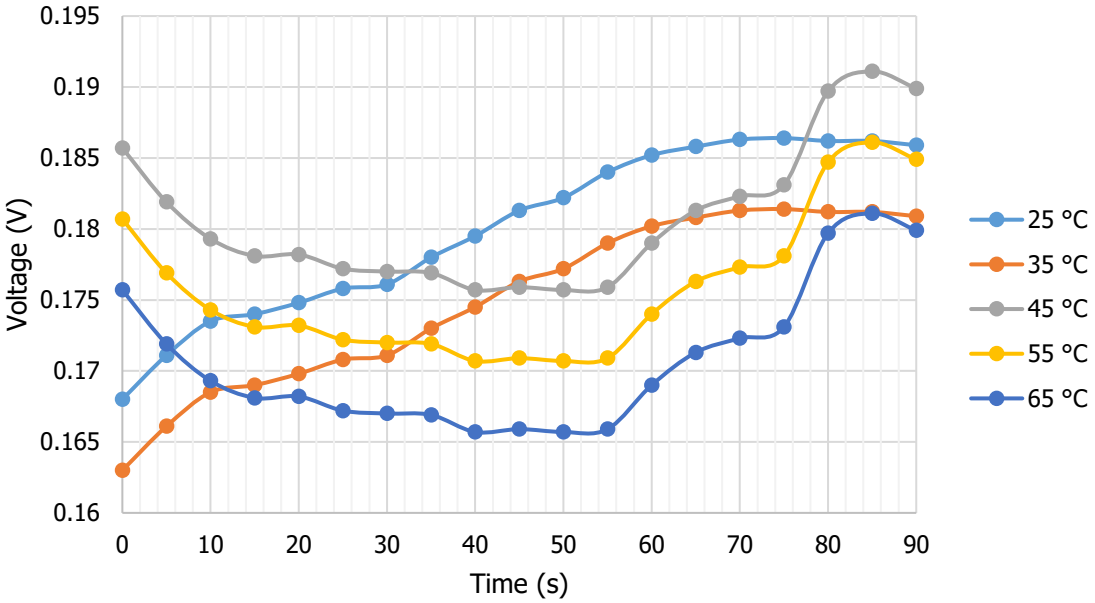

Figure 5.8 The voltage values of the cell containing 1 M KOH with 1 M urea as the anolyte at different temperatures over time

This graph shows that the voltage output is highest and most stable at 45°C, indicating that this temperature is optimal for the given anolyte composition. The performance at 35°C and 55°C is also relatively high but slightly lower than at 45°C. At 25°C and 65°C, the voltage values are lower, indicating reduced efficiency at these temperatures. The data suggest that moderate temperatures around 45°C provide the best performance, while extremes at both low and high temperatures result in decreased efficiency.

Figure 5.9 illustrates the measured voltage values of the cell containing 5 M KOH with 1 M urea as the anolyte at different temperatures. The highest and most stable voltage is observed at 25°C, suggesting that this temperature provides optimal performance for this anolyte composition. At higher temperatures, the voltage values are lower and relatively stable but do not match the performance at 25°C. The voltage slightly decreases as the temperature increases, indicating that higher temperatures negatively impact performance. Further testing beyond 90 seconds at 25°C demonstrated that the voltage continued to stabilize, confirming the consistency and reliability of the cell's performance at this

temperature. Therefore, for the 5 M KOH with 1 M urea anolyte, lower temperatures around 25°C are preferable for achieving higher and more stable voltage outputs.

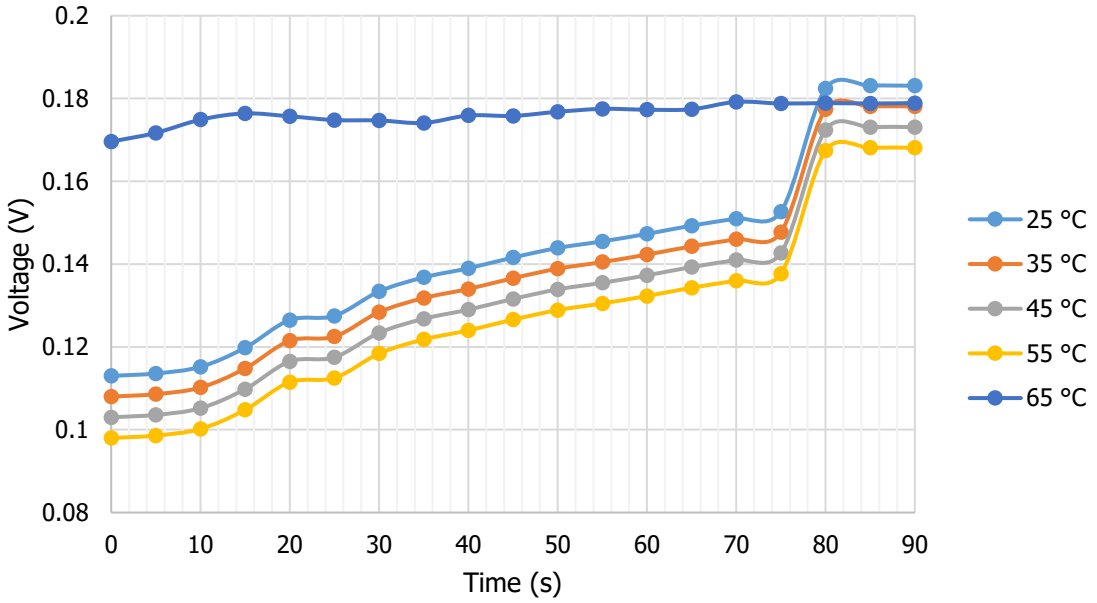

Figure 5.9 The voltage values of the cell containing 5 M KOH with 1 M urea as the anolyte at different temperatures over time

Figure 5.10 illustrates the measured voltage values of the cell containing 9 M KOH with 1 M urea as the anolyte at different temperatures. It indicates that the highest voltage is observed at 35°C, suggesting that this temperature provides optimal performance for the cell with this anolyte composition. The voltage at 45°C is also relatively high but slightly lower than at 35°C. At 55°C and 65°C, the voltage values are significantly lower, indicating reduced performance at these higher temperatures. The lowest voltage is observed at 25°C, where the performance is the least efficient.

For 0.33 M urea concentration, Figure 5.11 illustrates the measured voltage values of the cell containing 1 M KOH with 0.33 M urea as the anolyte at different temperatures. The graph indicates that the highest voltage is consistently observed at 25°C, suggesting that this temperature provides the best performance for this anolyte composition. At higher temperatures, the voltage values are lower and more consistent, but none surpass the performance at 25°C. Among the higher temperatures, 35°C shows the lowest voltage. These results suggest that for the 1 M KOH with 0.33 M urea anolyte, lower temperatures around 25°C are optimal, while increasing temperatures reduce efficiency.

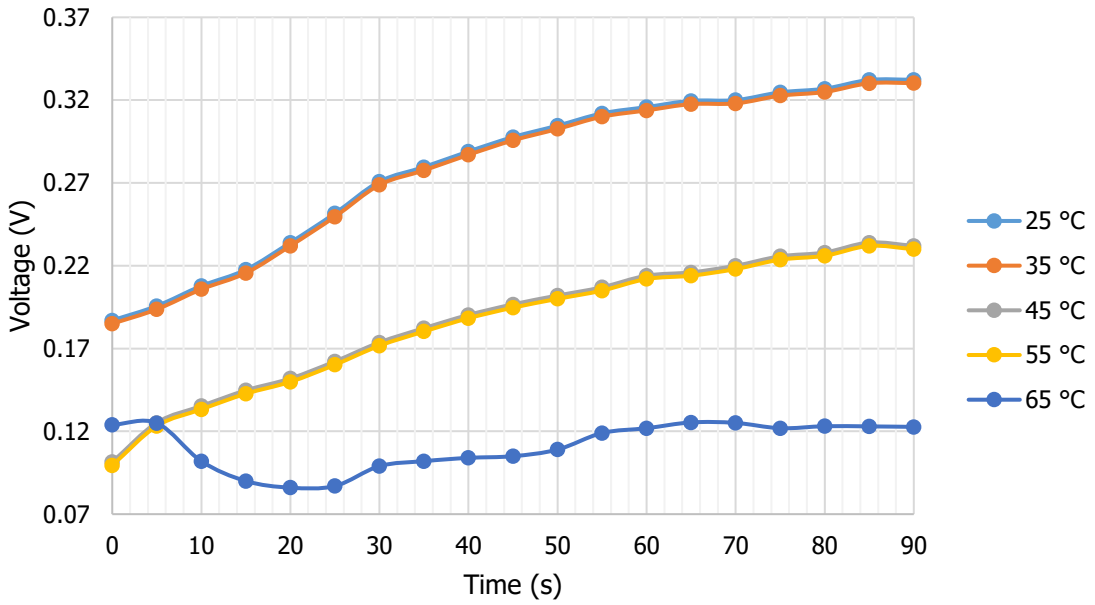

Figure 5.10 The voltage values of the cell containing 9 M KOH with 1 M urea as the anolyte at different temperatures over time

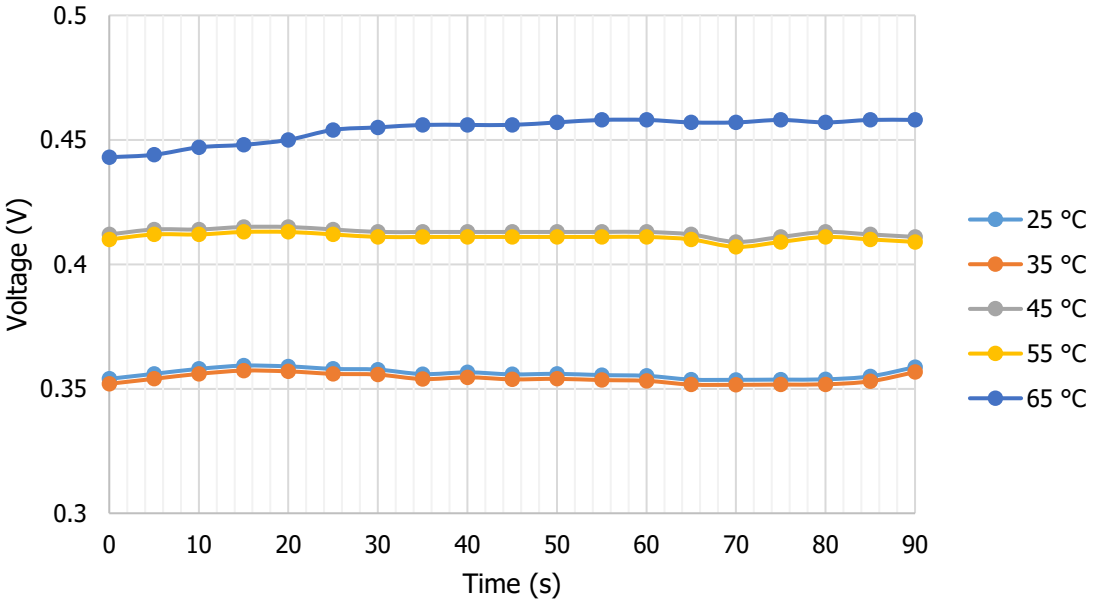

Figure 5.11 The voltage values of the cell containing 1 M KOH with 0.33 M urea as the anolyte at different temperatures over time

Figure 5.12 illustrates the measured voltage values of the cell containing 5 M KOH with 0.33 M urea as the anolyte at different temperatures.

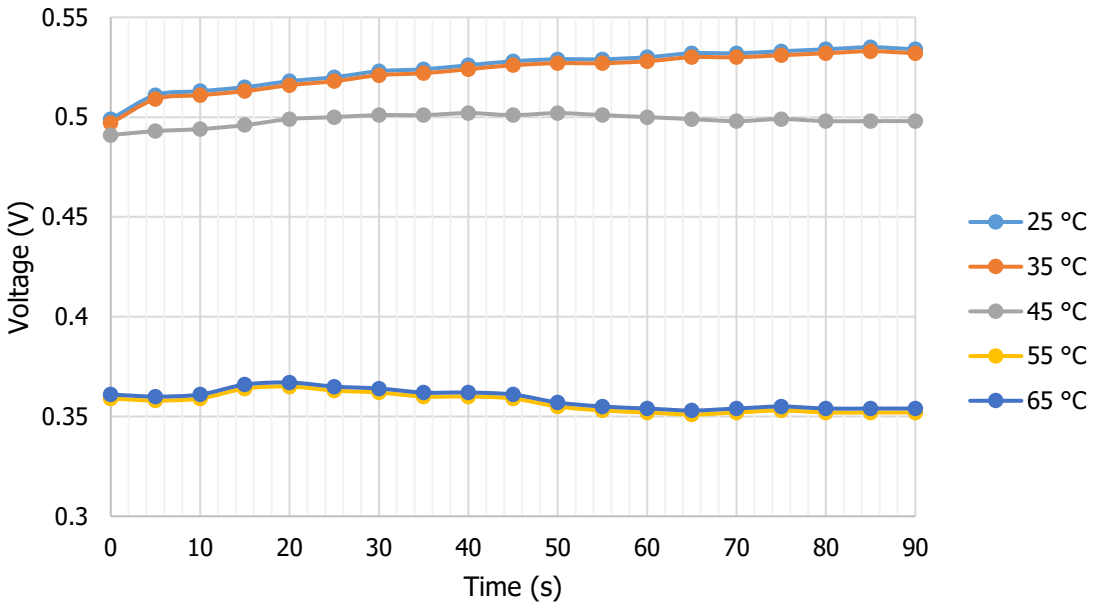

Figure 5.12 The voltage values of the cell containing 5 M KOH with 0.33 M urea as the anolyte at different temperatures over time

The voltage is highest and most stable at 35°C, indicating optimal performance at this temperature. The voltage values at 45°C and 55°C are slightly lower but still relatively stable. At 25°C and 65°C, the voltage is significantly lower, suggesting less efficient performance at these temperatures. This suggests that moderate temperatures around 35°C are ideal for achieving the best performance with this anolyte composition.

Figure 5.13 illustrates the measured voltage values of the cell containing 9 M KOH with 0.33 M urea as the anolyte at different temperatures.

In this figure, the voltage is highest and most stable at 25°C, indicating optimal performance at this lower temperature. The voltage values at 35°C and 45°C are slightly lower but still stable. At 55°C, the voltage fluctuates significantly, suggesting instability in performance. The voltage at 65°C is stable but the lowest among all temperatures, indicating the least efficient performance. These fluctuations at higher temperatures may indicate the influence of dynamic responses within the cell, particularly the development of capacitive behavior as temperature increases. The observed voltage fluctuations, particularly at higher temperatures such as 55°C and 65°C, can be attributed to several underlying electrochemical phenomena. One significant factor is the development of capacitive behavior within the fuel cell. Capacitive behavior arises from the accumulation

and discharge of charges on the electrode surfaces, which can lead to fluctuations in the cell voltage over time. This effect is likely exacerbated at higher temperatures, where increased thermal energy may enhance charge mobility, leading to more pronounced fluctuations. Higher temperatures cause the electrochemical processes in the cell to proceed more quickly, which usually results in better performance. But this acceleration may also set off unintended consequences or other destabilizing mechanisms, which add to the voltage instability that is being seen. Higher temperatures, for example, can speed up undesirable reactions in the electrolyte, including urea breakdown or the emergence of intermediate species, which could lead to variations in the voltage output. Moreover, temperature alters the behavior of the electrolyte itself. As the temperature rises, the ionic conductivity of the KOH and urea combination may change, which could cause an unequal distribution of current across the cell. Voltage swings may be the result of this unequal distribution, especially at temperatures when the electrolyte's behavior becomes less stable or predictable. A possible explanation for these dynamics could be microstructural alterations at the electrode surfaces. The microstructure of the electrodes may change with temperature, affecting the total electrochemical interface as well as the double-layer capacitance. These modifications may have an impact on how charges build up and dissipate, which could intensify the capacitive effects and consequent voltage variations. Despite these fluctuations, the overall performance of the cell at lower temperatures, particularly around 25°C, remains relatively stable and higher compared to higher temperature conditions. This suggests that lower temperatures are preferable for achieving consistent and reliable performance in the DUHPFC system. The stability observed at 25°C can be linked to more controlled reaction kinetics and fewer side reactions, resulting in a more stable and predictable voltage output. This suggests that lower temperatures around 25°C are preferable for achieving higher and more stable voltage outputs with this anolyte composition. Moreover, this temperature-dependent behavior highlights the importance of optimizing operating conditions to balance ionic conductivity and electrochemical stability. Further investigation into the thermal effects on electrode microstructure and reaction pathways could provide deeper insights into improving the long-term durability and efficiency of the DUHPFC system.

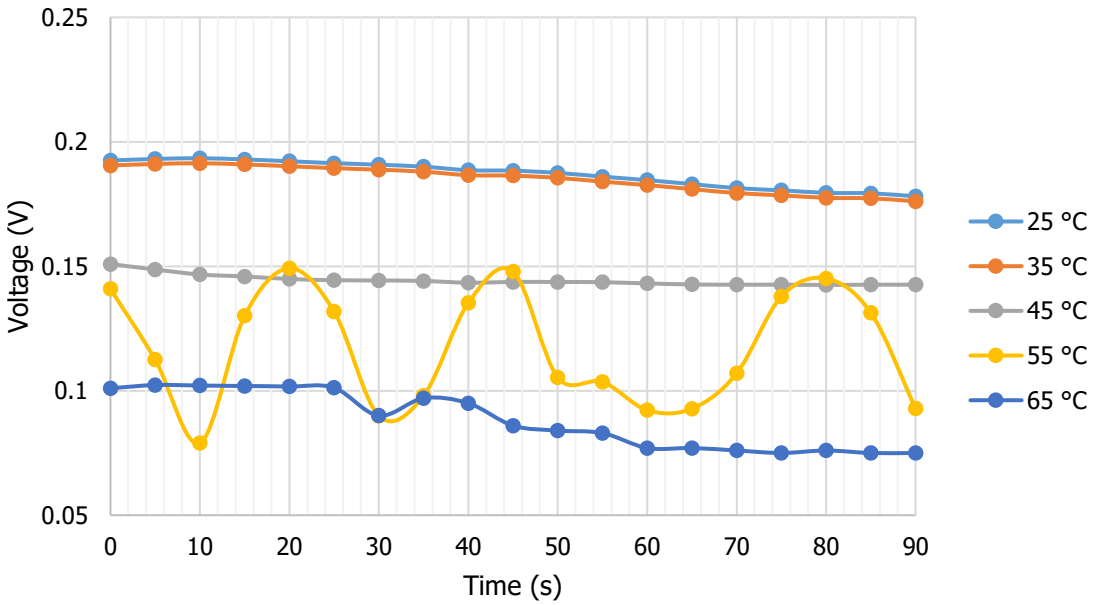

Figure 5.13 The voltage values of the cell containing 9 M KOH with 0.33 M urea as the anolyte at different temperatures over time

Upon examining the graphs, it is evident that temperature has a significant impact on the performance of DUHPFC. Measurements taken for cells with different urea and KOH concentrations indicate that each combination exhibits optimal performance within a specific temperature range. Generally, cells perform best within the moderate temperature range of 25°C to 45°C. Specifically, the combination of 9 M KOH and 0.5 M urea as the anolyte achieves the highest and most stable voltage values at 35°C. These findings suggest that optimal performance depends on the concentrations of urea and KOH, with the best results typically occurring within the lower to moderate temperature range. The optimum performance is obtained with the anolyte concentration of 9 M KOH and 0.5 M urea at a temperature of 35°C. These results underscore the importance of temperature control and the selection of appropriate concentrations in the design and operation of DUHPFC systems.

5.2.2 Investigation of Effect of KOH Concentration on DUHPFC

In this part, the impact of varying KOH concentrations on the performance of DUHPFC has been investigated through parametric studies conducted in an H-type electrolytic cell at 25°C, which was previously determined as the optimal temperature. By analyzing

different concentrations, the aim is to determine the optimal KOH concentration that enhances the efficiency and stability of the fuel cell.

Figure 5.14 shows the voltage values of the cell containing 0.5 M urea with varying concentrations of KOH (1 M, 5 M, and 9 M) as the anolyte at 25°C over time.

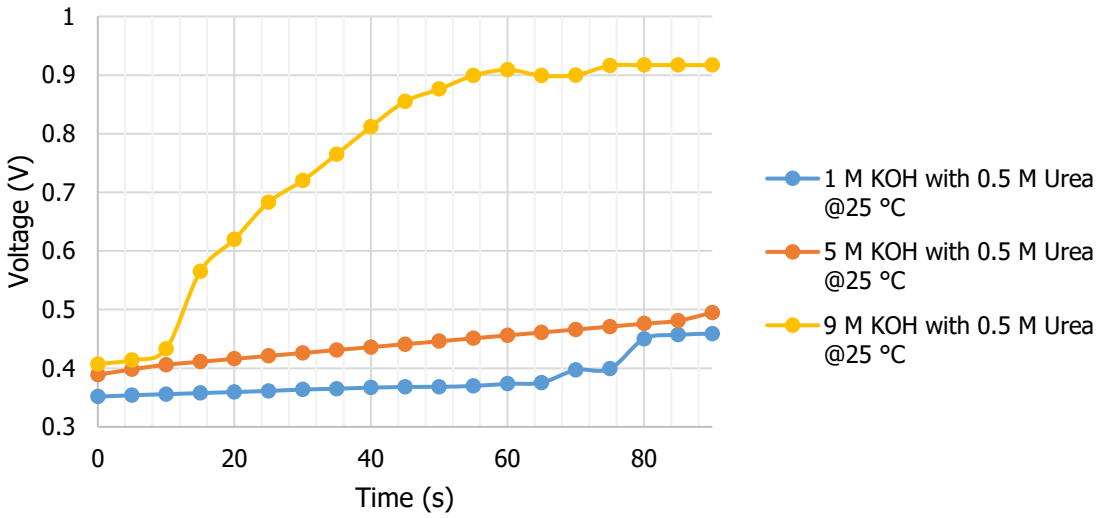

Figure 5.14 Voltage values of the cell containing 0.5 M urea with varying concentrations of KOH at 25°C over time

From this figure, the concentration of KOH significantly affects the cell's performance. The highest and most stable voltage is achieved with 9 M KOH, reaching approximately 0.9 V. This indicates that a higher KOH concentration substantially enhances the electrochemical activity and overall efficiency of the cell. The performance with 5 M KOH is moderate, with a voltage around 0.5 V, showing better performance than 1 M KOH but still significantly lower than 9 M KOH. The lowest performance is observed with 1 M KOH, with a voltage around 0.4 V. As observed in the graph, increasing the KOH concentration leads to higher cell voltage. However, using even higher concentrations could have several effects. Initially, a higher KOH concentration might enhance ionic conductivity, resulting in a further increase in voltage and more efficient electrochemical reactions. However, excessively high concentrations could also promote side reactions, leading to the formation of unwanted products, potential damage to the electrodes, and a loss of voltage stability. There may also be a threshold concentration beyond which the benefits of increased KOH are diminished or even reversed, potentially causing a decrease

in overall cell efficiency. Therefore, determining the optimal KOH concentration is crucial to balancing performance and the longevity of the cell.

These results suggest that increasing the KOH concentration in the anolyte improves the voltage output and stability of the DUHPFC at 25°C. Therefore, for optimal performance, a higher concentration of KOH, such as 9 M, is recommended.

5.2.3 Investigation of Performance Result for Effect of Urea Concentration on DUHPFC

In this part, the performance of DUHPFC will be examined at 25°C with varying urea concentrations using a H-cell electrolytic cell setup. This study follows the previous analysis, where 9 M KOH was selected as the optimal concentration for enhancing cell performance. The aim is to determine the effect of different urea concentrations on the efficiency and stability of the fuel cell under the previously identified optimal conditions. Figure 5.15 shows the voltage values of the cell containing 9 M KOH with varying urea concentrations (0.33 M, 0.5 M, and 1 M) as the anolyte at 25°C over time.

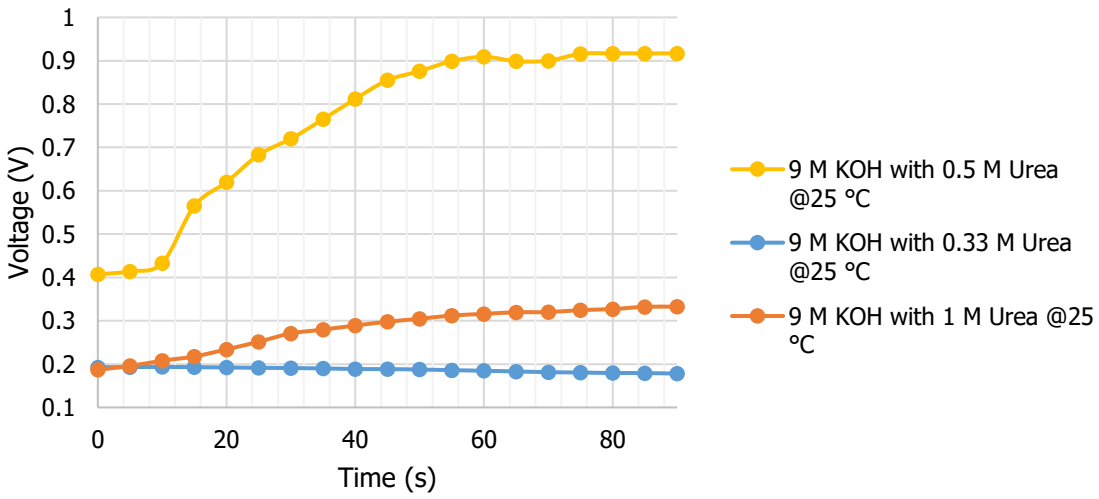

Figure 5.15 The voltage values of the cell containing 9 M KOH with varying urea concentrations at 25°C over time

The graph indicates that the urea concentration has a significant impact on the performance of the DUHPFC. The highest and most stable voltage is observed with 0.5 M urea, reaching approximately 0.9 V. This suggests that 0.5 M urea provides the optimal concentration for efficient electrochemical reactions within the cell.

The performance with 0.33 M urea is significantly lower, with the voltage stabilizing around 0.3 V. This indicates that lower urea concentration is not sufficient to achieve high performance, likely due to insufficient reactant availability for the electrochemical processes. On the other hand, the performance with 1 M urea is better than 0.33 M but still lower than 0.5 M, stabilizing around 0.4 V. This suggests that too high a concentration of urea may also be detrimental, possibly due to increased viscosity or other limiting factors that reduce the efficiency of the cell.

The voltage profile's observed transients, especially the rise and subsequent stabilization exhibited in the 0.5 M urea concentration with 9 M KOH, are representative of the intricate electrochemical reactions taking place inside the cell as it gets closer to equilibrium. The electrochemical system first undergoes a fast alignment of charge transfer mechanisms, ion transport dynamics, and reaction kinetics during cell activation. The development of double-layer capacitance at the electrode-electrolyte interface, which is a key component of the voltage transients that are seen, characterizes this phase. The electrolyte's ions move in the first few minutes to the electrode surfaces, where they take part in the electrochemical reactions. As the system overcomes initial resistive losses and starts to generate a continuous flow of electrons through the external circuit, the voltage rise represents the growing rate of these reactions. This phase is also linked to the alignment of the potential distribution between the electrodes and electrolyte when the cell's electric field stabilizes. The voltage then stabilizes, indicating that the system has reached a dynamic equilibrium where ionic conduction in the electrolyte and the rates of electron transfer at the electrodes are balanced. This balance reduces additional voltage fluctuations and shows that the cell is performing at its best given the reactant concentrations. The concentration of the reactants (urea and KOH), the intrinsic resistance of the cell's constituent parts, and the particular electrode materials employed are some of the variables that affect the size and length of these transients. Higher urea concentrations, for example, might cause more noticeable transients if the system takes longer to reach equilibrium because of higher reaction rates or the presence of side reactions. In a similar vein, the transient response can be impacted by the electrode material's nature, which can change the rate of charge accumulation and discharge.

These results indicate that for the DUHPFC using 9 M KOH, the optimal urea concentration at 25°C is 0.5 M, as it provides the highest and most stable voltage output. Both lower and higher urea concentrations result in decreased performance, highlighting the importance of optimizing the urea concentration for maximum efficiency.

5.3 Single Cell- DUHPFC

In this section, the performance results of the single cell DUHPFC are presented. A single cell was constructed, and previous parametric studies identified 0.5 M urea as the optimal concentration for the anolyte. Therefore, this investigation focuses on evaluating the single cell performance at 0.5 M urea concentration with varying KOH concentrations and different temperatures. Electrochemical tests, including Open Circuit Potential (OCP), Linear Sweep Voltammetry (LSV), Polarization Resistance (POLRES), Cyclic Voltammetry (RCV), and Electrochemical Impedance Spectroscopy (EIS), were conducted using a Gamry reference 3000 instrument to thoroughly assess the single cell's performance under these conditions.

5.3.1 Effects of KOH Concentration on Performance of The Single-Cell Arrangement Fuel Cell

In this section, the effects of varying KOH concentrations on the performance of the single-cell arrangement of the DUHPFC are investigated. Direct Urea-Hydrogen Peroxide Fuel Cells (DUHPFC) are promising for their potential in sustainable energy production due to the availability and low cost of urea. Previous parametric studies have identified 0.5 M urea as the optimal anolyte concentration for enhancing performance. The aim is to determine how different concentrations of KOH, as the supporting electrolyte, impact the efficiency and stability of the fuel cell. By systematically varying the KOH concentration while maintaining the urea concentration at 0.5 M, the electrolyte composition is optimized to achieve the best possible performance for the single-cell DUHPFC.

The performance of the developed DUHPFC single cell arrangement was evaluated using electrochemical tests at 25°C with an anolyte solution of 0.5 M urea and 1, 5, 9 M KOH, and a catholyte solution of 2 M H_2SO_4 with 2 M H_2O_2. The results are presented in the form of current density vs. cell voltage and current density vs. power density graphs.

Figure 5.16 and 5.17 shows the relationship between current density vs cell voltage and power density vs current density for 1 M KOH with 0.5 M urea as an anolyte solution,

respectively. This graph represents the average results of three independent tests, with the error points highlighted to indicate minor variations observed across the measurements, confirming the overall consistency of the data. The Open Circuit Voltage (OCV) was observed to be approximately 0.5 V, indicating a healthy initial potential. The cell voltage decreased with increasing current density, exhibiting a typical behavior due to internal resistance and polarization losses, with the short-circuit current density around 62 mA/cm².

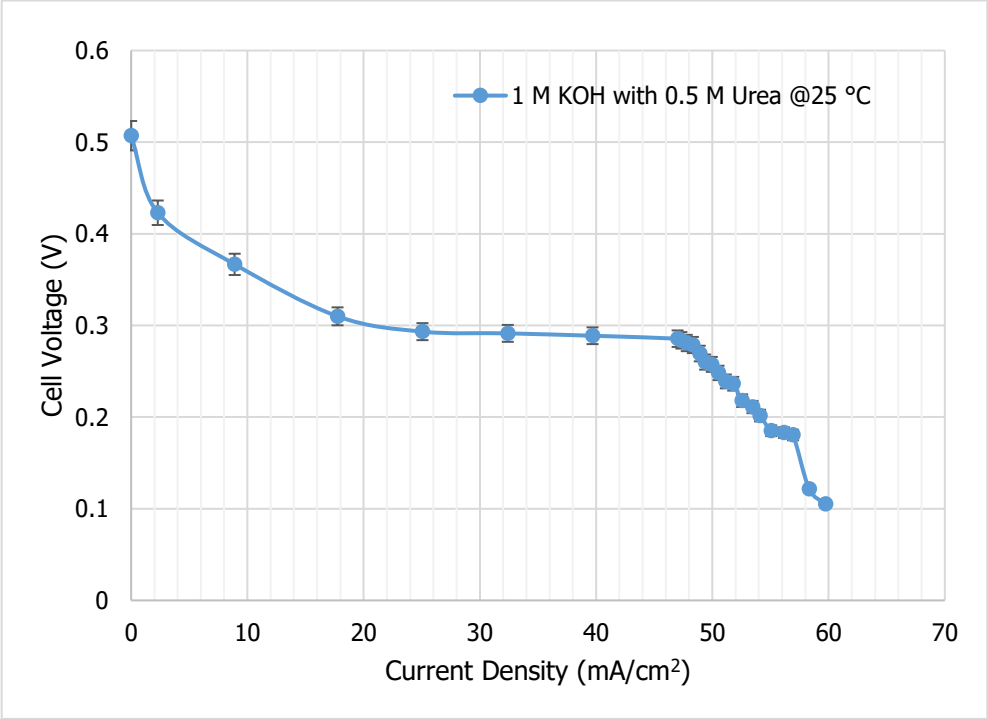

Figure 5.16 Cell voltage vs current density curves for 1 M KOH with 0.5 M urea at 25°C

The power density increased with current density, reaching a peak power density of approximately 12 mW/cm² at 50 mA/cm², beyond which it declined, indicating significant losses when operating beyond the optimal range. These results suggest that the DUHPFC single cell exhibits good electrochemical performance with these conditions, demonstrating substantial power delivery at the optimal point. The sharp voltage drop at low current densities is attributed to activation losses, while the gradual decline at higher current densities is due to ohmic and mass transport losses [78, 79, 80, 81]. Mass transport limits, in which reactant diffusion to the electrode surface is insufficient to maintain the reaction rates necessary for greater current densities, are another reason for the power density drop after the peak. The observed drop is also attributed to increasing internal

resistance and the development of concentration gradients within the cell, underscoring the significance of maintaining efficiency by operating within the ideal current density range.

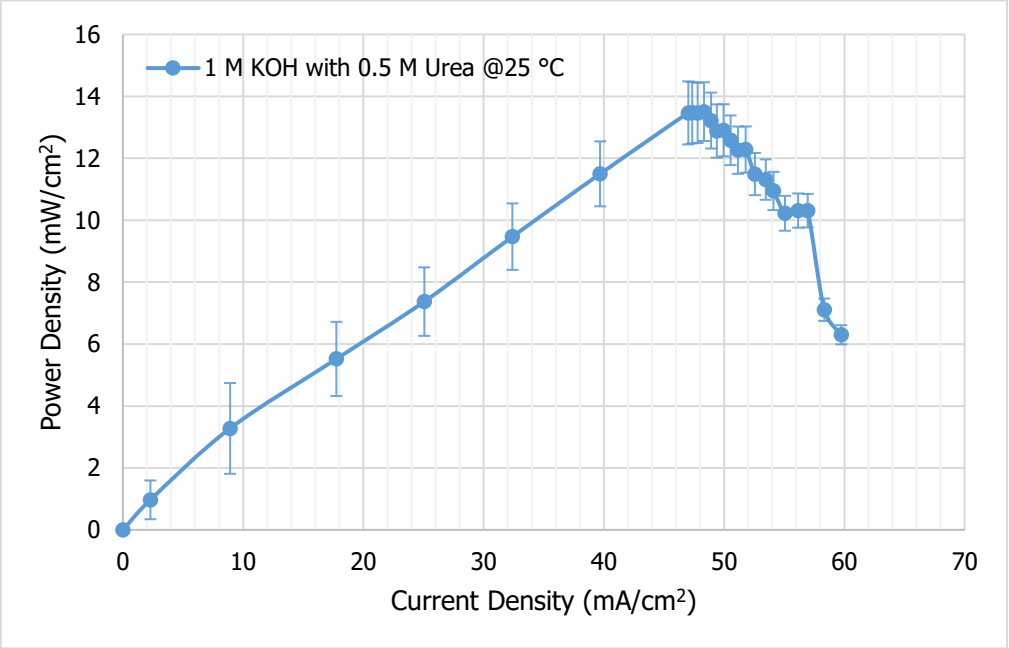

Figure 5.17 Power density vs current density curves for 1 M KOH with 0.5 M urea at 25°C

Figure 5.18 and 5.19 shows the relationship between current density vs cell voltage and power density vs current density for 5 M KOH with 0.5 M urea as an anolyte solution, respectively. The Open Circuit Voltage (OCV) was observed to be approximately 0.6 V, indicating a strong initial potential. As the current density increased, the cell voltage decreased, showing a typical trend due to internal resistance and polarization losses, with the short-circuit current density around 70 mA/cm². The power density increased with current density, reaching a peak power density of approximately 20 mW/cm² at 60 mA/cm², beyond which it declined, indicating significant losses when operating beyond the optimal range.

Compared to the 1 M KOH scenario, the 5 M KOH configuration achieved a higher OCV and peak power density, suggesting improved performance. The higher performance can be attributed to better ionic conductivity and reduced internal resistance with the increased KOH concentration. However, the sharp voltage drop at low current densities indicates activation losses, while the gradual decline at higher current densities is due to ohmic and mass transport losses. Overall, these results indicate that increasing the KOH concentration to 5 M enhances the DUHPFC performance, demonstrating substantial

power delivery at the optimal point while highlighting the importance of balancing electrolyte concentration to minimize losses [82,83,84].

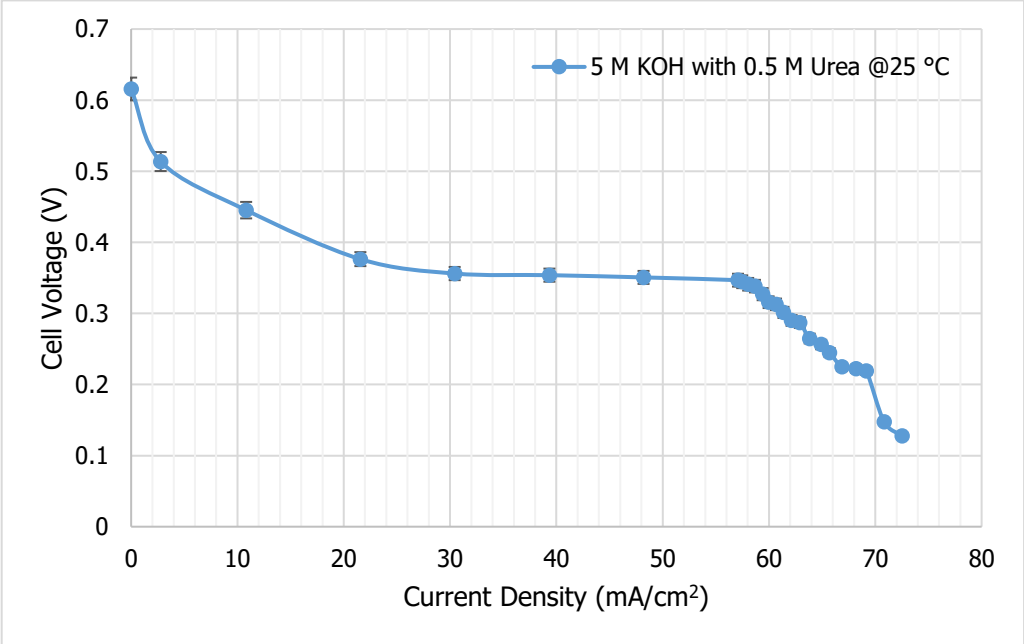

Figure 5.18 Cell voltage vs current density curves for 5 M KOH with 0.5 M urea at 25°C

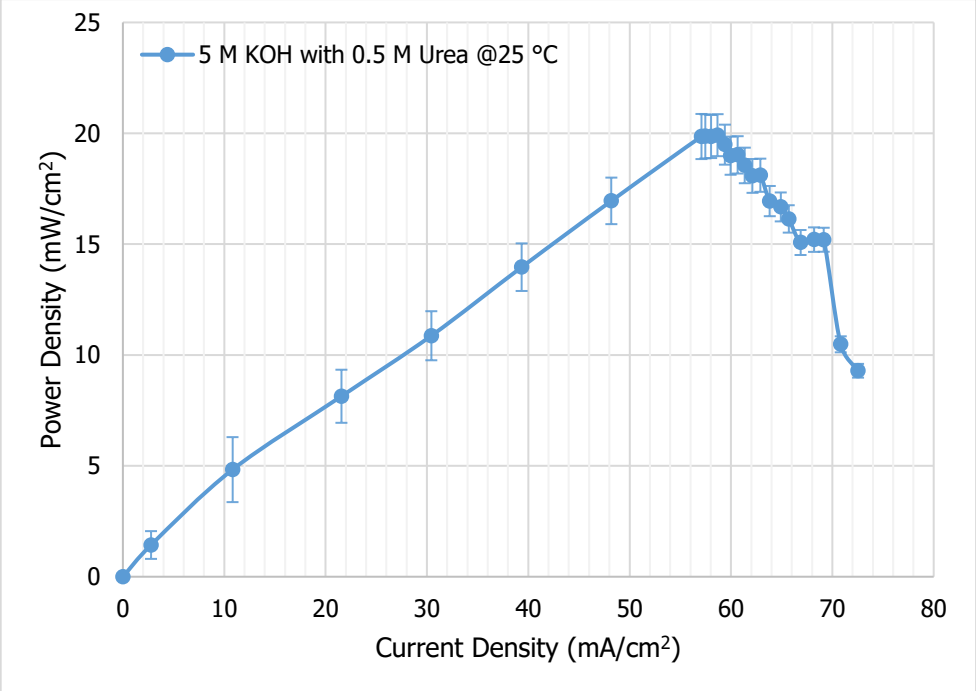

Figure 5.19 Power density vs current density curves for 5 M KOH with 0.5 M urea at 25°C

The relationship between power density and current density and current density and cell voltage for a 9 M KOH anolyte solution containing 0.5 M urea is depicted in Figures 5.20 and 5.21, respectively. The Open Circuit Voltage (OCV) achieved was approximately 0.7 V, reflecting a robust initial potential. As the current density increased, the cell voltage exhibited a typical decline due to internal resistance and polarization effects, with the short-circuit current density reaching around 80 mA/cm².

The power density increased with current density, peaking at approximately 47 mW/cm² at 20 mA/cm² before declining, indicating significant losses when surpassing the optimal operational range. Compared to previous configurations with lower KOH concentrations, the 9 M KOH setup demonstrated a higher OCV and peak power density, suggesting enhanced cell performance.

This improvement can be attributed to superior ionic conductivity and reduced internal resistance provided by the higher KOH concentration. Despite the improved performance, the sharp voltage drop at lower current densities indicates activation losses, while the gradual decrease at higher current densities points to ohmic and mass transport losses. These findings underscore that increasing the KOH concentration to 9 M significantly enhances the DUHPFC's performance, yielding substantial power output at the optimal point, while also highlighting the importance of optimizing electrolyte concentration to balance and minimize losses.

According to Figure 22 and Figure 23, results indicate that the concentration of KOH significantly affects the cell's electrochemical performance, with varying impacts on key metrics such as Open Circuit Voltage (OCV), peak power density, short-circuit current density, and overall stability.

Increasing the KOH concentration from 1 M to 9 M consistently improved the cell's overall performance. The enhancements observed can be attributed to the increased ionic conductivity and reduced internal resistance that come with higher KOH concentrations. As the concentration of KOH increased, the cell exhibited higher open circuit voltages (OCV) and peak power densities, indicating that the electrochemical reactions were more efficient and that the cell could deliver greater power.

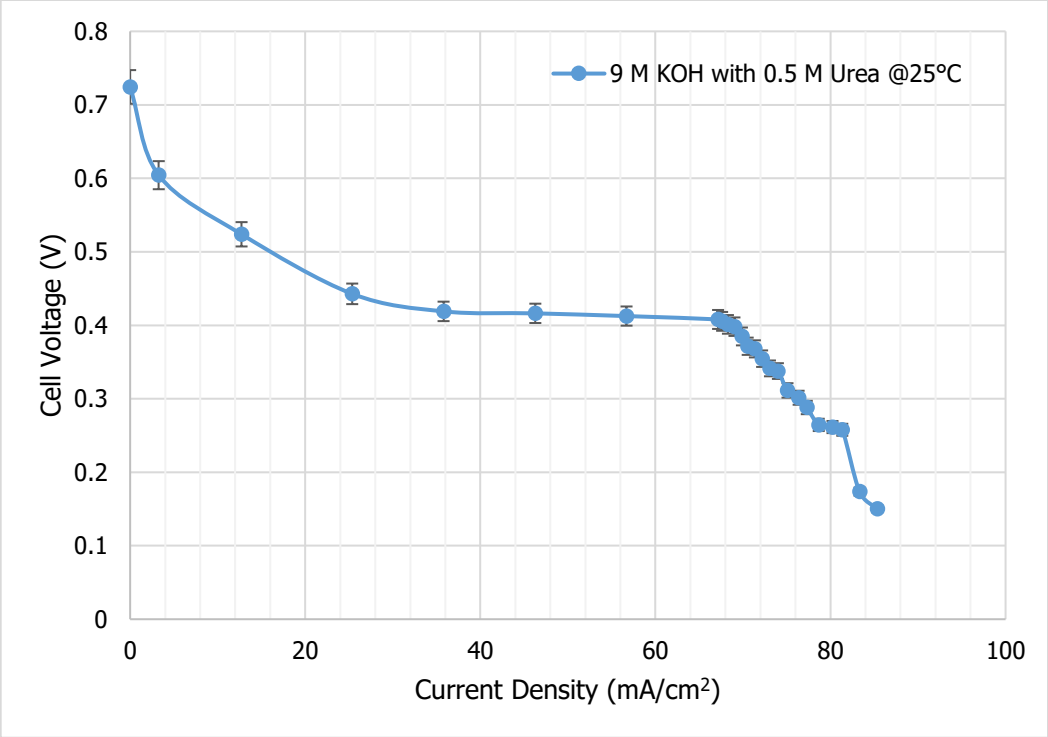

Figure 5.20 Cell voltage vs current density curves for 9 M KOH with 0.5 M urea at 25°C

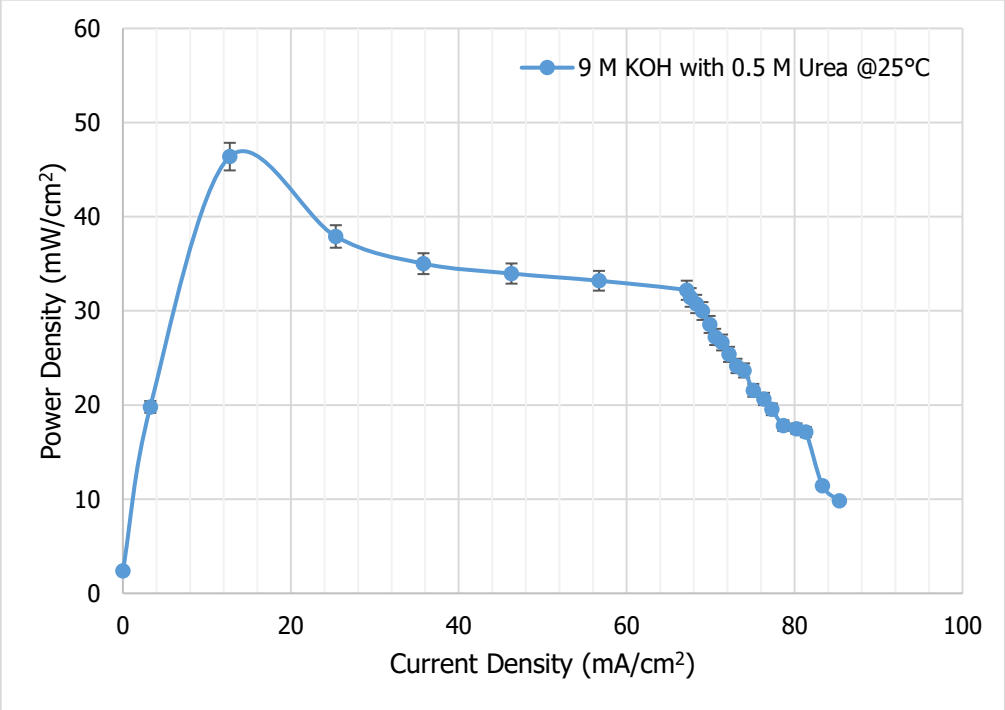

Figure 5.21 Power density vs current density curves for 9 M KOH with 0.5 M urea at 25°C

With lower KOH concentrations, such as 1 M, the cell performance was moderate, likely due to insufficient ionic conductivity and higher internal resistance, which limited the efficiency of the electrochemical processes. At this concentration, the voltage drop was more pronounced at lower current densities, indicating significant activation losses.

At an intermediate concentration of 5 M KOH, there was a noticeable improvement in performance compared to 1 M KOH. The higher ionic conductivity reduced internal resistance, leading to better overall efficiency and power output. However, some limitations persisted, particularly at higher current densities where ohmic and mass transport losses became more apparent.

The highest KOH concentration of 9 M yielded the best performance, demonstrating the greatest efficiency and power output. This configuration benefited from optimal ionic conductivity and minimized internal resistance, allowing the cell to operate more effectively. Nevertheless, even at this concentration, the cell experienced activation losses at lower current densities and ohmic/mass transport losses at higher current densities, which are typical challenges in fuel cell operation.

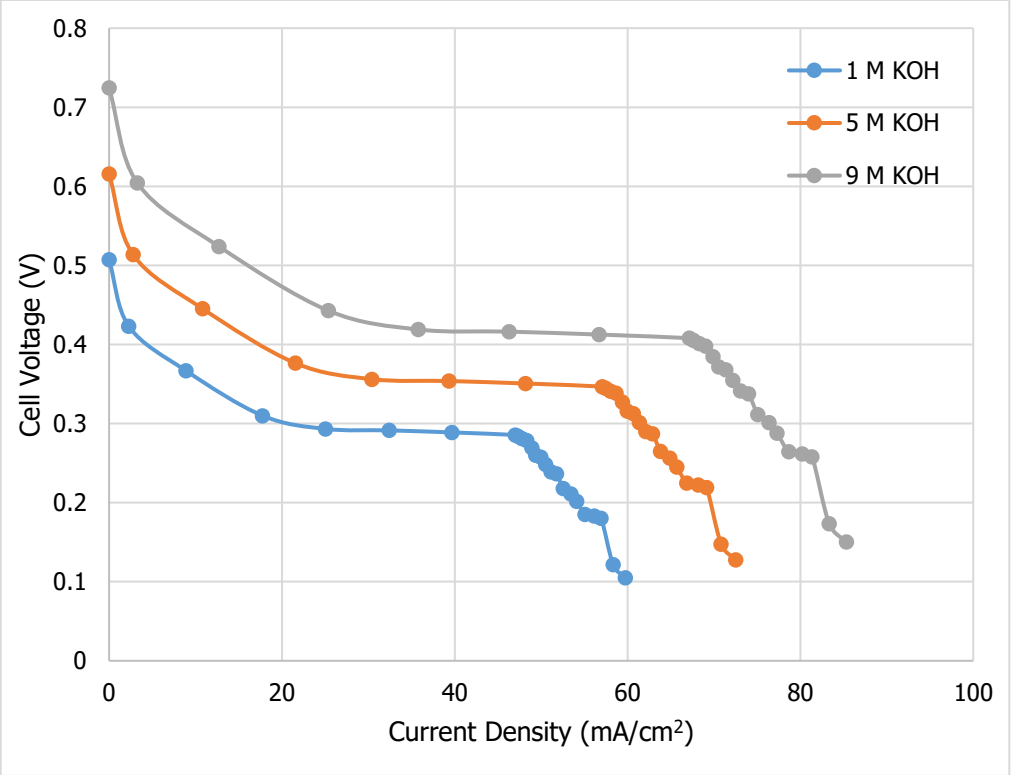

Figure 5.22 Cell voltage vs current density curves for different concentration of KOH with 0.5 M urea at 25°C

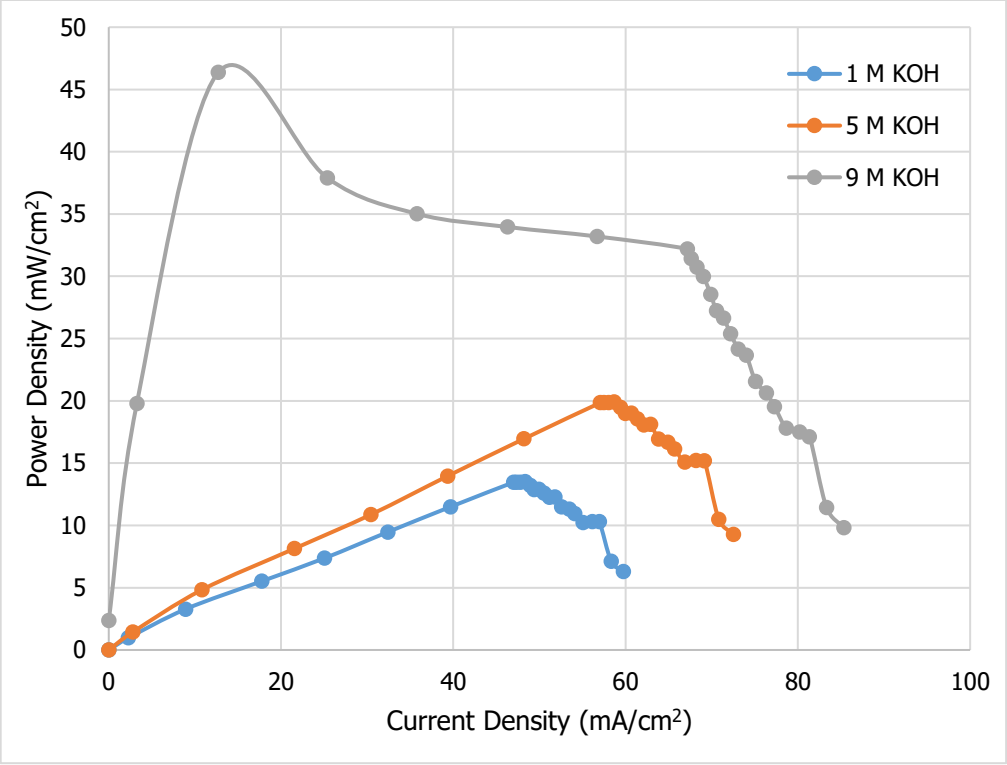

Figure 5.23 Power density vs current density curves for different concentration of KOH with 0.5 M urea at 25°C

Higher KOH concentrations generally lead to improved efficiency and power output by enhancing ionic conductivity and reducing internal resistance. However, balancing these benefits against potential losses due to activation and mass transport effects is essential for achieving the best possible performance. These findings emphasize the importance of careful electrolyte optimization in the design and operation of DUHPFC systems.

5.3.2 Effects of Temperature on Performance of The Single-Cell Arrangement Fuel Cell

In this part, the effects of temperature on the performance of the single-cell arrangement of the DUHPFC are investigated. Previous part has demonstrated that increasing the KOH concentration improves cell performance, with 9 M KOH providing optimal results. Based on these findings, electrochemical tests were conducted to observe the performance of a single cell with an anolyte solution of 9 M KOH and 0.5 M urea, and a catholyte solution of 2 M H_2SO_4 with 2 M H_2O_2 at various temperatures (25°C, 35°C, 45°C, 55°C, and 65°C).

These tests aim to determine how temperature variations impact the efficiency and stability of the fuel cell under optimal KOH concentration conditions.

The test results for 9M KOH with 0.5M urea at 25°C were previously presented in Figures 5.20 and 5.21. Figure 5.24 shows the LSV test result at a cell temperature of 25°C. The onset potential of around 0.35 V vs. Ag/AgCl indicates that the cell can effectively initiate electrochemical reactions at a relatively low voltage, enhancing overall efficiency. The sharp increase in current density with potential reflects the cell's high efficiency and strong performance at this temperature. The maximum current density of approximately 70 mA/cm², consistent across multiple tests, highlights the reproducibility and stability of the cell's performance, which is crucial for practical applications. The plateau region further confirms the cell's ability to maintain stable operation within a specific potential range.

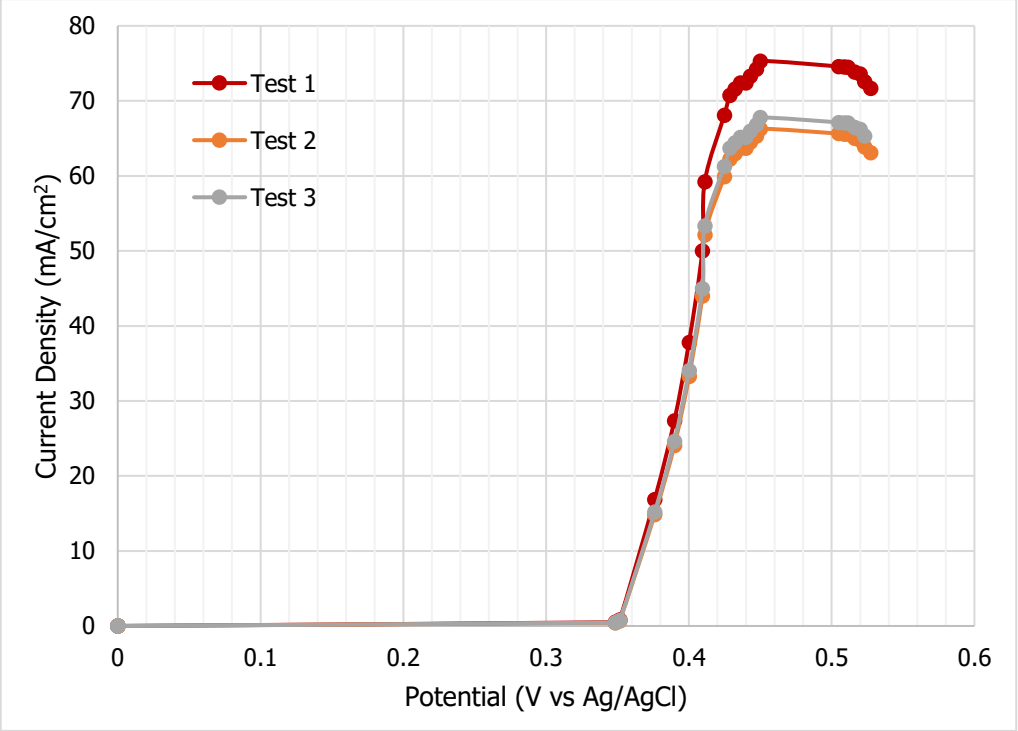

Figure 5.24 LSV results for 9 M KOH with 0.5 M urea at 25°C

Figure 5.25 shows the relationship between current density and cell voltage for the DUHPFC single cell at 35°C. Open Circuit Voltage (OCV) of approximately 0.7 V, with the cell voltage decreasing as current density increased, and a short-circuit current density around 90 mA/cm².

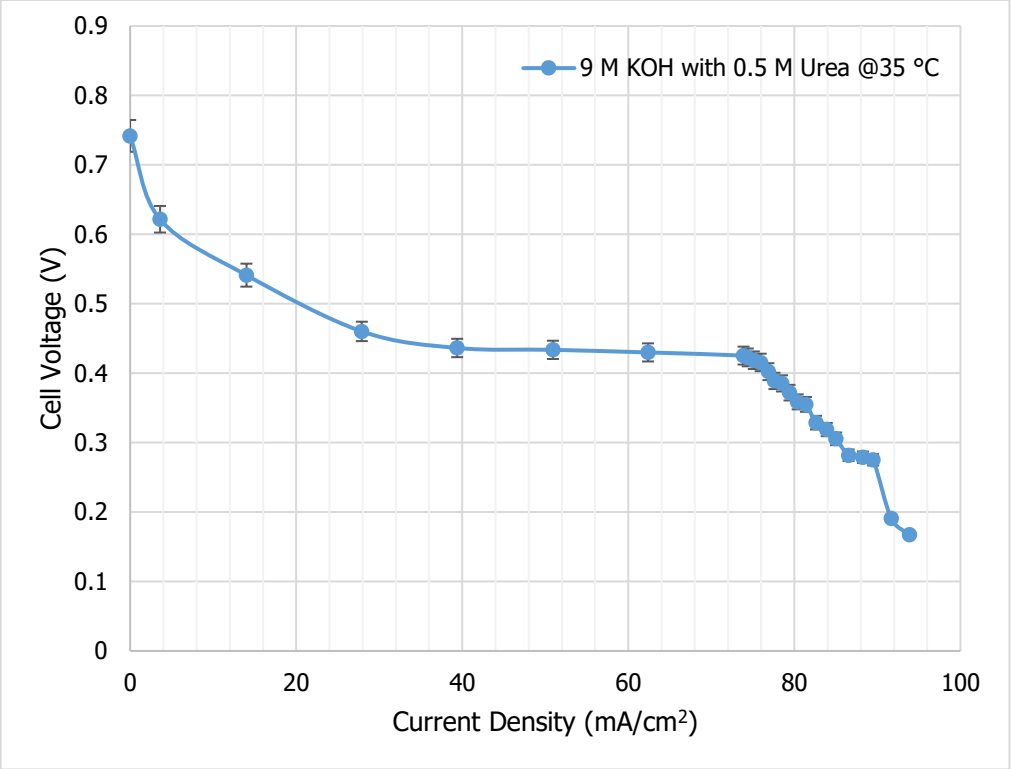

Figure 5.25 Cell voltage vs current density curves for 9 M KOH with 0.5 M urea at 35°C

According to Figure 5.26, power density peaked at about 32 mW/cm² at a current density of 80 mA/cm², demonstrating efficient performance at this temperature.

The LSV test results in Figure 5.27, showing consistent behavior across three tests, revealed an onset potential of around 0.4 V vs. Ag/AgCl and a maximum current density of 80 mA/cm², indicating robust catalytic activity and good reproducibility. These findings suggest that 35°C is an optimal temperature for the DUHPFC single cell with this electrolyte composition, providing high efficiency, stability, and reproducibility. The enhanced performance at this temperature can be attributed to improved reaction kinetics and ionic conductivity. However, the decline in power density beyond the peak points to polarization and mass transport losses at higher current densities. To further improve performance, optimizing the electrode structure and flow management within the cell could help mitigate these losses. Future studies could explore different electrolyte compositions and operating conditions to push the limits of efficiency and minimize the observed losses at higher current densities.

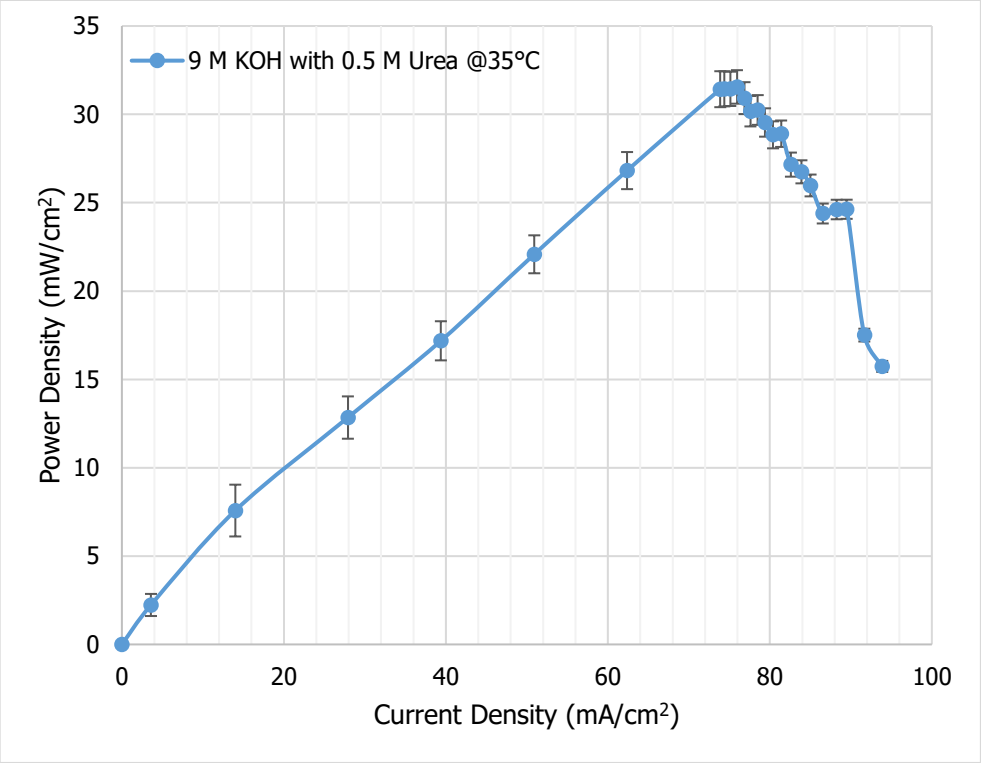

Figure 5.26 Power density vs current density curves for 9 M KOH with 0.5 M urea at 35°C

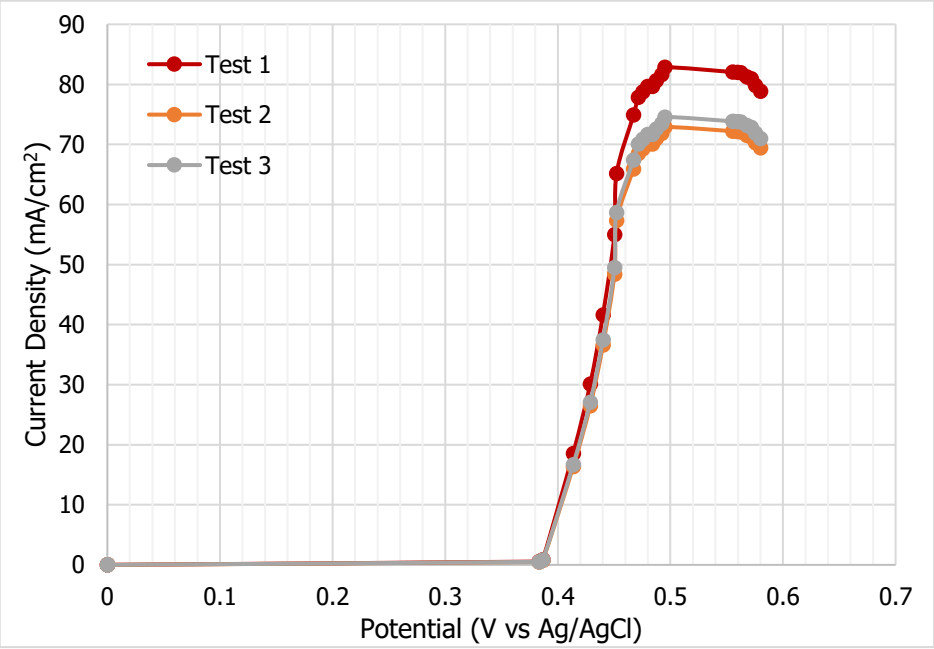

Figure 5.27 LSV results for 9 M KOH with 0.5 M urea at 35°C

Figures 5.28, 5.29, and 5.30 respectively illustrate the cell voltage versus current density, power density versus current density, and LSV analyses obtained at a cell

temperature of 45°C with 9M KOH and 0.5M urea. The polarization graph illustrates the relationship between current density and cell voltage for the DUHPFC single cell at 45°C. The Open Circuit Voltage (OCV) is approximately 0.7 V, which indicates a strong initial potential. As the current density increases, the cell voltage decreases, with the short-circuit current density reaching around 100 mA/cm². This decline in voltage with increasing current density is typical due to the internal resistance and polarization effects within the cell. The power density graph shows that it increases with current density, peaking at about 34 mW/cm² at a current density of around 85 mA/cm². Beyond this peak, the power density declines, indicating that the cell experiences significant losses when operating beyond its optimal range. The high peak power density at 45°C suggests that the cell operates efficiently at this temperature, delivering substantial power output. The Linear Sweep Voltammetry (LSV) graph shows consistent behavior across three tests, with the current density sharply increasing as the potential rises. The onset potential is around 0.4 V vs. Ag/AgCl, and the maximum current density achieved is about 90 mA/cm². This indicates robust catalytic activity and good reproducibility, highlighting the cell's stable performance at 45°C.

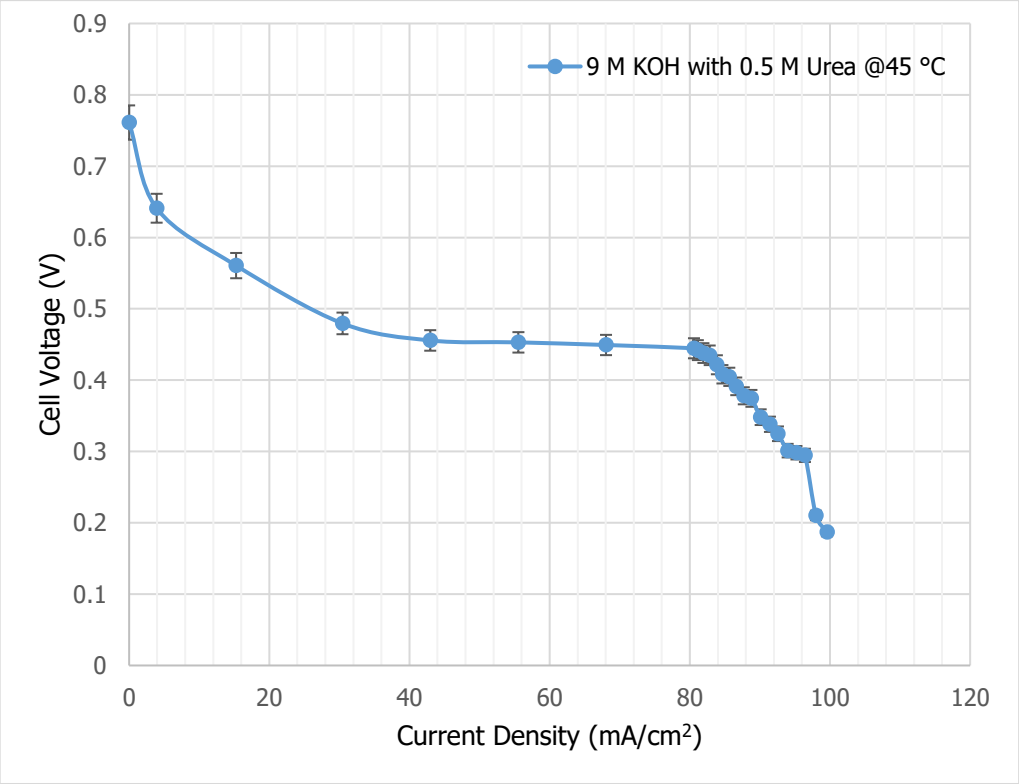

Figure 5.28 Cell voltage vs current density curves for 9 M KOH with 0.5 M urea at 45°C

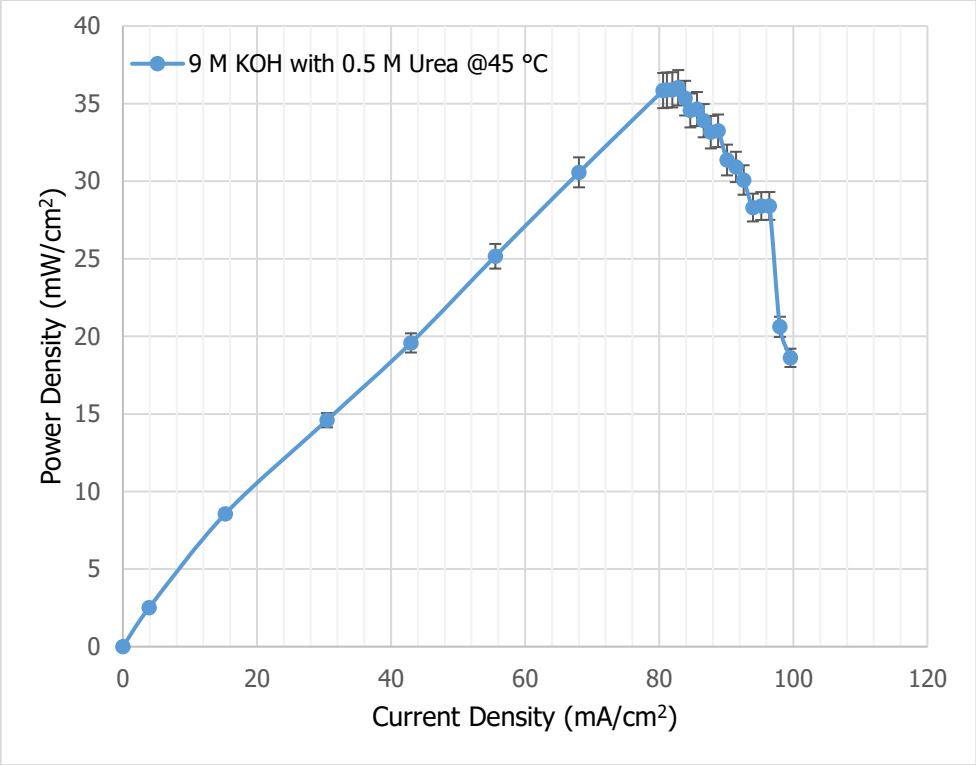

Figure 5.29 Power density vs current density curves for 9 M KOH with 0.5 M urea at 45°C

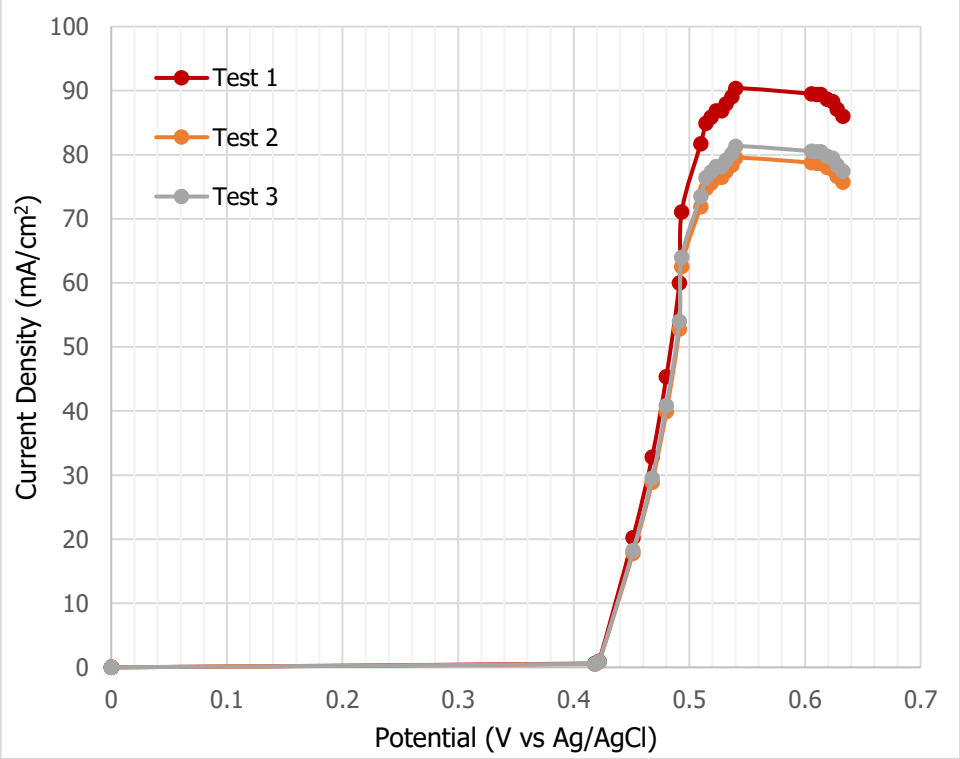

Figure 5.30 LSV results for 9 M KOH with 0.5 M urea at 45°C

The enhanced performance at this temperature can be attributed to improved reaction kinetics and ionic conductivity. The cell's ability to deliver higher current densities and power outputs suggests that 45°C is an optimal temperature for this configuration. The consistent LSV results across multiple tests highlight the robustness and reproducibility of the cell's performance. However, the decline in power density beyond the peak indicates limitations due to polarization and mass transport losses, which become more pronounced at higher current densities. Overall, these findings suggest that 45°C enhances the DUHPFC single cell's performance, providing a balance between efficiency, stability, and reproducibility, while also emphasizing the need to manage operating conditions to minimize losses and optimize efficiency.

The cell voltage versus current density, power density vs current density, and LSV analyses conducted at a 55°C cell temperature with 9 M KOH and 0.5 M urea are shown in Figures 5.31 and 5.32, respectively.

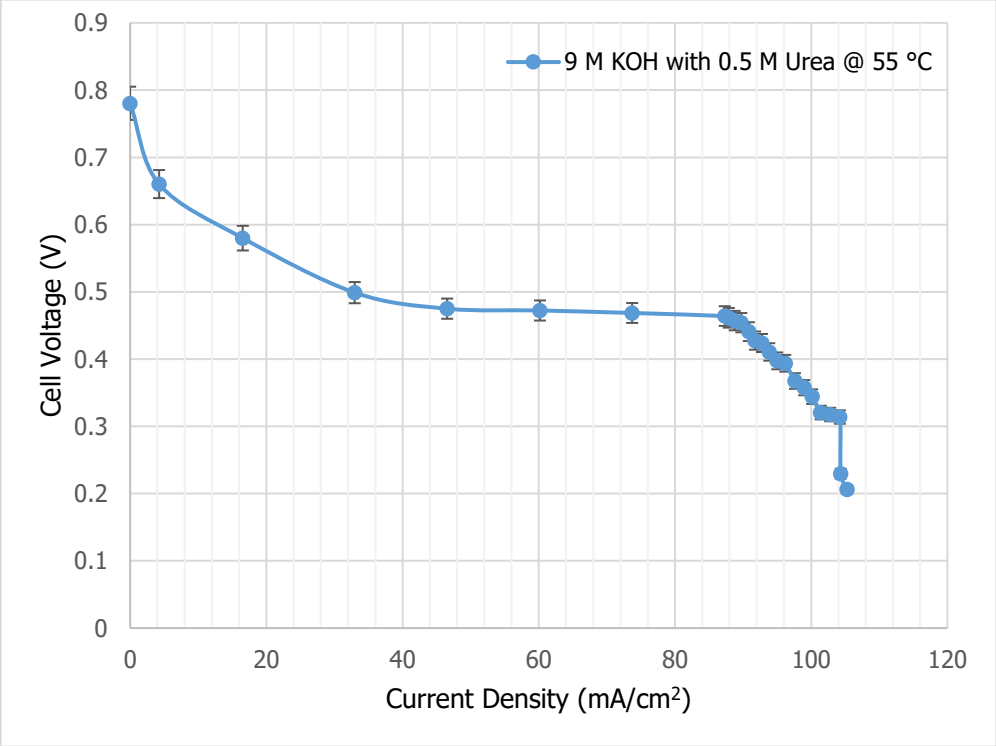

Figure 5.31 Cell voltage vs current density curves for 9 M KOH with 0.5 M urea at 55°C

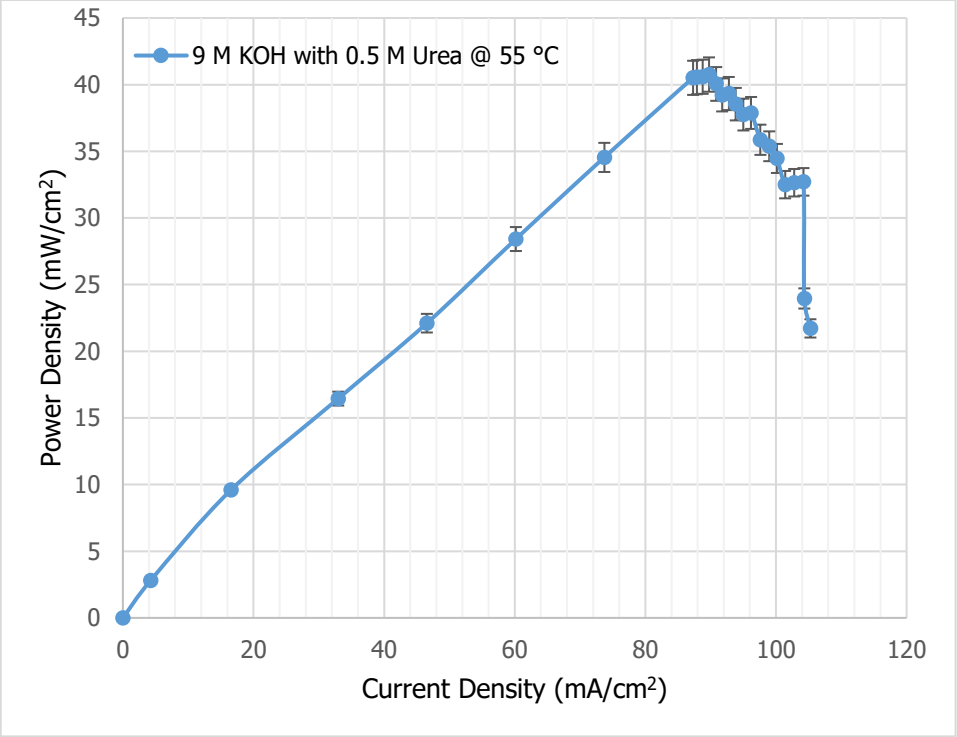

Figure 5.32 Power density vs current density curves for 9 M KOH with 0.5 M urea at 55°C

The Open Circuit Voltage (OCV) is approximately 0.7 V, indicating a strong initial potential. As the current density increases, the cell voltage decreases, and the short-circuit current density is around 110 mA/cm². This behavior is consistent with internal resistance and polarization effects that occur as current density rises. The power density graph shows an increase with current density, peaking at about 38 mW/cm² at a current density of around 95 mA/cm². Beyond this peak, the power density declines, indicating significant losses when operating beyond the optimal range. The higher peak power density at 55°C suggests that the cell operates efficiently at this elevated temperature, delivering substantial power output. The Linear Sweep Voltammetry (LSV) data indicates consistent behavior across three tests, with the current density sharply increasing as the potential rises. The onset potential is around 0.4 V vs. Ag/AgCl, and the maximum current density achieved is about 100 mA/cm². This suggests robust catalytic activity and good reproducibility, indicating stable performance of the cell at 55°C.

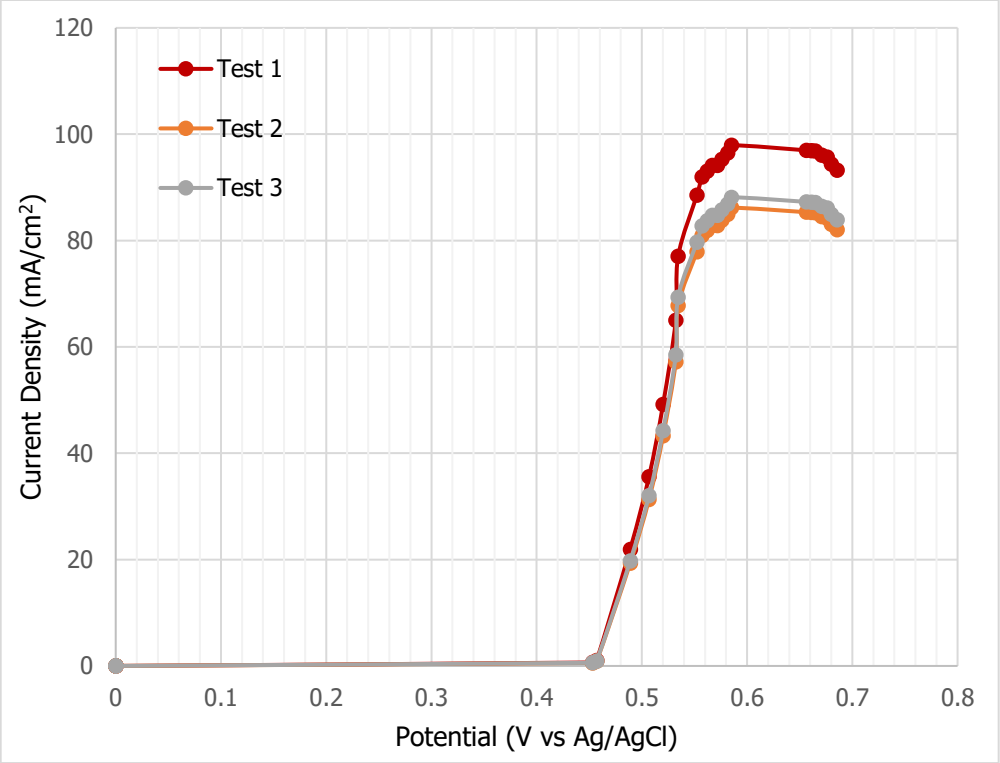

Figure 5.33 LSV results for 9 M KOH with 0.5 M urea at 55°C

Figures 5.34, 5.35, and 5.36, respectively, display the cell voltage vs current density, power density vs current density, and LSV analyses carried out at a 55°C cell temperature with 9 M KOH and 0.5 M urea. At 65°C, the DUHPFC single cell with 9 M KOH and 0.5 M urea demonstrates enhanced performance, evidenced by a high Open Circuit Voltage (OCV) of approximately 0.7 V, a peak power density of about 42 mW/cm² at a current density of 110 mA/cm², and stable results from the Linear Sweep Voltammetry (LSV) tests.

The cell voltage decreases with increasing current density, showing a short-circuit current density around 120 mA/cm², which is typical due to internal resistance and polarization effects. The elevated temperature improves reaction kinetics and ionic conductivity, allowing the cell to deliver higher current densities and power outputs. However, the decline in power density beyond the peak highlights the impact of polarization and mass transport losses at higher current densities.

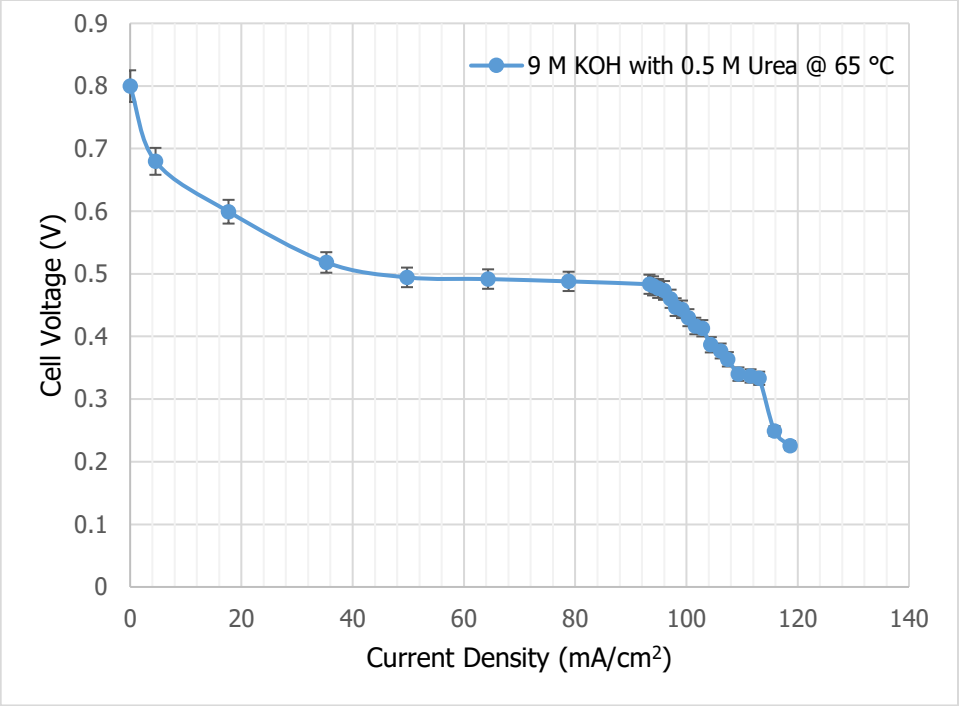

Figure 5.34 Cell voltage vs current density curves for 9 M KOH with 0.5 M urea at 65°C

The consistent LSV results, with an onset potential around 0.4 V vs. Ag/AgCl and maximum current density of about 110 mA/cm², indicate robust catalytic activity and reproducibility. These findings suggest that 65°C is a favorable operating temperature, enhancing efficiency, stability, and reproducibility of the DUHPFC single cell, while also emphasizing the need to manage polarization and mass transport losses for optimal performance [85,86,87,88]. The improved reaction kinetics and ionic conductivity at 65°C contribute significantly to the enhanced performance observed. However, to fully capitalize on these benefits, further optimization of the electrode and electrolyte configurations may be necessary to minimize the impact of polarization and mass transport limitations at higher current densities. Additionally, exploring alternative catalysts and membrane materials could offer pathways to further improve the overall efficiency and durability of the DUHPFC system under these operating conditions. Moreover, conducting long-term stability tests at this temperature could provide valuable insights into the durability of the cell over extended periods of operation. Investigating the effects of varying the electrolyte concentration and flow rates may also help in fine-tuning the system for even better performance and reduced degradation over time.

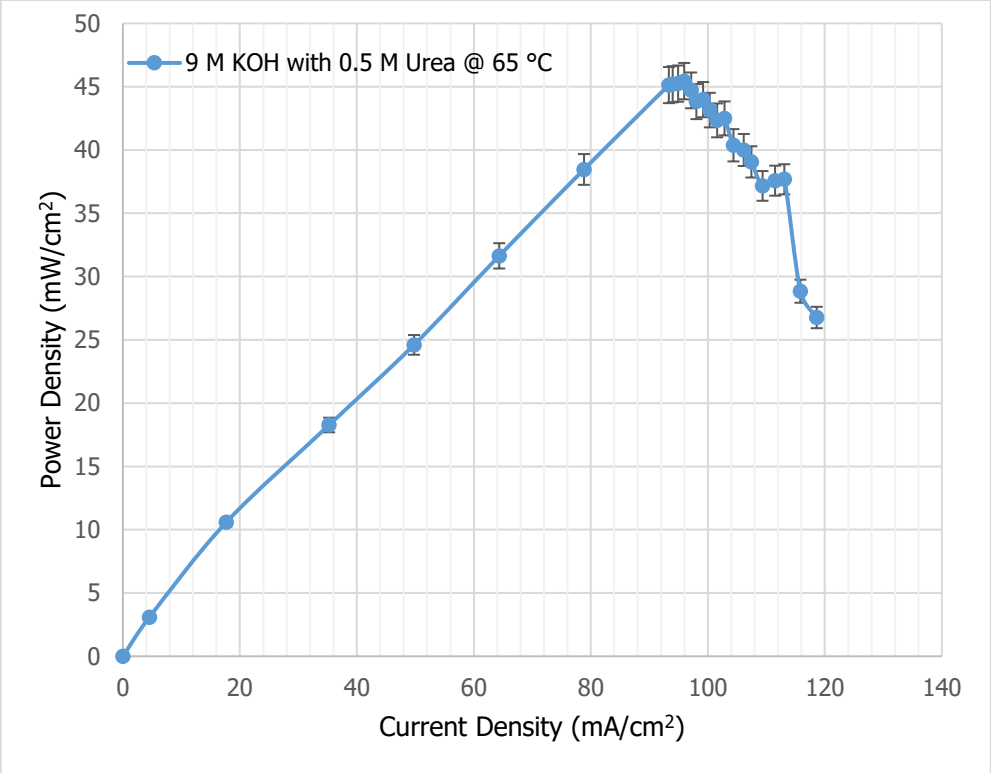

Figure 5.35 Power density vs current density curves for 9 M KOH with 0.5 M urea at 65°C

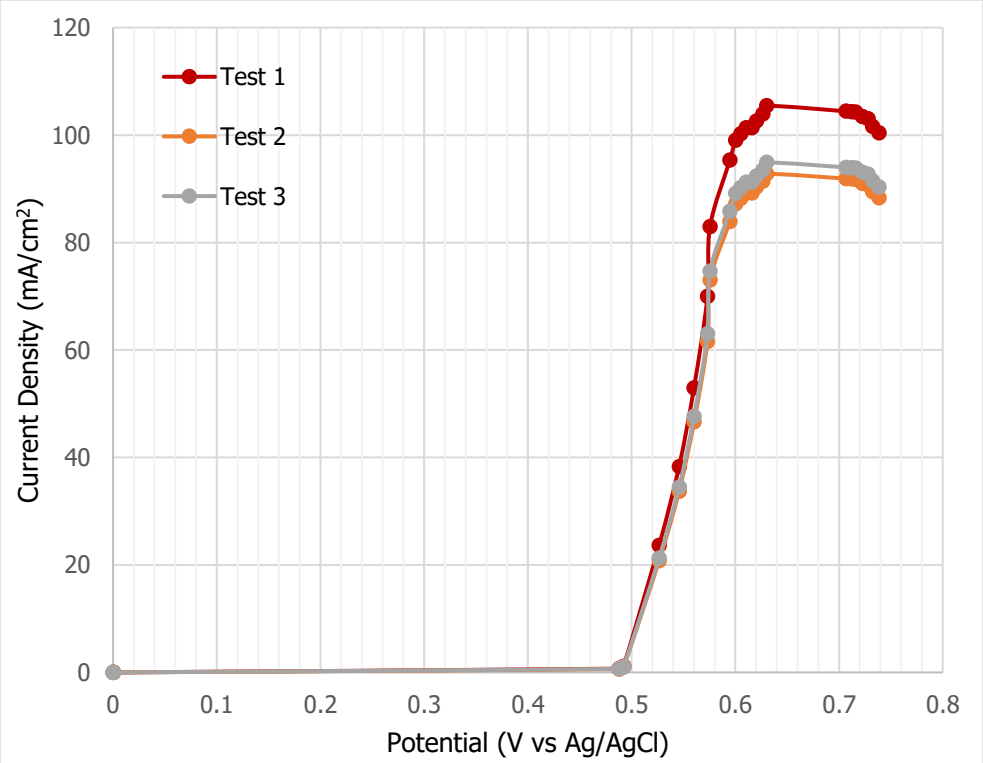

Figure 5.36 LSV results for 9 M KOH with 0.5 M urea at 65°C

5.3.3 Electrochemical Impedance Spectroscopy (EIS) Results of Single-Cell Arrangement Fuel Cell

In this part, the Electrochemical Impedance Spectroscopy (EIS) results for the DUHPFC single cell arrangement are presented and analyzed, focusing on how varying cell temperatures impact the impedance characteristics and electrochemical behavior of the anode electrode.

Figures 5.36, 5.37, and 5.38 present the EIS test results for 9M KOH with 0.5M urea at different cell temperatures, showcasing the corresponding Bode and Nyquist plots. These analyses are performed to evaluate the impedance characteristics and understand the electrochemical behavior of the anode electrode under varying thermal conditions, which is crucial for optimizing the performance and efficiency of the fuel cell.

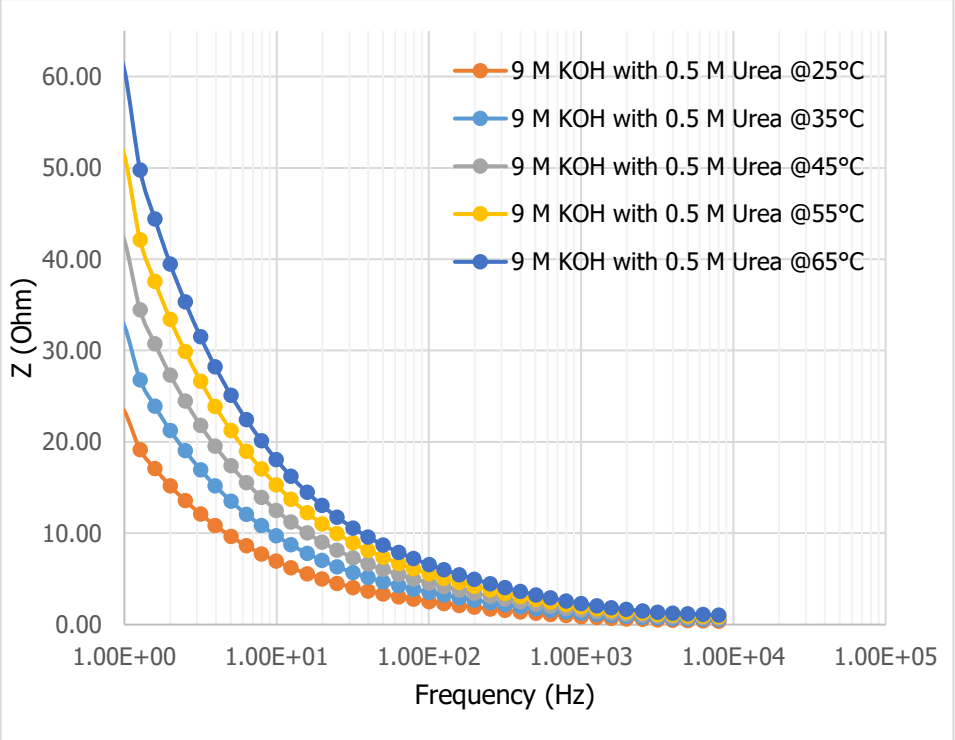

Figure 5.37 Bode plot of 9 M KOH with 0.5 M urea for impudence magnitude obtained from EIS at different cell temperature

The EIS test results for the DUHPFC single cell with 9 M KOH and 0.5 M urea at varying temperatures (25°C, 35°C, 45°C, 55°C, and 65°C) reveal significant insights into the cell's impedance characteristics and electrochemical behavior. The Bode plots show that the impedance decreases with increasing temperature, indicating enhanced ionic

conductivity and reduced resistance at higher temperatures, with the lowest impedance observed at 55°C and 65°C. The phase angle shifts towards more negative values as the temperature increases, reflecting improved charge transfer processes and more dominant resistive behavior.

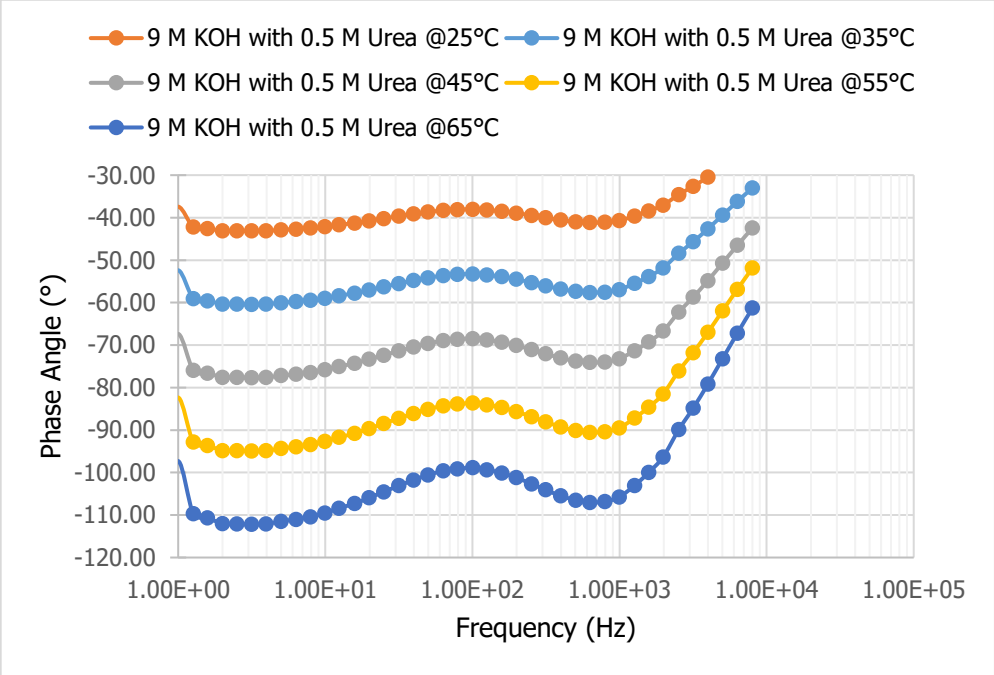

Figure 5.38 Bode plot of 9 M KOH with 0.5 M urea for phase angle obtained from EIS at different cell temperature

The Nyquist plots further corroborate these findings, with the semicircles' diameters decreasing as temperature rises, indicating reduced charge transfer resistance and more efficient electrochemical kinetics. At 25°C, the impedance is highest, showing higher resistance and lower ionic conductivity. As the temperature increases, the impedance reduces significantly, reaching its lowest at 65°C, where the cell exhibits the most efficient electrochemical reactions.

These results suggest that higher temperatures improve the cell's performance by facilitating better ionic mobility, accelerating electrochemical reactions, and reducing charge transfer resistance. However, while higher temperatures enhance performance, they also introduce potential challenges such as material degradation and thermal management issues. Therefore, optimizing the operating temperature is crucial for balancing performance improvements with the fuel cell's longevity and stability. In conclusion, the EIS analysis underscores the importance of temperature optimization in maximizing the

efficiency and durability of DUHPFC systems, highlighting that temperatures around 55°C to 65°C provide the best electrochemical performance while necessitating careful thermal management [89, 90, 91].

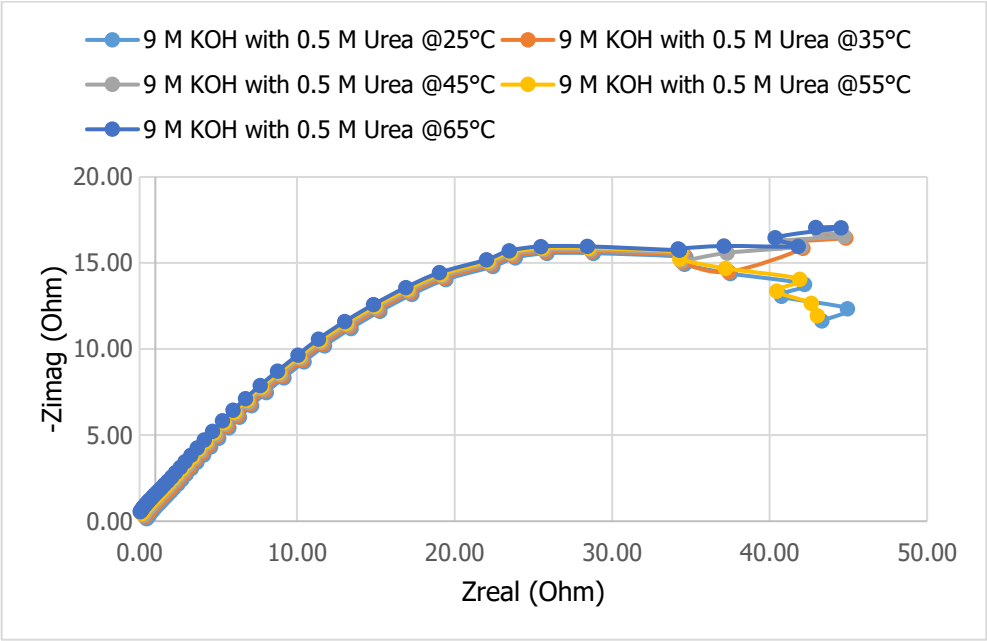

Figure 5.39 Nyquist plot of 9 M KOH with 0.5 M urea obtained from EIS at different cell temperature

EIS results and temperature effects analysis indicate that the DUHPFC single cell performs best at 55°C and 65°C. While 65°C shows the lowest impedance and charge transfer resistance, suggesting the highest efficiency, it may pose challenges related to thermal management and material durability. Therefore, 55°C is the most suitable temperature, balancing high performance and long-term stability.

5.4 Fuel Cell Stack- DUHPFC

In this section, the performance results of a Direct Urea-Hydrogen Peroxide Fuel Cell (DUHPFC) stack, consisting of 16 individual cells, are presented and analyzed. The fuel cell stack was constructed and tested under varying thermal conditions. The tests were conducted using an anolyte solution of 9 M KOH with 0.5 M urea, chosen based on previous sections' findings, which demonstrated this combination as optimal for enhancing electrochemical performance. The catholyte consisted of 2 M H_2SO_4 with 2 M H_2O_2. Detailed electrochemical testing, including measurements of voltage, current density, and power density, was performed to evaluate the stack's performance across the different

temperatures, providing insights into the thermal effects on the overall efficiency and stability of the fuel cell stack.

5.4.1 Effects of Temperature on Performance of Fuel Cell Stack

This section explores the effects of temperature on the performance of a DUHPFC fuel cell stack, consisting of 16 cells, by analyzing its electrochemical behavior at 25°C, 45°C, and 65°C. The investigation aims to determine how varying thermal conditions impact the efficiency, stability, and overall performance of the fuel cell stack, using an optimal anolyte solution of 9 M KOH with 0.5 M urea, as identified in previous studies.

Figure 5.40 and Figure 5.41 presents the relationship between stack voltage and stack power density according to current density for the DUHPFC fuel cell stack at different stack temperatures. At 25°C, the stack voltage starts around 8 V and decreases significantly with increasing current density, dropping to below 1 V at higher current densities. The stack achieves a peak power density of approximately 200 mW/cm² at around 25 mA/cm². However, this temperature exhibits significant instability, as indicated by the sharp drops and fluctuations in power density. At this temperature the stack shows high initial voltage and peak power density but suffers from instability and sharp declines in both voltage and power density at higher current densities. This indicates that while the stack can perform well at lower temperatures, it struggles to maintain stability under higher loads. At 45°C, the stack voltage shows a more stable decline, maintaining higher voltages at increased current densities compared to 25°C. The stack achieves a peak power density of around 180 mW/cm² at approximately 50 mA/cm².

The power density curve is much smoother, indicating more stable performance. The stack demonstrates a balance between voltage stability and power output, with a smoother decline in voltage and a stable power density curve. The peak power density at this temperature suggests that the cell reactions are more efficient, likely due to improved ionic conductivity and reaction kinetics at this moderate temperature. At 65°C, the initial voltage is like that at 45°C, but the decline in voltage is more gradual, indicating better performance at higher temperatures. The peak power density is slightly lower, around 160 mW/cm² at 55 mA/cm², but the performance remains stable and consistent across a wider range of current densities. In this high stack temperature, the stack shows the most gradual decline in voltage and a stable power density curve, though with a slightly lower peak

power density compared to 45°C. The performance stability at 65°C indicates that higher temperatures further enhance ionic mobility and reduce internal resistance. However, the lower peak power density compared to 45°C might be due to thermal effects that could impact material stability or other operational factors.

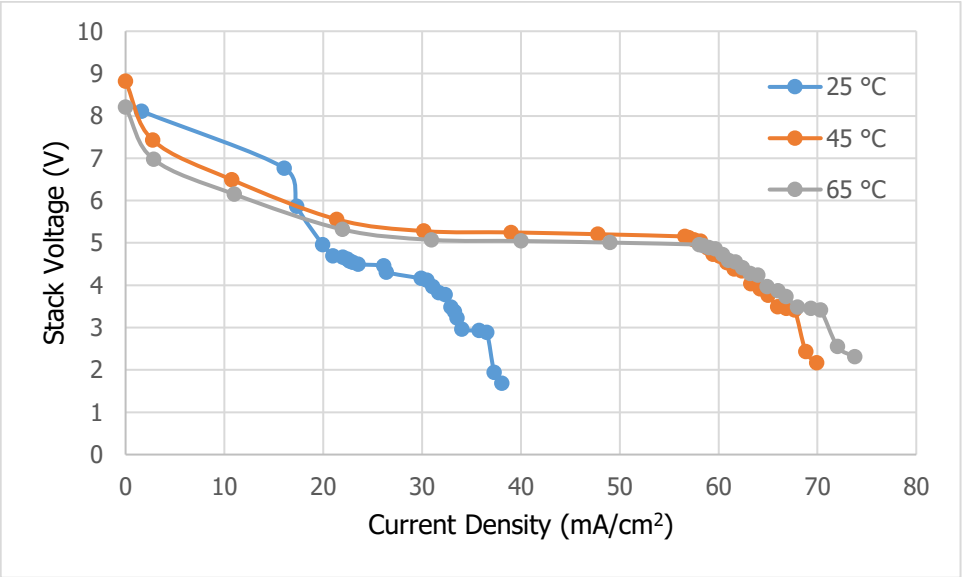

Figure 5.40 Stack voltage vs current density curves for 9 M KOH with 0.5 M urea at different stack temperatures

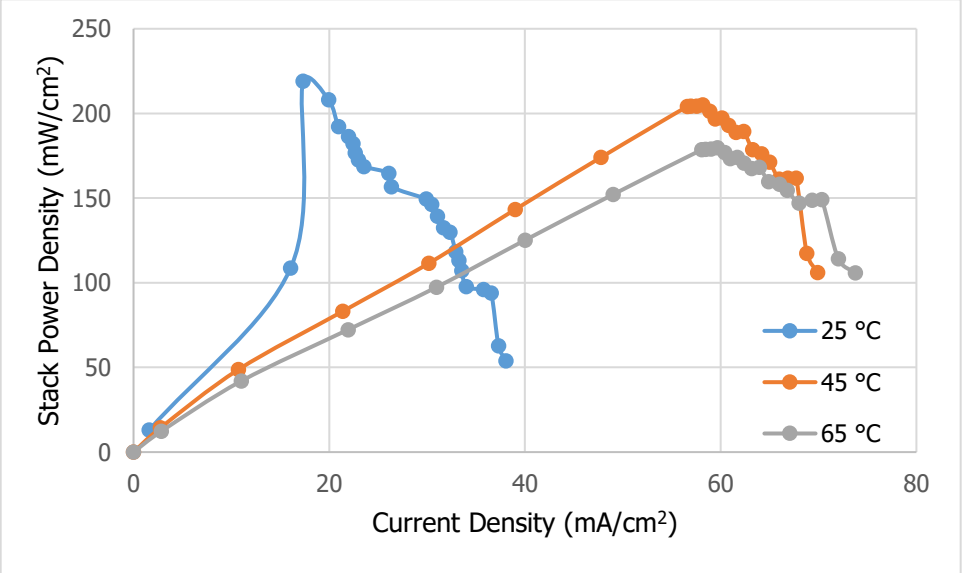

Figure 5.41 Stack power density vs current density curves for 9 M KOH with 0.5 M urea at different stack temperatures

In summary, the DUHPFC fuel cell stack performs best at 65°C, offering superior voltage stability and consistent performance across a wide range of current densities. the

overall stability and gradual voltage decline at 65°C make it the optimal temperature for achieving reliable and efficient fuel cell operation. The enhanced ionic mobility and reduced internal resistance at 65°C contribute to its superior performance, ensuring that the fuel cell stack can maintain high efficiency and stability under various operating conditions. These findings emphasize the importance of temperature optimization in enhancing the efficiency and stability of fuel cell stacks, with 65°C emerging as the most effective operating temperature.

5.4.2 Electrochemical Impedance Spectroscopy (EIS) Results of Fuel Cell Stack

In the previous section, it was found that 65°C provided the best performance for the fuel cell stack. Consequently, an Electrochemical Impedance Spectroscopy (EIS) test was conducted at this optimal temperature to further analyze the impedance characteristics and understand the electrochemical behavior of the fuel cell stack. EIS tests are crucial for identifying resistance components, optimizing operational conditions, and enhancing overall efficiency and stability of the fuel cell stack.

Figures 5.42 and Figure 5.43 shows the Bode plot and Nyquist plot of 9 M KOH with 0.5 M urea obtained from EIS at 65°C stack temperature, respectively. The experimental impedance data shows a clear trend with increasing frequency, indicating typical impedance behavior for the fuel cell stack. The modeling data closely follows the experimental data, validating the accuracy of the model. The impedance is relatively high at lower frequencies, indicating higher resistance, which gradually decreases as frequency increases. The phase angle starts at a relatively low negative value and decreases further as frequency increases, reaching a peak around -90 degrees at higher frequencies. The experimental phase angle data closely matches the modeling phase angle data, demonstrating consistent behavior.

The Nyquist plot displays a semicircular arc, typical of fuel cell impedance behavior, with a clear experimental data trend closely followed by the modeling data. The diameter of the semicircle represents the charge transfer resistance, which appears moderate in this case. The high-frequency intercept on the real axis (Zreal) indicates the ohmic resistance, while the diameter of the semicircle represents the charge transfer resistance.

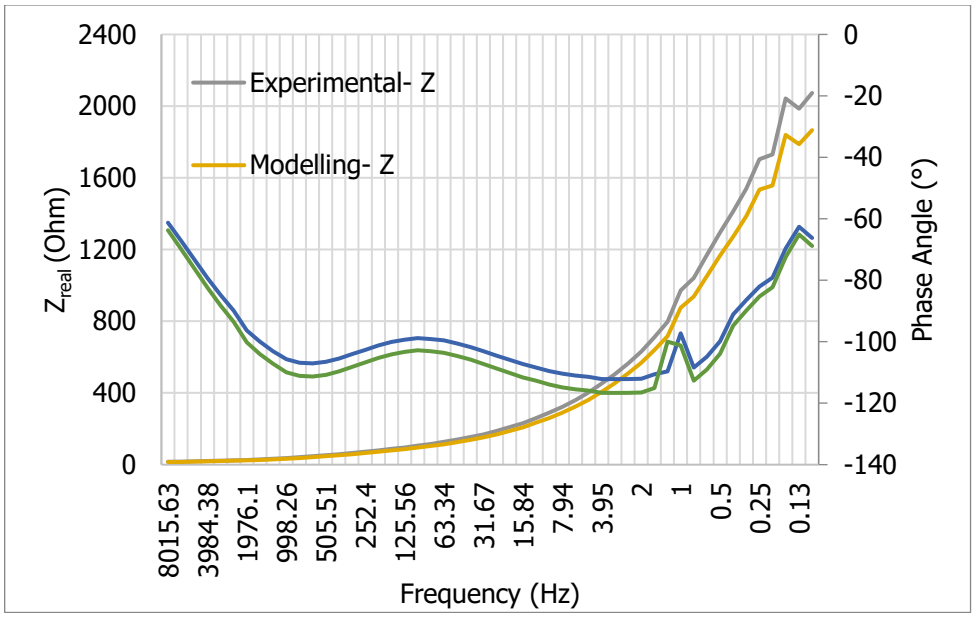

Figure 5.42 Bode plot of 9 M KOH with 0.5 M urea obtained from EIS at 65°C stack temperature

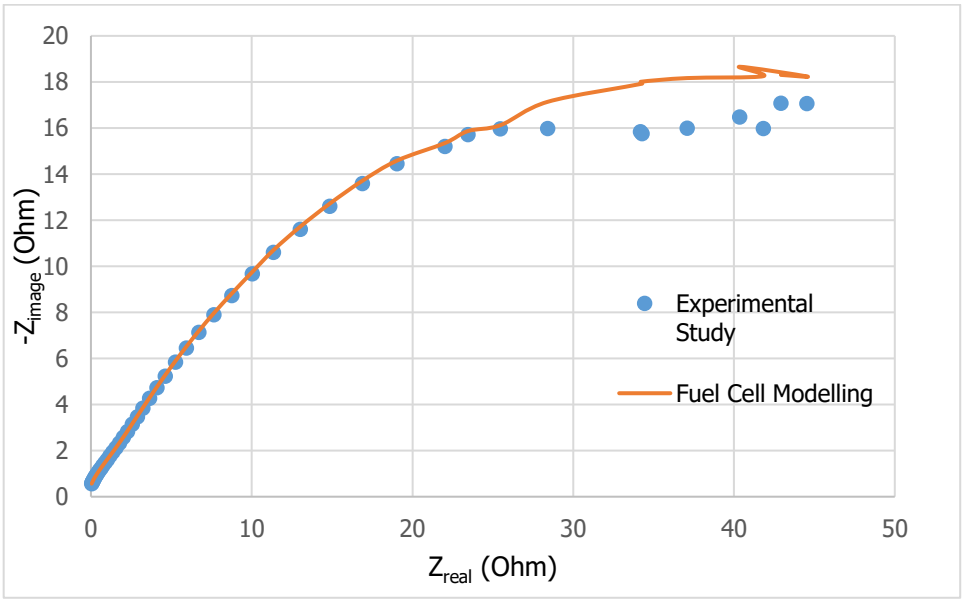

Figure 5.43 Nyquist plot of 9 M KOH with 0.5 M urea obtained from EIS at 65°C stack temperature

The EIS results for the 16-cell DUHPFC stack at 65°C indicate that this temperature optimizes the fuel cell's performance by reducing overall impedance and charge transfer resistance. The decrease in impedance with increasing frequency in the Bode plot suggests improved ionic conductivity, while the phase angle behavior points to efficient charge transfer processes. The Nyquist plot reveals a moderate charge transfer resistance, indicating effective electrochemical reactions. These findings can be attributed to the

enhanced ionic mobility and reduced internal resistance at elevated temperatures, which facilitate better electrochemical dynamics [92, 93, 94, 95].

Figure 5.44 represents the time-dependent changes in temperature and conductivity for the anolyte solution containing 9 M KOH and 0.5 M urea. In this graph, it is observed that while the temperature steadily increases over time, the conductivity decreases inversely. Typically, an increase in temperature would enhance the mobility of ions in the solution, leading to higher conductivity; however, the observed decline here might be due to changes in the composition of the anolyte solution as the temperature rises. Specifically, the chemical transformations of urea and KOH during the reaction could reduce the ion concentration in the solution, resulting in a decrease in conductivity. The reduction in conductivity negatively impacts the ability of ions to be transported between the electrodes. This, in turn, reduces the efficiency of the electrochemical reactions and weakens the overall performance of the system. Although the reaction rates increase with temperature, the decrease in conductivity could lead to an increase in internal resistance and a subsequent drop in cell performance. This effect becomes more pronounced, particularly in scenarios requiring high power outputs.

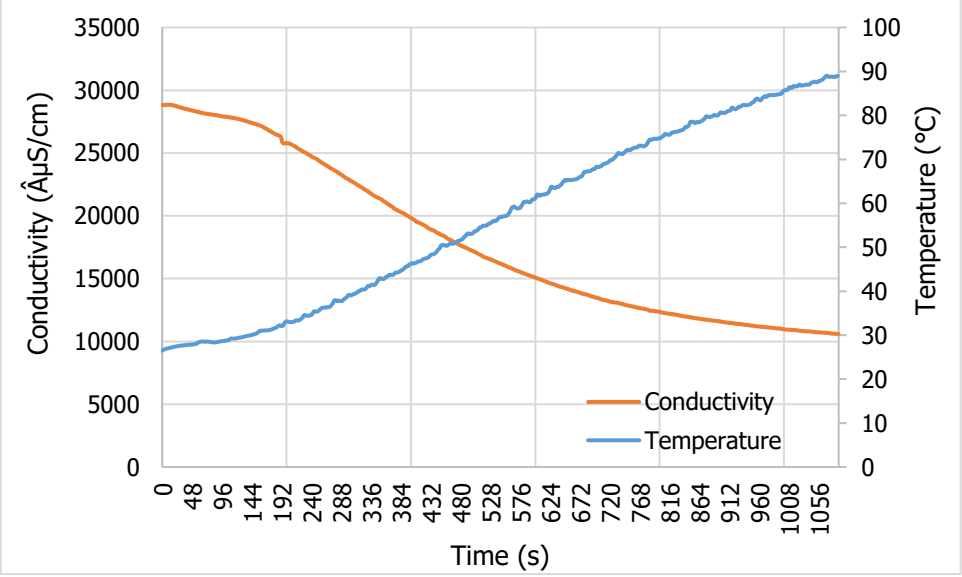

Figure 5.44 Representation of the time-dependent changes in temperature and conductivity for the anolyte solution containing 9 M KOH and 0.5 M urea.

When examining the power density graph (Figure 5.41), we can better understand why the high-power density observed at 25°C drops significantly when the temperature

increases to 45°C. The higher conductivity at 25°C allows for more efficient ion transport within the cell, enabling higher power density. However, when the temperature rises to 45°C, the decrease in conductivity makes ion transport more difficult, leading to increased internal resistance in the system, which, combined with the higher temperature, causes a drop in power density.

The drop in power density observed in the graph results from the combined positive and negative effects of the temperature increase. While the rise in temperature initially boosts performance by accelerating reaction kinetics, the accompanying decrease in conductivity, along with the increase in internal resistance within the system, limits efficiency and eventually leads to a decrease in power density. Therefore, it is crucial to closely monitor and control the balance between temperature and conductivity to optimize the performance of DUHPFC systems.

5.5 Energy and Exergy Efficiencies of Single Cell and Fuel Cell Stack

In this section, the performance analysis focuses on the energy and exergy efficiencies of both the single cell and the fuel cell stack. For the single cell, the energy and exergy efficiency values were calculated and compared at 25°C using different KOH concentrations with 0.5 M urea. For the fuel cell stack, the efficiencies were evaluated at various stack temperatures using 9 M KOH with 0.5 M urea. These comparisons are presented in the form of charts. The calculation of the energy and exergy efficiencies is essential for understanding the overall performance and thermodynamic viability of the fuel cell systems. These efficiencies provide insights into how effectively the fuel cell converts chemical energy into electrical energy and how much of the input energy is available for useful work, considering both energy losses and irreversibility within the system.

Figure 5.45 presents the energy and exergy efficiencies of the single cell at 25°C using different KOH concentrations (1 M, 5 M, and 9 M) with 0.5 M urea. At 1 M KOH, the energy efficiency is 39% and the exergy efficiency is 16%, indicating notable system irreversibility. The highest efficiencies are observed at 5 M KOH, with the energy and exergy efficiencies reaching 58% and 24%, respectively, suggesting optimal ionic conductivity and reduced internal losses at this concentration, leading to better overall performance. At 9 M KOH, the energy efficiency drops to 34%, while the exergy efficiency

increases to 29%. This indicates that while the overall energy conversion is less efficient at this concentration, the quality of the energy converted (exergy) is relatively higher, possibly due to more effective utilization of the available energy in overcoming internal losses. These results highlight that the 5 M KOH concentration provides the best balance between sufficient ionic conductivity and minimal resistive losses, emphasizing the importance of optimizing electrolyte concentration to achieve maximum performance in fuel cells. The efficiency analysis underscores that 5 M KOH with 0.5 M urea is optimal for the single cell at 25°C, achieving the highest energy efficiency and significantly high exergy efficiency, thus enhancing the overall conversion of chemical energy to electrical energy.

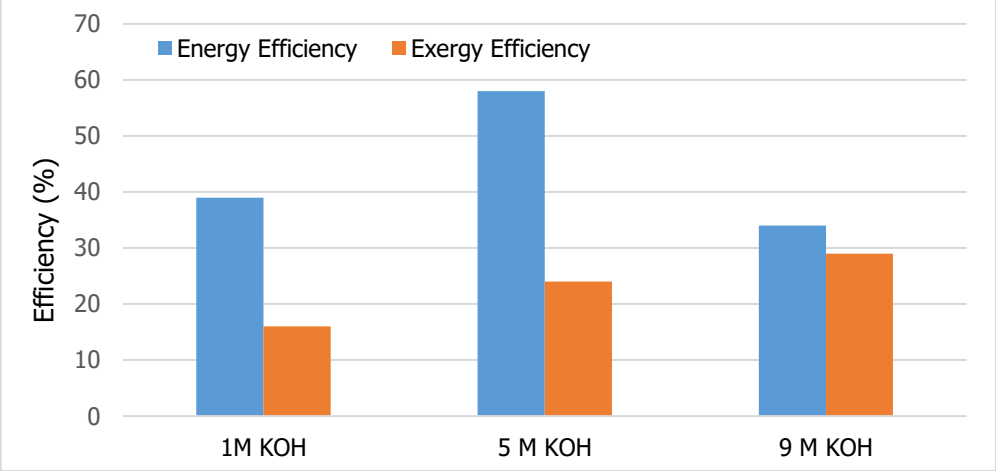

Figure 5.45 Energy and exergy efficiency values for DUHPFC- single cell arrangement for various KOH concentration with 0.5 M urea at 25°C

Figure 5.46 illustrates the energy and exergy efficiency values for DUHPFC- stack for 9 M KOH with 0.5 M urea at different stack temperatures. At 25°C, the energy efficiency is approximately 43.35% and the exergy efficiency is around 36.80%. These values indicate that while a significant portion of the chemical energy is converted to electrical energy, there are still notable irreversibility in the system. At 45°C, the energy efficiency increases to approximately 48.52%, and the exergy efficiency rises to about 40.32%. This improvement suggests that the fuel cell stack operates more efficiently at this moderate temperature, likely due to enhanced ionic conductivity and reduced internal losses. At 65°C, the energy efficiency reaches the highest value of about 48.89%, and the exergy efficiency increases to 41.27%. This indicates that higher temperatures further

enhance the overall performance by improving ionic mobility and reducing internal resistance, although the gains in exergy efficiency are marginal compared to 45°C. These results suggest that 65°C is the optimal temperature for achieving the highest energy and exergy efficiencies in the fuel cell stack. The efficiency analysis underscores the importance of temperature optimization in fuel cell systems, highlighting that operating at 65°C maximizes both energy conversion and the quality of the energy converted, thus enhancing the overall performance and minimizing system irreversibility [96, 97].

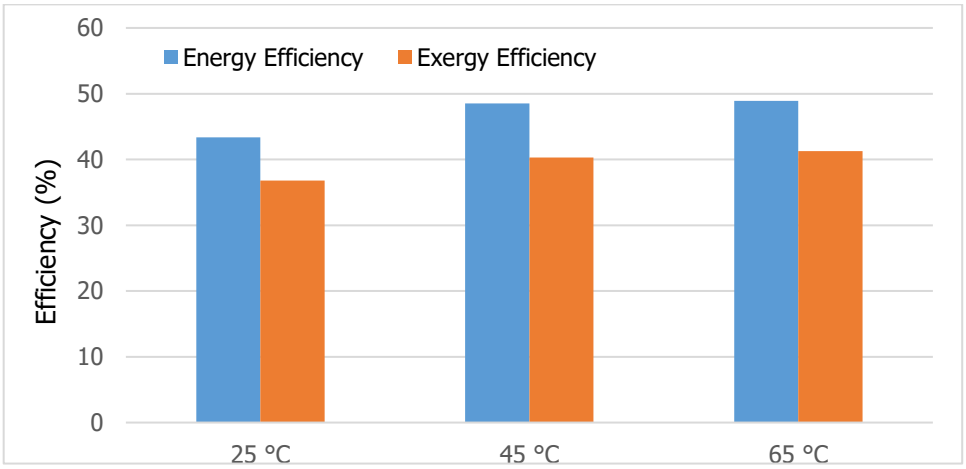

Figure 5.46 Energy and exergy efficiency values for DUHPFC- stack for 9 M KOH with 0.5 M urea at different stack temperatures

5.6 Comparison with Literature Studies

In this section, the performance of the developed DUHPFC system is compared with results from existing literature studies to evaluate its relative efficiency, effectiveness, and potential improvements. This comparison helps to contextualize the findings within the broader scope of fuel cell research and highlights the advancements and remaining challenges in the field.

Figure 5.47 and 5.48 shows comparison of open circuit voltage and power density obtained for the DUHPFC test in the current study with other previous studies. The comparison of Open Circuit Voltage (OCV) and power density values from various studies with those obtained in the present study reveals significant insights. While the present study's single cell OCV (0.72 V) is lower than the values reported by Pei et al. (0.89 V), Hao et al. (1.43 V), Xie et al. (0.99 V), and Yin et al. (0.98 V), it achieves the highest power density (46.38 mW/cm²), indicating effective energy conversion despite the lower OCV.

The fuel cell stack in the present study exhibits a substantially higher OCV (8.8 V) due to the series connection of 16 cells, resulting in a significantly amplified voltage output.

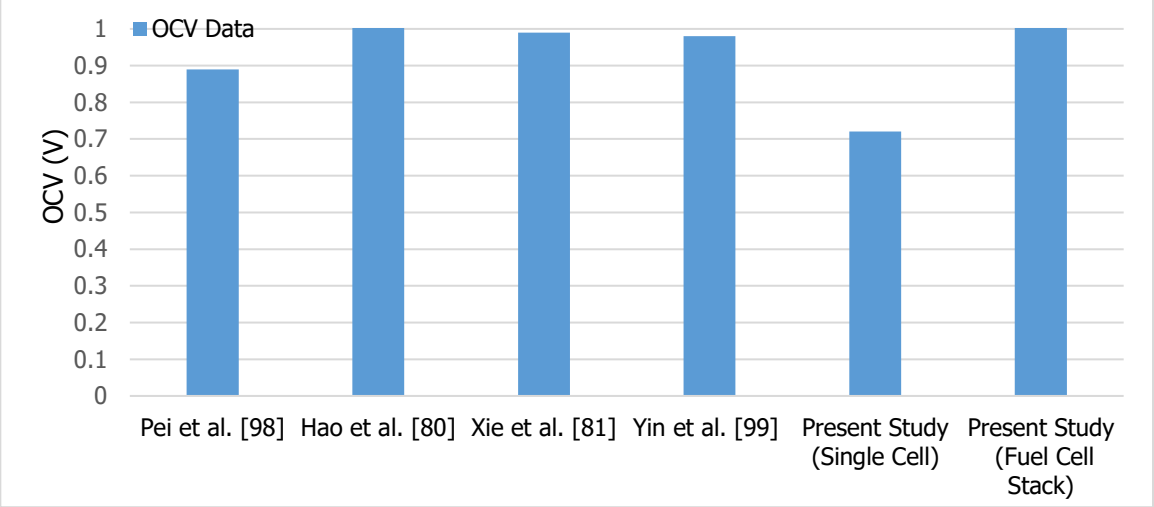

Figure 5.47 A comparison of open circuit voltage obtained for the DUHPFC in the current study with other previous studies

Additionally, the stack achieves a power density of 151.7 mW/cm², which is considerably higher than those reported in the literature. This high-power density underscores the efficiency and effectiveness of the stack configuration in delivering substantial power, making it highly suitable for applications requiring higher power outputs. These results suggest that while there is room for improving the single cell's OCV, its high-power density demonstrates excellent energy conversion efficiency.

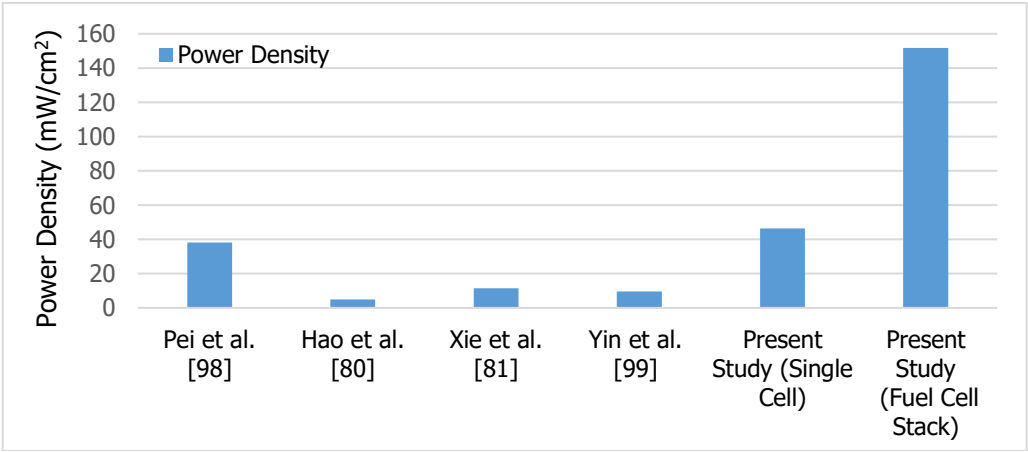

Figure 5.48 A comparison of power density obtained for the DUHPFC in the current study with other previous studies

CHAPTER 6: CONCLUSIONS AND RECOMMENDATIONS

6.1 Conclusions

This section summarizes the key findings from the study on Direct Urea-Hydrogen Peroxide Fuel Cells (DUHPFC), focusing on the electrode preparation, performance evaluation of single cells and fuel cell stacks, and the impact of various operational parameters. The research has provided significant insights into optimizing DUHPFCs for enhanced performance and efficiency, addressing critical gaps in the current literature.

- Nickel zinc iron oxide was successfully deposited onto stainless steel foil via electrodeposition, resulting in an anode with high catalytic activity and stability, making it suitable for DUHPFC applications. The best performance was observed with an electrode prepared using 9 M KOH and 0.5 M urea at an operating temperature of 35°C, emphasizing the critical role of material selection and preparation techniques. The performance of the DUHPFC was significantly influenced by temperature and KOH concentration, with optimal single-cell performance achieved under these conditions, producing a peak power density of 46.38 mW/cm^2.
- For the fuel cell stack, the highest power output of 0.307 kW was obtained at 65°C, demonstrating the crucial impact of operating temperature on efficiency and output. The OCV of the single cell reached 0.72 V, indicating strong potential for power generation under no-load conditions, while the fuel cell stack achieved an OCV of 8.8 V, showcasing its capability for higher voltage applications. Additionally, the energy and exergy efficiencies of the single cell at 25°C were highest with 5 M KOH, achieving values of 58% and 24%, respectively. For the fuel cell stack, the highest efficiencies were observed at 65°C, with the energy and exergy efficiencies of 48.88% and 41.27%, respectively, highlighting the importance of temperature optimization.
- The EIS results demonstrated that impedance decreased with increasing temperature, with the lowest impedance observed at 55°C and 65°C, suggesting enhanced ionic conductivity and reduced resistance at these higher temperatures. Correspondingly, the phase angle shifts towards more negative values as the temperature increases, reflecting improved charge transfer processes and more

dominant resistive behavior. The single cell achieved a power output of 0.00227 kW, suitable for small-scale applications, while the 16-cell fuel stack significantly outperformed it with a power output of 0.307 kW, demonstrating the scalability and effectiveness of the DUHPFC system for larger-scale energy generation.

- Overall, the performance of the DUHPFC system, both in single-cell and stack configurations, shows considerable promise compared to traditional fuel cells. The optimized conditions identified in this study provide a robust foundation for further improvements and practical applications of DUHPFCs.

6.2 Recommendations

Based on the findings and limitations of this study, the following recommendations are proposed for future research to further enhance the performance and understanding of Direct Urea-Hydrogen Peroxide Fuel Cells (DUHPFC):

- Micro-scale Exploration and Optimization: To optimize the structure and composition of electrode materials, future studies may start with micro-scale investigations. This would entail investigating novel catalysts for the electrochemical oxidation of urea, such as nickel, iron oxide, gold, rhenium, and iridium. Beyond what was covered in the first studies, more research into other electrode kinds and configurations as well as thorough parametric studies on variables like electrode surface area and catalyst loading may provide insights into improving catalytic activity and stability. On a smaller scale, evaluating the effects of different electrolyte compositions, membrane thicknesses, and flow field designs may also help to improve the system's performance.
- Scaling Up and System-Level Analysis: The DUHPFC system would need to be scaled up for practical use when micro-scale optimizations have been found. This entails building larger prototypes and analyzing stacked cells thoroughly to assess how well they function in real-world situations. Maintaining optimal performance through precise temperature control systems, especially at higher operating temperatures, and evaluating the fuel cell's long-term stability under these circumstances could be important areas of emphasis. Furthermore, doing exergoeconomic evaluations on this scale can yield insightful information about

cost-effective design improvements, especially with regard to the anion exchange membrane and other crucial parts.

- Environmental and Lifecycle Assessments: To fully comprehend the environmental effects of DUHPFCs, life cycle assessments (LCAs) must be carried out in addition to scaling up. These evaluations can point out any negative effects of using urea as fuel in addition to any potential environmental advantages, like waste management and a decrease in greenhouse gas emissions. More ecologically friendly and sustainable fuel cell technologies will be developed with the help of the lessons learned from these life cycle assessments.
- Further Parametric Studies: It would be beneficial to conduct additional parametric studies that extend beyond the initial scope. These studies should focus on optimizing operating conditions not previously explored, allowing for a more precise identification of optimal conditions for the system. Such studies could include variations in cathode conditions, cell voltage settings, or flow rates, providing a more comprehensive understanding of how to achieve peak performance in DUHPFC systems. Conducting additional parametric studies to capture dynamics beyond the range presented here and to focus more precisely on the optimal operating conditions identified in this study.

REFERENCES

[1] Introduction to Climate Action" United Nations Framework Convention on Climate Change. https://unfccc.int/climate-action/introduction-climate-action (accessed May 22, 2023).

[2] CO_2 Emissions in 2022 IEA Report." International Energy Agency. https://www.iea.org/reports/CO_2 -emissions-in-2022 (accessed May 22, 2023).
[3] BP Statistical Review of World Energy 2021.

[4] Hassan, Q., Viktor, P., Al-Musawi, T. J., Ali, B. M., Algburi, S., Alzoubi, H. M., ... & Jaszczur, M. (2024). The renewable energy role in the global energy Transformations. Renewable Energy Focus, 48, 100545.

[5] IRENA – International Renewable Energy Agency. (n.d.). IRENA – International Renewable Energy Agency. https://www.irena.org/

[6] GWEC in 2020 - Global Wind Energy Council. (n.d.). Global Wind Energy Council. https://gwec.net/gwec-in-2020/

[7] Renewable Energy Directive. (n.d.). Energy. https://energy.ec.europa.eu/topics/renewable-energy/renewable-energy-directive-targets-and-rules/renewable-energy-directive_en

[8] Energy storage - IEA. (n.d.). IEA. https://www.iea.org/energy-system/electricity/grid-scale-storage

[9] Zhang, Y., & Zhang, W. (2021). Urea as a Hydrogen Carrier: Properties and Application. Journal of Hydrogen Energy, 46(10), 6553-6561.

[10] Kumar, R., & Maity, S. K. (2020). Direct Urea Fuel Cells: An Overview. Energy Reports, 6, 401-409.

[11] U.S. Department of Energy. (2022). Hydrogen Production from Urea. DOE Technical Reports.

[12] Li, X., & Liu, Y. (2019). Performance of Urea-Hydrogen Peroxide Fuel Cells. Electrochimica Acta, 302, 74-80.

[13] Global Energy Research. (2021). Sustainable Energy Solutions: Urea-Based Fuel Cells.

[14] Gnana kumar, G., Farithkhan, A., & Manthiram, A. (2020). Direct Urea Fuel Cells: Recent Progress and Critical Challenges of Urea Oxidation Electrocatalysis. Advanced Energy and Sustainability Research, 1(1), 2000015.

[15] [Zhang, X., et al. (2020). "Non-Noble Metal Catalysts for Urea Oxidation: Advances and Challenges." Electrochimica Acta, 354, 136852.]

[16] Gao, X., Zhang, S., Wang, P., Jaroniec, M., Zheng, Y., & Qiao, S.-Z. (2024). Urea catalytic oxidation for energy and environmental applications. Chemical Society Reviews.

[17] Gnana kumar, G., Farithkhan, A., & Manthiram, A. (2020b). Direct Urea Fuel Cells: Recent Progress and Critical Challenges of Urea Oxidation Electrocatalysis. Advanced Energy and Sustainability Research, 1(1), 2000015.

[18] Masjedi, S. K., Kazemi, A., Moeinnadini, M., Khaki, E., & Olsen, S. I. (2023). Urea production: An absolute environmental sustainability assessment. Science of The Total Environment, 168225.

[19] Xia, M., Mao, C., Gu, A., Tountas, A. A., Qiu, C., Wood, T. E., Li, Y. F., Ulmer, U., Xu, Y., Viasus, C. J., Ye, J., Qian, C., & Ozin, G. (2021). Solar Urea: Towards a Sustainable Fertilizer Industry. Angewandte Chemie, 134(1).

[20] Guzmán, R. O., & Lazo, A. B. (2022). Simulation of a reactor considering the Stamicarbon, Snamprogetti, and Toyo patents for obtaining urea. Open Chemistry, 20(1), 424–430.

[21] Yurekli, Y., Zhang, T., & Qiu, F. (2024b). Process intensification through enzymatic decomposition of urea with simultaneous recovery of ammonia. Journal of Environmental Chemical Engineering, 112888.

[22] Hopsort, G., Carmo, D. P. D., Latapie, L., Loubière, K., Serrano, K. G., & Tzedakis, T. (2023). Progress toward a better understanding of the urea oxidation by electromediation of Ni(II)/Ni(III) system in alkaline media. Electrochimica Acta, 141898.

[23] Nemati, H., & Shekoohi, S. A. (2022). Particle sized distribution simulation for an industrial fluidised bed urea granulator by PNB method considering non-uniform growth rate. Indian Chemical Engineer, 1–14.

[24] Weerakoon, D., Bansal, B., Padhye, L. P., Rachmani, A., Wright, L. J., Silyn Roberts, G., & Baroutian, S. (2023). A critical review on current urea removal technologies from water: An approach for pollution prevention and resource recovery. Separation and Purification Technology, 123, 123652.

[25] Knagenhjelm, S. (2010). Mer om nakkesleng. Tidsskrift for Den norske legeforening, 130(24), 2449–2450.

[26] Waheed, H., & Hussain, A. (2019). Fabrication of Cellulose Acetate/Polyaziridine Blended Flat Sheet Membranes for Dialysis Application. BioNanoScience, 9(2), 256–265.

[27] Redirecting. (n.d.). Home Page.

[28] Shen, S., Li, M., Li, B., & Zhao, Z. (2014). Catalytic hydrolysis of urea from wastewater using different aluminas by a fixed bed reactor. Environmental Science and Pollution Research, 21(21), 12563–12568.

[29] Zhang, J., Yan, B., He, C., Hao, Y., Sun, S., Zhao, W., & Zhao, C. (2020). Urease-Immobilized Magnetic Graphene Oxide as a Safe and Effective Urea Removal Recyclable Nanocatalyst for Blood Purification. Industrial & Engineering Chemistry Research, 59(19), 8955–8964.

[30] Chávez, A. M., Torres-Pinto, A., Álvarez, P. M., Faria, J. L., Silva, C. G., & Silva, A. M. T. (2023). One-pot synthesis and immobilization of urea-derived graphitic

carbon nitride onto ceramic foams for visible-light photocatalytic wet peroxide oxidation in water treatment. Chemical Engineering Journal, 148141.

[31] Wang, Q., Huang, N., Wang, W., Wu, Y., Xue, S., Xu, H., Chen, Z., Wu, Y., Wu, Q., & Hu, H. (2023). Urea removal for ultrapure water production by VUV/UV/chlorine under acidic aqueous conditions: Facile elimination and efficient denitrification. Journal of Cleaner Production, 401, 136732.

[32] Kim, J., Kim, M., Han, S. S., & Cho, K. (2024). Accessible Ni-Fe-Oxalate Framework for Electrochemical Urea Oxidation with Radically Enhanced Kinetics. Advanced Functional Materials.

[33] Davies, G. M., Blinkhorn, F. A., & Duxbury, J. T. (2001). Caries among 3-year-olds in Greater Manchester. British Dental Journal, 190(7), 381–384.

[34] Qasem, N. A. A. (2024). A recent overview of proton exchange membrane fuel cells: Fundamentals, applications, and advances. Applied Thermal Engineering, 252, 123746.

[35] Chen, R., Gao, Y., Gao, J., Zhang, H., Motola, M., Bilal Hanif, M., & Li, C.-X. (2024). From concept to commercialization: A review of tubular solid oxide fuel cell technology. Journal of Energy Chemistry.

[36] Wang, M., Ruan, J., Zhang, J., Jiang, Y., Gao, F., Zhang, X., Rahman, E., & Guo, J. (2024). Modelling, thermodynamic performance analysis, and parameter optimization of a hybrid power generation system coupling thermogalvanic cells with alkaline fuel cells. Energy, 130557.

[37] Biebl, M., Roes, J., & Hoster, H. (2024). Investigation of the technical potential of a hydrogen powered phosphoric acid fuel cell (PAFC) for CHP. Journal of Physics: Conference Series, 2689(1), 012014.

[38] Putri, Y. M. T. A., Syauqi, M. I., Rahmawati, I., Aliyah, A., Sanjaya, A. R., & Ivandini, T. A. (2024). Advancements in Ni-based Catalysts for Direct Urea Fuel Cells: A Comprehensive Review. ChemElectroChem.

[39] Fang, T., Vairin, C., von Jouanne, A., Agamloh, E., & Yokochi, A. (2024). Review of Fuel-Cell Electric Vehicles. Energies, 17(9), 2160.

[40] Marcinkoski, J., James, B. D., Kalinoski, J. A., Podolski, W., Benjamin, T., & Kopasz, J. (2011). Manufacturing process assumptions used in fuel cell system cost analyses. Journal of Power Sources, 196(12), 5282–5292.

[41] Kampker, A., Heimes, H., Kehrer, M., Hagedorn, S., Reims, P., & Kaul, O. (2023). Fuel cell system production cost modeling and analysis. Energy Reports, 9, 248–255.

[42] Putri, Y. M. T. A., Gunlazuardi, J., Yulizar, Y., Wibowo, R., Einaga, Y., & Ivandini, T. A. (2021). Recent progress in direct urea fuel cell. Open Chemistry, 19(1), 1116–1133.

[43] Ke, K., Wang, G., Cao, D., & Wang, G. (2020). Recent advances in the electro-oxidation of urea for direct urea fuel cell and urea electrolysis. Electrocatalysis, 41-78.

[44] Sayed, E. T., Eisa, T., Mohamed, H. O., Abdelkareem, M. A., Allagui, A., Alawadhi, H., & Chae, K. J. (2019). Direct urea fuel cells: Challenges and opportunities. Journal of Power Sources, 417, 159-175.

[45] Putri, Y. M., Syauqi, M. I., Rahmawati, I., Aliyah, A., Sanjaya, A. R., & Ivandini, T. A. (2024). Advancements in Ni-based Catalysts for Direct Urea Fuel Cells: A Comprehensive Review. ChemElectroChem, 11(5), e202300637.

[46] Tawalbeh, M., Alarab, S., Al-Othman, A., & Javed, R. M. N. (2022). The Operating Parameters, Structural Composition, and Fuel Sustainability Aspects of PEM Fuel Cells: A Mini Review. Fuels, 3(3), 449–474.

[47] Vedharathinam V, Botte GG. Understanding the electro-catalytic oxidation mechanism of urea on nickel electrodes in alkaline medium. Electrochim Acta. 2012;81:292–300.

[48] Ajayan J, Nirmal D, Mohankumar P, Saravanan M, Jagadesh M, Arivazhagan L. A review of photovoltaic performance of organic/inorganic solar cells for future renewable and sustainable energy technologies. Superlattices Microstruct. 2020;143:106549.

[49] Balajii M, Niju S. Banana peduncle – A green and renewable heterogeneous base catalyst for biodiesel production from Ceiba pentandra oil. Renew Energy. 2020;146:2255–69.

[50] Espinoza-Acosta JL, Torres-Chávez PI, Olmedo-Martínez JL, Vega-Rios A, Flores-Gallardo S, Zaragoza-Contreras EA. Lignin in storage and renewable energy applications: A review. J Energy Chem. 2018;27:1422–38.

[51] Nagaraju G, Sekhar SC, Ramulu B, Yu JS. An integrated approach toward renewable energy storage using rechargeable Ag@Ni0.67Co0.33 S-based hybrid supercapacitors. Small. 2019;15:1–14.

[52] Edrisi A, Mansoori Z, Dabir B. Urea synthesis using chemical looping process – Techno-economic evaluation of a novel plant configuration for a green production. Int J Greenh Gas Control. 2016;44:42–51.

[53] Zheng Y, Jiao Y, Zhu Y, Li LH, Han Y, Chen Y, et al. Hydrogen evolution by a metal-free electrocatalyst. Nat Commun. 2014;5:1–8.

[54] O'hayre R, Suk-Won Cha WGC. Fuel cell fundamentals. Open Med (Warsaw, Pol). 2016;14:271–8.

[55] Serban EC, Balan A, Iordache AM, Cucu A, Ceaus C, Necula M, et al. Urea/hydrogen peroxide fuel cell. Dig J Nanomater Biostruct. 2014;9:1647–54.

[56] An L, Jung CY. Transport phenomena in direct borohydride fuel cells. 2017;205:1270–82.

[57] Guo F, Cheng K, Ye K, Wang G, Cao D. Preparation of nickel–cobalt nanowire arrays anode electro-catalyst and its application in direct urea/hydrogen peroxide fuel cell. Electrochim Acta. 2016;199:290–6.

[58] Lan R, Tao S. Preparation of nano-sized nickel as anode catalyst for direct urea and urine fuel cells. J Power Sources. 2011;196:5021–6.

[59] Rao, N. N., Alex, C., Mukherjee, M., Roy, S., Tayal, A., Datta, A., & John, N. S. (2024). Evidence for Exclusive Direct Mechanism of Urea Electro-Oxidation Driven by In Situ-Generated Resilient Active Species on a Rare-Earth Nickelate. ACS Catalysis, 14(2), 981-993.

[60] Guo, F., Ye, K., Du, M., Huang, X., Cheng, K., Wang, G., & Cao, D. (2016). Electrochemical impedance analysis of urea electro-oxidation mechanism on nickel catalyst in alkaline medium. Electrochimica Acta, 210, 474-482.

[61] Daramola DA, Singh D, Botte GG. Dissociation rates of urea in the presence of NiOOH catalyst: A DFT analysis. J Phys Chem A. 2010;2:11513–21.

[62] Tesfaye RM, Das G, Park BJ, Kim J, Yoon HH. Ni–Co bimetal decorated carbon nanotube aerogel as an efficient anode catalyst in urea fuel cells. Sci Rep. 2019;9:1–9.

[63] Yan W, Wang D, Botte GG. Nickel and cobalt bimetallic hydroxide catalysts for urea electro-oxidation. Electrochim Acta. 2012;61:25–30.

[64] Akkari, S., Vivier, V., & Sánchez-Sánchez, C. M. (2024). Urea electro-oxidation byproducts impact on NiO/NiOOH anode performance studied by operando electrochemical impedance spectroscopy. Electrochimica Acta, 474, 143526.

[65] Tesfaye RM, Das G, Park BJ, Kim J, Yoon HH. Ni–Co bimetal decorated carbon nanotube aerogel as an efficient anode catalyst in urea fuel cells. Sci Rep. 2019;9:1–9.

[66] Li, X., Zheng, H., Liao, Y., Huang, K., Ye, Y., Xin, H., ... & Liu, G. (2024). Urine Treatment in a Stacked Membraneless Direct Urea Fuel Cell with Honeycomb-like Nickel–Molybdenum Bimetal Phosphide as the Anodic Electrocatalyst. ACS Sustainable Chemistry & Engineering, 12(9), 3621-3631.

[67] Wang, J., & Ma, Y. (2023). Copper and nickel-based oxides delicately tailored via galvanic reaction as electrocatalyst for solid-state direct urea fuel cell. International Journal of Hydrogen Energy, 48(74), 28882-28890.

[68] Shah, S. S., Niaz, F., Ehsan, M. A., Das, H. T., Younas, M., Khan, A. S., ... & Aziz, M. A. (2024). Advanced strategies in electrode engineering and nanomaterial modifications for supercapacitor performance enhancement: A comprehensive review. Journal of Energy Storage, 79, 110152.

[69] McMaster-Carr.(n.d.).McMasterCarr. https://www.mcmaster.com/products/stainless-steel-foil/stainless-steel-foil-tape/?s=stainless-steel-foil

[70] CXM-200 (CMI-7000) Cation Exchange Membranes | Technical Specifications - Membranes International Inc. (n.d.). Membranes International Inc. https://ionexchangemembranes.com/cmi-7000-cation-exchange-membranes-technical-specifications/

[71] Kravos, A., Ritzberger, D., Tavčar, G., Hametner, C., Jakubek, S., & Katrašnik, T. (2020). Thermodynamically consistent reduced dimensionality electrochemical model for

proton exchange membrane fuel cell performance modelling and control. Journal of Power Sources, 454, 227930.

[72] Yuan, H., Dai, H., Wei, X., & Ming, P. (2021). Internal polarization process revelation of electrochemical impedance spectroscopy of proton exchange membrane fuel cell by an impedance dimension model and distribution of relaxation times. Chemical Engineering Journal, 418, 129358.

[73] Li, H., Wei, W., Liu, F., Xu, X., Li, Z., & Liu, Z. (2023). Identification of internal polarization dynamics for solid oxide fuel cells investigated by electrochemical impedance spectroscopy and distribution of relaxation times. Energy, 267, 126482.

[74] Verma, S., Arya, S., Gupta, V., Mahajan, S., Furukawa, H., & Khosla, A. (2021). Performance analysis, challenges and future perspectives of nickel based nanostructured electrodes for electrochemical supercapacitors. Journal of Materials Research and Technology, 11, 564-599.

[75] Xu, Z., Hu, X., Wan, Y., Xue, S., Zhang, S., Zhang, L., ... & Xia, C. (2020). Electrochemical performance and anode reaction process for Ca doped Sr2Fe1· 5Mo0· 5O6-δ as electrodes for symmetrical solid oxide fuel cells. Electrochimica Acta, 341, 136067.

[76] Osinkin, D. A. (2022). Detailed analysis of electrochemical behavior of high–performance solid oxide fuel cell using DRT technique. Journal of Power Sources, 527, 231120.

[77] Tzelepis, S., Kavadias, K. A., Marnellos, G. E., & Xydis, G. (2021). A review study on proton exchange membrane fuel cell electrochemical performance focusing on anode and cathode catalyst layer modelling at macroscopic level. Renewable and Sustainable Energy Reviews, 151, 111543.

[78] Li, B., Song, C., Yan, J., Ye, K., Cheng, K., Cao, D., & Wang, G. (2020). Effect of graphene on the performance of nickel foam-based CoNi nanosheet anode catalyzed direct urea-hydrogen peroxide fuel cell. International Journal of Hydrogen Energy, 45(17), 10569-10579.

[79] Eisa, T., Park, S. G., Mohamed, H. O., Abdelkareem, M. A., Lee, J., Yang, E., ... & Chae, K. J. (2021). Outstanding performance of direct urea/hydrogen peroxide fuel cell based on precious metal-free catalyst electrodes. Energy, 228, 120584.

[80] Hao, J., Zhao, S., Mao, R., & Zhao, X. (2021). Nickel phosphide on Ni foam as anode and peroxymonosulfate as the chemical oxidizer for effective direct urea fuel cell. Journal of Environmental Sciences, 110, 84-91.

[81] Xie, J., Ding, R., Li, Y., Guo, J., Zhang, Y., Fang, Q., ... & Liu, E. (2024). Surface reconstruction and synergistic electrocatalysis of perovskite K-Ni-Zn-F for efficient urea-based energy conversion. Nano Energy, 126, 109669.

[82] Kim, B., Das, G., Park, B. J., & Yoon, H. H. (2020). A free-standing NiCr-CNT@ C anode mat by electrospinning for a high-performance urea/H2O2 fuel cell. Electrochimica Acta, 354, 136657.

[83] Le, T. H., Thakur, D., & Nguyen, P. K. T. (2022). Modeling and optimization of direct urea-hydrogen peroxide fuel cell using the integration of artificial neural network and bio-inspired algorithms. Journal of Electroanalytical Chemistry, 922, 116783.

[84] Yin, X., Zhu, K., Ye, K., Yan, J., Cao, D., Zhang, D., ... & Wang, G. (2024). FeNi supported on carbon sponge for efficient urea oxidation in direct urea fuel cell. Journal of Colloid and Interface Science, 654, 36-45.

[85] Karaoglan, M. U., Ince, A. C., Glüsen, A., Colpan, C. O., Müller, M., Stolten, D., & Kuralay, N. S. (2021). Comparison of single-cell testing, short-stack testing and mathematical modeling methods for a direct methanol fuel cell. International Journal of Hydrogen Energy, 46(6), 4844-4856.

[86] Kim, O. H., Choi, H. J., Kang, S. Y., Jang, G. Y., Karuppannan, M., Park, J. E., ... & Cho, Y. H. (2022). Towards outstanding performance of direct urea fuel cells through optimization of anode catalyst layer and operating conditions. Journal of Electroanalytical Chemistry, 921, 116661.

[87] Nguyen, P. K. T., Kim, J., Yoon, Y. S., Yoon, H. H., & Hur, J. (2023). Mathematical modeling of a direct urea fuel cell. International Journal of Hydrogen Energy, 48(6), 2314-2327.

[88] Nguyen, T. L., Tran, Q. N., & Nguyen, P. K. T. (2023). Mathematical modeling of anion exchange membrane-based direct urea/O2 fuel cell incorporating the effects of under-rib mass transport and gaseous bubble formation. Journal of Electroanalytical Chemistry, 945, 117682.

[89] Tang, Z., Huang, Q. A., Wang, Y. J., Zhang, F., Li, W., Li, A., ... & Zhang, J. (2020). Recent progress in the use of electrochemical impedance spectroscopy for the measurement, monitoring, diagnosis and optimization of proton exchange membrane fuel cell performance. Journal of Power Sources, 468, 228361.

[90] Lv, J., Kuang, J., Yu, Z., Sun, G., Liu, J., & Leon, J. I. (2023). Diagnosis of PEM fuel cell system based on electrochemical impedance spectroscopy and deep learning method. IEEE Transactions on Industrial Electronics, 71(1), 657-666.

[91] Najafi, B., Bonomi, P., Casalegno, A., Rinaldi, F., & Baricci, A. (2020). Rapid fault diagnosis of PEM fuel cells through optimal electrochemical impedance spectroscopy tests. Energies, 13(14), 3643.

[92] Raeesi, M., Changizian, S., Ahmadi, P., & Khoshnevisan, A. (2021). Performance analysis of a degraded PEM fuel cell stack for hydrogen passenger vehicles based on machine learning algorithms in real driving conditions. Energy Conversion and Management, 248, 114793.

[93] Zhou, S., Fan, L., Zhang, G., Gao, J., Lu, Y., Zhao, P., ... & Hu, Z. (2022). A review on proton exchange membrane multi-stack fuel cell systems: architecture, performance, and power management. Applied Energy, 310, 118555.

[94] Chen, D., Pei, P., Li, Y., Ren, P., Meng, Y., Song, X., & Wu, Z. (2022). Proton exchange membrane fuel cell stack consistency: Evaluation methods, influencing factors,

membrane electrode assembly parameters and improvement measures. Energy Conversion and Management, 261, 115651.

[95] Zhong, D., Lin, R., Jiang, Z., Zhu, Y., Liu, D., Cai, X., & Chen, L. (2020). Low temperature durability and consistency analysis of proton exchange membrane fuel cell stack based on comprehensive characterizations. Applied Energy, 264, 114626.

[96] Nanadegani, F. S., & Sunden, B. (2023). Review of exergy and energy analysis of fuel cells. International Journal of Hydrogen Energy, 48(84), 32875-32942.

[97] Bayat, M., Özalp, M., & Gürbüz, H. (2022). Comprehensive performance analysis of a high-temperature PEM fuel cell under different operating and design conditions. Sustainable Energy Technologies and Assessments, 52, 102232.

[98] Pei, C., Chen, S., Zhou, M., Chen, X., Sun, B., Lan, S., Hahn, H., & Feng, T. (2023). Direct Urea/H2O2 Fuel Cell with a Hierarchical Porous Nanoglass Anode for High-Efficiency Energy Conversion. ACS Applied Materials & Interfaces.

[99] Yin, X., Zhu, K., Ye, K., Yan, J., Cao, D., Zhang, D., Yao, J., & Wang, G. (2023). FeNi supported on carbon sponge for efficient urea oxidation in direct urea fuel cell. Journal of Colloid and Interface Science.